FRACTURE CHARACTERIZATION OF KNITTING FABRIC REINFORCED LAMINATED COMPOSITES

MASTER OF SCIENCE THESIS

DERVİŞ YALÇIN

SUPERVISOR
Assoc. Prof. Dr. Mehmet AKTAŞ

Graduate School of Natural and Applied Sciences of Usak University

APRIL 2016

GRADUATE SCHOOL OF NATURAL AND APPLIED SCIENCES

OF

USAK UNIVERSITY

DEPARTMENT OF MECHANICAL ENGINEERING

FRACTURE CHARACTERIZATION OF KNITTING FABRIC REINFORCED LAMINATED COMPOSITES

MASTER OF SCIENCE THESIS

DERVİŞ YALÇIN

APRIL 2016

GRADUATE SCHOOL OF NATURAL AND APPLIED SCIENCES

OF

USAK UNIVERSITY

DEPARTMENT OF MECHANICAL ENGINEERING

FRACTURE CHARACTERIZATION OF KNITTING FABRIC REINFORCED LAMINATED COMPOSITES

MASTER OF SCIENCE THESIS

DERVİŞ YALÇIN

APRIL 2016

M. Sci. THESIS EXAMINATION RESULT FORM

We have read the thesis entitled **"FRACTURE CHARACTERIZATION OF KNITTING FABRIC REINFORCED LAMINATED COMPOSITES"** completed by **DERVİŞ YALÇIN** under supervision of **ASSOC. PROF. DR. MEHMET AKTAŞ** and we certify that in our opinion it is fully adequate, in scope and in quality, as a thesis for the degree of Master of Science.

ASSOC. PROF. DR. MEHMET AKTAŞ ……..
Supervisor, Department of Mechanical Engineering

This study was certified with unanimity by committee member as Master of Science Thesis at Department of Mechanical Engineering.

PROF. DR. HALİT GÜN ……..
Department of Mechanical Engineering, Usak University

ASSOC. PROF. DR. MEHMET ŞENEL ……..
Department of Mechanical Engineering, Dumlupınar University

Date: 06/04/2016

This thesis was certified as Master of Science Thesis by board of director Usak University Graduate School of Natural and Applied Sciences.

PROF. DR. LÜTFULLAH TÜRKMEN ……..
Director, Graduate School of Natural and Applied Sciences

THESIS DECLARATION

This thesis is a presentation of my original research work. Wherever contributions of others are involved, every effort is made to indicate this clearly, with due reference to the literature, and acknowledgement of collaborative research and discussions. This master thesis was completed under the guidance of Assoc. Prof. Dr. Mehmet AKTAŞ at the Graduate School of Natural and Applied Sciences of Usak University.

DERVİŞ YALÇIN

FRACTURE CHARACTERIZATION OF KNITTING FABRIC REINFORCED LAMINATED COMPOSITES
(M. Sci. Thesis)

Derviş YALÇIN

USAK UNIVERSITY
GRADUATE SCHOOL OF NATURAL AND APPLIED SCIENCES

April 2016

ABSTRACT

Features such as strength and lightness come into prominence in the engineering application with the development of technology. This situation obligates the use of composite materials, which are as strong as metallic materials but lighter than the metallic materials, instead. Polymeric composites have been used in many engineering applications due to their high strength in proportion to their weight, high stability, rigidity, superior corrosion, and fatigue resistance. For this aim, glass and carbon fibers used as reinforcement materials in the polymeric composites must be improved in order to constitute more strength in the structures.

Composite materials used as a structure material can be damaged during manufacturing, assembly, and usage of them. These damages can cause breaking of the construction under environmental effects and external loadings in some period of times. One of these damages is creating crack and fracture, which depends on crack propagation. Fracture, which is dangerous for composite structures, can cause loss of life and property. To improve safety level of the structures, strength value of materials for crack propagation named fracture toughness must be known.

In this study, fracture characterizations of laminated composites reinforcing with hybrid and non-hybrid knitting fabric were investigated under different loading conditions. For this purposes, hybrid and non-hybrid fabrics were knitted in 1x1 rib knitting structure by using glass and carbon fibers. Non-hybrid fabrics were knitted with pure glass fibers (100%) and pure carbon fibers (100%) and hybrid fabrics were knitted with equal as weight glass-carbon fibers (50%-50%). Also, hybrid fabrics were knitted in 3 different pattern widths in order to investigate the effect of knitting pattern width on the fracture toughness. Laminated composites, which reinforced with knitted fabrics, were manufactured by hand lay-up method and Arcan test specimens having desired sizes were obtained from manufactured laminated composites. After that crack having 4mm length was created on the each manufactured Arcan test specimens. Fracture toughness of cracked Arcan test specimens were determined under mode I (0°), mode I-II (30°, 45°, and 60°), and mode II (90°) loading conditions. After Arcan tests, morphology of fracture surfaces was examined by using scanning electron microscope (SEM).

Another study in this thesis is determination of fracture toughness of laminated composites, which reinforced with hybrid and non-hybrid glass and carbon fabrics by using J-integral method in ANSYS package program, numerically. Mechanical properties of each composite structure, which is needed for numerical study, were also determined experimentally.

Keywords: Fracture toughness, glass-carbon knitting fabric, hybrid knitting structure, Arcan test, scanning electron microscope (SEM), finite element analysis (FEA).

Science Code: 625.03.00

Number of Page: 142

Supervisor: Assoc. Prof. Dr. Mehmet AKTAŞ

ÖRGÜ KUMAŞ TAKVİYELİ TABAKALI KOMPOZİTLERİN KIRILMA KARAKTERİSTİĞİ
(Yüksek Lisans Tezi)

Derviş YALÇIN

UŞAK ÜNİVERSİTESİ
FEN BİLİMLERİ ENSTİTÜSÜ

Nisan 2016

ÖZET

Sağlamlık ve hafiflik gibi özellikler teknolojinin ilerlemesi ile birlikte mühendislik uygulamalarında ön plana çıkmıştır. Bu durum metalik malzemelerin yerine onun kadar sağlam ve ondan daha hafif olan kompozit malzemelerin kullanımını zorunlu kılmıştır. Polimerik kompozitler, ağırlıklarına oranla yüksek dayanım, yüksek rijitlik ve stabilite, üstün korozyon ve yorulma dayanımlarından ötürü birçok mühendislik uygulamasında kullanılmaktadır. Bu amaçla polimer esaslı kompozitlerde takviye elemanı olarak kullanılan cam ve karbon lifleri daha mukavim yapılar oluşturma açısından geliştirilmelidir.

Yapı elamanı olarak kullanılan kompozit malzemeler üretim, montaj veya kullanım sırasında çeşitli şekillerde hasara uğrayabilirler. Bu hasarlar çevresel etkiler ve dış yükler altında yapının zamanla bozulmasına neden olurlar. Bu hasarlardan biri de çatlak oluşumu ve çatlak yayılımına bağlı olarak meydana gelen kırılmadır. Kompozit yapılarda tehlikeli bir durum olan kırılma, can ve mal kaybıyla sonuçlanan hasarlara sebep olabilir. Yapılardaki güvenliği arttırmak için, kırılma tokluğu olarak adlandırılan malzemenin çatlak ilerlemesine karşı dayanımının bilinmesi gerekir.

Bu çalışmada, hibrit ve hibrit olmayan örgü kumaşlarla takviye edilmiş tabakalı kompozitlerin farklı yükleme durumlarındaki kırılma karakteristiği incelenmiştir. Bu

amaçla 1x1 rib örgü yapısına sahip cam ve karbon lifleri kullanılarak hibrit ve hibrit olmayan kumaşlar örülmüştür. Hibrit olmayan kumaşlar sadece cam (%100) ve sadece karbon (%100) lifi ile örülürken, hibrit kumaşlar ise ağırlıkça eşit cam-karbon (%50-%50) liflerinden örülmüştür. Ayrıca örgü desen genişliğinin kırılma tokluğuna etkisini incelemek için hibrit kumaşlar 3 farklı desen genişliğinde örülmüştür. Örgü kumaşlarla takviye edilecek tabakalı kompozitler el yatırma yöntemiyle üretilmiş ve üretilen tabakalı kompozitlerden istenilen ölçülerde Arcan test numunesi elde edilmiştir. Daha sonra üretilen her bir Arcan test numunesine 4mm uzunluğunda çatlak açılmıştır. Çatlaklı Arcan test numunelerinin mod I (0°), mod I-II (30°, 45° ve 60°), ve mod II (90°) yükleme şartlarındaki kırılma toklukları belirlenmiştir. Arcan testleri sonrası taramalı elektron mikroskobu (SEM) kullanılarak kırılma yüzeylerinin morfolojisi incelenmiştir.

Bu tezde yapılan bir diğer çalışma ise, cam ve karbon hibrit ve hibrit olmayan kumaşlarla takviye edilmiş kompozit malzemelerin kırılma tokluklarının J-integral yöntemi ile ANSYS paket programı kullanılarak nümerik olarak belirlenmesidir. Ayrıca, nümerik çalışma için gerekli olan her bir yapıya ait mekanik özellikler deneysel olarak belirlenmiştir.

Anahtar Kelimeler: Kırılma tokluğu, cam-karbon örgü kumaş, hibrit örgü yapısı, Arcan test, tarama elektron mikroskobu (TEM), sonlu elemanlar analizi (SEA).

Bilim Kodu: 625.03.00

Sayfa Adedi: 142

Tez Yöneticisi: Doç. Dr. Mehmet AKTAŞ

ACKNOWLEDGEMENT

Assoc. Prof. Dr. Mehmet AKTAŞ

"I would like to express my sincere gratitude to you for friendship, encouragement and patience that you have shown in all circumstances throughout the thesis. Since the first day I got down to, you have always believed in me and my abilities. This was the most important thing for me to proceed. This thesis would not have been completed without your guidance and support. And most importantly, from you, I learned that life is a climb, but the view is great."

Res. Asst. H. Ersen BALCIOĞLU

"How do I characterise you? A good scholar, a good teacher, a good friend or a good brother… You were more than these for me during the entire time we were together. I am grateful to you for your support, motivation, encouragement, friendship and valuable advises through not only my study but also my life and also for sharing all your precious work experiences with me."

Res. Asst. H. Aslı YALÇIN

"Without your help and love I could not complete this thesis. "Thanks" is such a little word to carry a big load. You're the only architect of my hope. I am really grateful to you for providing that peace inside of me by giving this inspiration and strength."

Derviş YALÇIN

TABLE OF CONTENTS

ABSTRACT v
ÖZET vii
ACKNOWLEDGEMENT ix
TABLE OF CONTENTS x
LIST OF FIGURES xiv
LIST OF TABLES xx
NOMENCLATURE xxii

CHAPTER ONE: INTRODUCTION

1.1. Introduction 2
1.2. Literature Review 4
1.3. Scope of Thesis 11
1.4. Outline of Thesis 12
1.5. Sponsorship & Material Supply 12

CHAPTER TWO: GENERAL INFORMATION ABOUT COMPOSITE MATERIALS

2.1. Introduction to Composite Materials 14
2.2. Advantages and Disadvantages of Composites Materials 17
2.2.1. Advantages of Composites Materials 17
2.2.2. Disadvantages of Composites Materials 18
2.2.3. Comparison with Metals 19
2.3. Reinforcement Elements 20
2.3.1. Glass Fibers 21
2.3.2. Carbon Fibers 22
2.3.2.1. Production of Carbon Fibers 25
2.3.3. Textile Reinforcements 26
2.4. Resin Systems 27
2.4.1. Thermosets 29

2.4.1.1. Epoxy Resin 30
2.4.1.2. Cure Reactions 31
2.3.1.3. Catalytic Cure 31
2.3.1.4. Co-reactive Cure 31
2.4.2. Thermoplastics 32
2.4.3. Comparison of Thermosets and Thermoplastics 32

CHAPTER THREE: FRACTURE MECHANICS

3.1. Introduction to Fracture Mechanics 35
3.2. The Importance of Fracture Mechanics 37
3.3. Linear Elastic Fracture Mechanics 37
3.3.1. Plane Stress and Plane Strain Conditions 38
3.3.2. Crack Tip Stress and Displacement Components 40
3.4. Elastic-Plastic Fracture Mechanics 43
3.4.1. Crack Tip Plastic Zone 43
3.4.2. Calculation of Crack Tip Plastic Zone 43
3.4.3. J-Integral Method 45

CHAPTER FOUR: PRODUCTION OF COMPOSITE MATERIALS

4.1. Reinforcement Elements 48
4.1.1. The Fibers used in Knitting Reinforcement 48
4.1.1.1. Carbon and Glass Fibers 48
4.1.2. The Production of Knitting Reinforcement Elements 49
4.2. Matrix Material 55
4.3. Production of Composite Materials 55
4.3.1. Production Parameters and Matters to Consider 56
4.4. Preparation of Test Samples 58
4.5. Preparation of Arcan Test Apparatus 62

CHAPTER FIVE: EXPERIMENTAL STUDIES

5.1. Introduction 64
5.1.1. Determination of Tensile Properties 64
5.1.2. Determination of Compressive Properties 65
5.1.3. Determination of Shear Properties 67
5.1.4. Determination of Fracture Toughness 69

CHAPTER SIX: FINITE ELEMENT ANALYSIS

6.1. Introduction 73
6.2. Program Overview: ANSYS 17.0 73
6.3. Fracture Analysis 73
6.3.1. Defining the Material Properties 73
6.3.2. Modelling of the Test Sample 75
6.3.3. Appointment of the Material Properties 75
6.3.4. Creation of the Coordinate System 77
6.3.5. Meshing Procedure 77
6.3.6. Identification of Crack Zone 77
6.3.7. Identification of Fracture Contour 78
6.3.8. Loading and Boundary Conditions 78
6.3.9. Identification of the Output Results 79
6.3.10. Reading the Results 80
6.4. Calculation of Fracture Toughness 81

CHAPTER SEVEN: RESULTS AND DISCUSSION

7.1. Introduction 84
7.2. Evaluation of Test Results 85
7.2.1. Pure Carbon Knitted Composites 85
7.2.2. Hybrid Knitted Composites with 50mm Pattern Width (Crack Initiation from Carbon Side) 87

7.2.3. Hybrid Knitted Composites with 25mm Pattern Width (Crack Initiation from Carbon Side) 90
7.2.4. Hybrid Knitted Composites with 12.5mm Pattern Width (Crack Initiation from Carbon Side) 92
7.2.5. Pure Glass Knitted Composites 95
7.2.6. Hybrid Knitted Composites with 50mm Pattern Width (Crack Initiation from Glass Side) 97
7.2.7. Hybrid Knitted Composites with 25mm Pattern Width (Crack Initiation from Glass Side) 100
7.2.8. Hybrid Knitted Composites with 12.5mm Pattern Width (Crack Initiation from Glass Side) 102
7.3. General evaluation of results 105
7.4. Evaluation of Scanning Electron Microscopy Images 107
7.5. Discussion 109

REFERENCES 111

LIST OF FIGURES

Figure 2.1 The evolution of engineering materials with time 15

Figure 2.2 The schematic illustration of engineering materials. The basic families of metals, ceramics, glasses, polymers, and elastomers can be combined in various geometries to create hybrids 16

Figure 2.3 Specific strength and modulus of some commercially important fibers . 20

Figure 2.4 Relative fiber cost and performance of some high-strength fibers..... 21

Figure 2.5 Tensile properties of carbon fibers 23

Figure 2.6 Compressive properties of carbon fibers 24

Figure 2.7 Electrical resistivity of carbon fibers 24

Figure 2.8 Thermal conductivity of carbon fibers 25

Figure 2.9 PAN and PITCH based carbon fibers 25

Figure 2.10 Examples of yarn-to-fabric preforms..... 27

Figure 2.11 Comparison of thermoset and thermoplastic polymer structures 28

Figure 2.12 Stages of cure for thermoset resin. (a) Polymer and curing agent prior to reaction. (b) Curing initiated with size of molecules increasing. (c) Gelation with full network formed. (d) Full cured and cross-linked..... 29

Figure 3.1 The examples of initial cracks and other damage phenomena, (a) welding line in pressure die cast aluminum, (b) corrosion attack on a rongeur forceps made of a martensitic stainless steel, (c) slag inclusion in a forged casing, and (d) crack in a connection rod..... 36

Figure 3.2 Fracture toughness versus strength of different engineering materials ·· 36

Figure 3.3 The modes of fracture crack separation a) Mode I: opening, b) Mode II: in-plane shear, c) Mode III: out of-plane shear 38

Figure 3.4 Plane stress and plane strain conditions for plates under biaxial positive tensile stresses 38

Figure 3.5 Thin body (plane stress condition) 39

Figure 3.6 Thin body (plane strain condition) 39

Figure 3.7 Location of local stresses near a crack tip 40

Figure 3.8 The shape of plastic zone for Ti-6Al-4V(ELI)RA (Titanium alloy) 45

Figure 3.9 Definition of the J-integral 46
Figure 4.1 V-bed semi-automatic knitting machine 49
Figure 4.2 The waxing apparatus 50
Figure 4.3 Passing fibers through the guides 50
Figure 4.4 The withdrawal of the knitted fabrics with concentric weights 51
Figure 4.5 A knitted loop 51
Figure 4.6 A needle movement for loop formation; (1) starting position, (2) half of the movement of the needle, (3) the highest position of the needle, (4) thread depositing, (5) "cast on" for new loop formation, and (6) new loop length setting 52
Figure 4.7 The wale and course directions of loops 52
Figure 4.8 Schematic representation of rib fabric 53
Figure 4.9 The production of 1x1 rib glass knitted non-hybrid fabric 53
Figure 4.10 The production of 1x1 rib carbon knitted non-hybrid fabric 54
Figure 4.11 The glass-carbon (50%-50%) knitted hybrid fabrics with 5 additional rows 54
Figure 4.12 DTE 1000 epoxy and DTS 1100 hardener 55
Figure 4.13 The knitted fabrics that in sample size 56
Figure 4.14 The produced composites: a) pure carbon and b) pure glass non-hybrid knitted composites, and glass-carbon hybrid knitted composites with c) 50mm, d) 25mm, and e)12.5mm pattern widths 57
Figure 4.15 The schematic representation of knitted composite production 58
Figure 4.16 The coordinate system for the knitted composite samples 58
Figure 4.17 The cutting process with the CNC router 59
Figure 4.18 The geometry of the fracture toughness test samples 60
Figure 4.19 The geometry of the mechanical test samples 61
Figure 4.20 The dimensions of arcan test apparatus 62
Figure 4.21 The image of arcan test apparatus 62
Figure 5.1 Tensile test and the extensometer connected to the composite samples . 64
Figure 5.2 The images of glass knitted composite samples (a) before and (b) after compression tests and of carbon knitted composite samples (c) before and (d) after compression tests 66

Figure 5.3 E_{45} knitted samples after the shear modulus tests (a) glass (b) carbon knitted composite samples 67
Figure 5.4 The shear test samples for (a) glass and (b) carbon knitted composites.. 68
Figure 5.5 The fracture toughness test samples and located in the arcan apparatus in 45° loading angle; a) non-hybrid carbon sample and hybrid glass-carbon samples with crack initiation from carbon side b) 50mm, c) 25mm, and d) 12.5mm pattern width and e) non-hybrid glass sample and hybrid glass-carbon samples with crack initiation from glass side f) 50mm, g) 25mm and h) 12.5mm pattern width 69
Figure 5.6 The average fracture toughness values (a) pure carbon and pure glass knitted samples and glass-carbon hybrid knitted samples with (b) 50mm, (c) 25mm and (d) 12.5mm pattern widths 71
Figure 6.1 Desktop image of ANSYS 17.0 74
Figure 6.2 Defining the material properties 74
Figure 6.3 The solid model of the arcan test sample 76
Figure 6.4 Entering material properties 76
Figure 6.5 Creating a coordinate system of arcan test sample 77
Figure 6.6 Meshing of arcan test sample 78
Figure 6.7 Defining the crack zone 78
Figure 6.8 Illustration of Fracture Contours 79
Figure 6.9 Entering the boundary conditions 79
Figure 6.10 Determination of the output results 80
Figure 6.11 Stresses at the crack tip 80
Figure 6.12 Distribution of J-integral values through the crack tip 81
Figure 7.1 The illustration of crack propagation and the loading direction of arcan fracture test 84
Figure 7.2 The experimental and numerical damage images of pure carbon knitted composite samples 86
Figure 7.3 The stress-loading angles curve for pure carbon knitted composite samples (a) and numerical damage images for 15° (b) and 75° (c) loading angles 86
Figure 7.4 The fracture toughness (a) and J-integral (b) variation depending on

the loading angles of the pure carbon knitted composite samples..... 87
Figure 7.5 The experimental and numerical damage images of hybrid glass-carbon knitted composite samples with 50mm pattern width (crack initiation from carbon side) 88
Figure 7.6 The stress-loading angles curve for hybrid glass-carbon knitted composite samples with 50mm pattern width (crack initiation from carbon side) (a) and numerical damage images for 15° (b) and 75° (c) loading angles 88
Figure 7.7 The fracture toughness (a) and J-integral (b) variation depending on the loading angles of hybrid glass-carbon knitted composite samples with 50mm pattern width (crack initiation from carbon side)..... 89
Figure 7.8 The experimental and numerical damage images of hybrid glass-carbon knitted composite samples with 25mm pattern width (crack initiation from carbon side) 90
Figure 7.9 The stress-loading angles curve for hybrid glass-carbon knitted composite samples with 25mm pattern width (crack initiation from carbon side) (a) and numerical damage images for 15° (b) and 75° (c) loading angles 91
Figure 7.10 The fracture toughness (a) and J-integral (b) variation depending on the loading angles of hybrid glass-carbon knitted composite samples with 25mm pattern width (crack initiation from carbon side)..... 92
Figure 7.11 The experimental and numerical damage images of hybrid glass-carbon knitted composite samples with 12.5mm pattern width (crack initiation from carbon side) 93
Figure 7.12 The stress-loading angles curve for hybrid glass-carbon knitted composite samples with 12.5mm pattern width (crack initiation from carbon side) (a) and numerical damage images for 15° (b) and 75° (c) loading angles 93
Figure 7.13 The fracture toughness (a) and J-integral (b) variation depending on the loading angles of hybrid glass-carbon knitted composite samples with 12.5mm pattern width (crack initiation from carbon side)..... 94
Figure 7.14 The experimental and numerical damage images of pure glass knitted

composite samples 95
Figure 7.15 The stress-loading angles curve for pure glass knitted composite samples (a) and numerical damage images for 15° (b) and 75° (c) loading angles 96
Figure 7.16 The fracture toughness (a) and J-integral (b) variation depending on the loading angles of the pure glass knitted composite samples 97
Figure 7.17 The experimental and numerical damage images of hybrid glass-carbon knitted composite samples with 50mm pattern width (crack initiation from glass side) 98
Figure 7.18 The stress-loading angles curve for hybrid glass-carbon knitted composite samples with 50mm pattern width (crack initiation from glass side) (a) and numerical damage images for 15° (b) and 75° (c) loading angles 98
Figure 7.19 The fracture toughness (a) and J-integral (b) variation depending on the loading angles of hybrid glass-carbon knitted composite samples with 50mm pattern width (crack initiation from glass side)..... 99
Figure 7.20 The experimental and numerical damage images of hybrid glass-carbon knitted composite samples with 25mm pattern width (crack initiation from glass side) 100
Figure 7.21 The stress-loading angles curve for hybrid glass-carbon knitted composite samples with 25mm pattern width (crack initiation from glass side) (a) and numerical damage images for 15° (b) and 75° (c) loading angles 101
Figure 7.22 The fracture toughness (a) and J-integral (b) variation depending on the loading angles of hybrid glass-carbon knitted composite samples with 25mm pattern width (crack initiation from glass side)..... 102
Figure 7.23 The experimental and numerical damage images of hybrid glass-carbon knitted composite samples with 12.5mm pattern width (crack initiation from glass side) 103
Figure 7.24 The stress-loading angles curve for hybrid glass-carbon knitted composite samples with 12.5mm pattern width (crack initiation from glass side) (a) and numerical damage images for 15° (b) and 75° (c)

loading angles 103
Figure 7.25 The fracture toughness (a) and J-integral (b) variation depending on the loading angles of hybrid glass-carbon knitted composite samples with 12.5mm pattern width (crack initiation from glass side)..... 104
Figure 7.26 The fracture toughness of the glass-carbon hybrid knitted composite samples (with crack initiation from carbon side) and pure carbon non-hybrid knitted composite samples for different loading angles and for different pattern widths..... 106
Figure 7.27 The fracture toughness of the glass-carbon hybrid knitted composite samples (with crack initiation from glass side) and pure glass non-hybrid knitted composite samples for different loading angles and for different pattern widths..... 106
Figure 7.28 The fracture toughness values for all non-hybrid and hybrid structures . 107
Figure 7.29 The fracture damage images of the glass knitted fibers in the pure glass knitted composites 108
Figure 7.30 The fracture images of the carbon knitted fibers in the pure carbon knitted composites 108
Figure 7.31 The matrix damages in the pure glass knitted composites during crack propagation 109

LIST OF TABLES

Table 2.1 A comparison of the textile reinforcement elements 26
Table 2.2 Relative characteristics of thermoset resin matrices 30
Table 2.3 The comparison of thermosets and thermoplastics 33
Table 4.1 The properties of the 3K carbon fibers 48
Table 4.2 The properties of the E glass fibers..... 49
Table 4.3 The row numbers of glass and carbon fibers for desired pattern widths ... 55
Table 5.1 The tensile properties of non-hybrid carbon and glass knitted composite samples..... 65
Table 5.2 The compressive properties of non-hybrid carbon and glass knitted composite samples 66
Table 5.3 The shear properties of glass and carbon knitted composite samples..... 68
Table 5.4 The fracture toughness values of non-hybrid and hybrid samples..... 71
Table 6.1 Mechanical properties of carbon and glass composites 75
Table 6.2 J-integral values obtained from ANSYS finite element software..... 82
Table 6.3 Calculated fracture toughness values 82
Table 7.1 The fracture toughness and J-integral values of the pure carbon knitted composite samples 86
Table 7.2 The fracture toughness and the J-integral values of hybrid glass-carbon knitted composite samples with 50mm pattern width (crack initiation from carbon side) 89
Table 7.3 The fracture toughness and the J-integral values of hybrid glass-carbon knitted composite samples with 25mm pattern width (crack initiation from carbon side) 91
Table 7.4 The fracture toughness and the J-integral values of hybrid glass-carbon knitted composite samples with 12.5mm pattern width (crack initiation from carbon side) 94
Table 7.5 The fracture toughness and the J-integral values of pure glass knitted composite samples 96
Table 7.6 The fracture toughness and the J-integral values of hybrid glass-carbon knitted composite samples with 50mm pattern width (crack initiation

from glass side) 99
Table 7.7 The fracture toughness and the J-integral values of hybrid glass-carbon knitted composite samples with 25mm pattern width (crack initiation from glass side) 101
Table 7.8 The fracture toughness and the J-integral values of hybrid glass-carbon knitted composite samples with 12.5mm pattern width (crack initiation from glass side) 104

NOMENCLATURE

W	Wale direction
C	Course direction
T	Transverse direction
E_W	The modulus of elasticity in wale direction
E_C	The modulus of elasticity in course direction
W_t	The tensile strength in wale direction
C_t	The tensile strength in course direction
W_C	The compressive strength in wale direction
C_C	The compressive strength in course direction
E_{45}	45° direction relative to the wale direction
G_{WC}	In plane shear modulus
ν_{WC}	Major Poisson's ratio
S_{WC}	In plane shear strength in the wale direction
S_{CW}	In plane shear strength in the course direction
P_{max}	Maximum load values in the stress-strength curve
a	The crack length
w	Specimen width
t	Specimen thickness
$f_{(a/w)}$	Geometrical factor
K	Stress intensity factor
K_I	Mode I or opening mode stress intensity factor
K_{II}	Mode II or shearing mode stress intensity factor
K_C	Fracture toughness in terms of stress intensity factor
K_{IC}	Mode I fracture toughness in terms of stress intensity factor
K_{IIC}	Mode II fracture toughness in terms of stress intensity factor
FEA	Finite element analysis
SEM	Scanning electron microscope

CHAPTER ONE

Introduction

Introduction

Literature Review

Scope of Thesis

Outline of Thesis

Sponsorship & Material Supply

1.1. Introduction

New discoveries and improvements in materials science played an important role in the development of technology. Nowadays, composite materials have a very important place in the materials science that was separated into many branches. The importance of composite materials in the areas of textile, construction, automotive and aeronautic has increased day by day and reached even more usage areas with the developing technology. In the modern World, composite materials can be found in almost every field. For example, a piece of paper that we use for writing can be made from a composite material.

Composite material is the combination of two or more materials which were combined in order to obtain superior properties in the macro scale. Components that form the structure are insoluble in each other. When looking at the internal structures, it is possible to see the components. Composites are the materials which are homogeneous in macro scale and heterogeneous in micro scale. Composite materials are better than metals in terms of many properties. The most important one of these properties is the low specific weight. They provide great advantages in light construction structures. Besides to that, another important feature of composites is to provide thermal, acoustic and electric insulation. In addition to all these features, it also has high strength, easy to take shape, chemical resistance, dampening vibration properties.

Like other materials, composite materials are separated into classes. The layered composite materials have the oldest and most common usage areas in this field. This continuous fiber reinforced composites are used extensively in the aerospace industry. In addition to being light, they are resistant against heat and humidity. In this type of composite, it is possible to produce the material with required strength. Laminated composites consist of load-bearing fibers and the matrix material that holding fibers together. Composite reinforcement elements that provide mechanical strength are fiber, woven fabrics, knit fabrics and similar materials.

In recent years, knit fabric reinforcement has increased in the composite industry. In terms of rigidity and strength, knitted fabric reinforced composite gives slightly lower results than the woven fabric reinforced composite and higher results than the non-woven reinforced composites. Also knitted fabrics are better than others in terms of production costs and styling. Because, the distribution of fibers during the knitting process can be determined by the knitting structure, the stiffness and strength performance of the knitted fabric reinforced composite is lower than the plane fabric reinforced composites.

Composite materials, which are used as structural members, are subjected to damage in several ways during production, installation and usage. This damages cause the structure to deteriorate over time under environmental impacts and loads. One of these damages is crack formation and fracture occurring due to crack propagation. Fracture, which is a dangerous situation for composite structure, may cause damage resulting in loss of life and property. Fracture is called the separation of two or more pieces of solids under the action of stress. Engineering materials, even though in micro scale, contain cracks or discontinuities zone resulting from production, installation or usage. These cracks, under different loading conditions, proceeds or form cracks in a larger size by combining with other cracks. The mechanical structures may be exposed to damage in a gradual manner by time, which are resulting in fracture. In terms of security, it is necessary to examine the critical crack size, the state of the cracks and the crack propagation mechanisms. To improve safety level in the structures, strength value of materials for crack propagation, which is named fracture toughness, must be known.

Composite materials are special materials that provide certain advantages in every aspect of our lives. Today, extensive facilities of raw material supply and combining methods make it possible to a number of combinations that provide maximum benefit to the user. The disadvantage is that they are more expensive than non-composite material. However, it can be seen as economic solution according to its usage areas and providing solutions to the problems such as strength, heat resistance etc. This issue is the driving force which open wider and new application areas for the day and future composites.

Glass fibers are the most used materials in the production of composites. They hold an important place in the composite production for their suitable mechanical properties and cheapness. However, the carbon fiber is one of the most widely used because of its properties such as, lightness, high modulus of elasticity and tensile strength. In particular, to accommodate needs of the aerospace industry the required strength and mechanical properties are available in carbon fiber. Besides the disadvantage of the low compressive strength and being expensive they have properties such as high tensile strength, low weight, high thermal conductivity and low thermal expansion coefficient.

Because of their high resistance to external influences, the petroleum-based synthetic fibers have extensively used in manufacturing of polymer matrix composites. In recent years, researchers have investigated the usability glass and carbon fibers as reinforcing elements and have made many efforts to increase their performance.

1.2. Literature Review

Polymer matrix composites reinforced with petroleum-based synthetic fibers are widely used in the engineering application area, because their resistance to impact and external influences. In recent years, the researchers have investigated the availability of glass and carbon fibers as reinforcing material and they have made many efforts to increase their performance. Some of the most important of these are given below.

Vieille and coworkers [1] have manufactured thermoplastic laminated composites by using woven carbon fabric reinforcement element. They have used polyetheretherketone (PEEK) and polyphenylene sulfide (PPS) as matrix elements. Then, the thermoplastic laminated composite samples were exposed to low velocity impact. By examining the results of experiments, the low speed impact resistance of carbon/PEEK composites with PEEK matrix material was found as the highest. Dai and Mishnaevsky [2] have investigated the fatigue life of the hybrid composites reinforced with the glass and carbon fibers using three-dimensional finite element model. The analysis results showed that the carbon fibers have the highest resistance under tensile loads. Dong and Davies [3] have studied the mechanical

properties of the hybrid composites reinforced with the glass and carbon fibers. It was observed that increase in hybrid ratio was enhanced the bending and tensile strength and also the increase in number of carbon layers in the hybrid structure had improved the tensile strength in the same proportion. The maximum tensile strength was achieved in composite sample composed of seven carbon layers and one glass layer.

Maples and coworkers [4] have manufactured three different laminated composites using carbon fibers and polystyrene matrix. They have investigated the mechanical properties of these composites at different temperatures. The results showed that the cracks were occured on the polystyrene layer after loading, however, it was not observed on the carbon fiber. In another study which is about hybrid composites using carbon fibers, Boroujeni and coworkers [5] have created a hybrid composite using carbon nanotubes and carbon fibers together. The produced composite samples were subjected to tensile test. They found that the ratio of carbon nanotube in the matrix material is useful up to a certain level. Pérez and his colleagues [6] have attempted to estimate the impact damage on the carbon fiber reinforced laminated composites using matrix-reinforced mixing theory. For this purpose, they have modelled the carbon fiber reinforced laminated composite samples and have exposed them to the impact loading and have calculated the impact damage using finite element method.

Elanchezhian and coworkers [7] have also studied the mechanical properties of glass and carbon fibers reinforced composites at different temperatures. According to the tensile test results, the strength of the carbon fiber reinforced composite was highest at 35°C, it was observed that the strength slightly decreases with the increasing temperature to the 70°C. However, there was a very significant drop in the strength of the glass fiber reinforcement composites when the temperature increased up to 70°C. Based on the results of the impact test, it was found that impact resistance of carbon fiber reinforced composite was better than the glass reinforced composites. In the study [8] that was conducted by Ocholo and his colleagues, the mechanical properties of glass fiber and carbon fiber reinforced composites under different stretching ratios were investigated. They have compared the results of different compression tests which were applied to glass fiber and carbon fiber reinforced

composites. As a result, the glass fiber reinforced composites have damaged further than the carbon fiber reinforced composites. Tehrani and coworkers [9] have investigated the mechanical properties and impact damage on the woven carbon fiber reinforced composites based on carbon nanotube and epoxy matrix. Experiments have shown that the mechanical properties obtained from nanocarbon reinforced composites have higher than the carbon fiber reinforced composites.

Qi and his colleagues [10] have studied the tensile strengths of the composites, which were composed of three, four, and five layers of fibers sewn with weft connections throughout their thickness, experimentally. The experimental test results showed that the three layered composites have the highest tensile strength, whereas the minimum tensile strength was found in the four layered composites. Leong et al. [11] have created the composite structures using a mixture of glass fiber based milano-rib knit with an epoxy matrix in different layers to investigate the mechanical properties of composite structures. As a result of experiments, the twelve-layered composites were showed better tensile and compression resistance than the six-layered composites. Sugie et al. [12] have investigated the impact behaviour of the hybrid composite materials created by sewing glass and carbon fabrics as a reinforcing element. According to the test results, the best impact strength were obtained from the hybrid composites with 0° carbon and 90° glass fiber orientations.

Solaimurugan and Velmurugan [13] have investigated the interlaminar fracture toughness of glass fiber reinforced composites in the case of mode I loading. As a result of the experiments, the composite with 45/-45 fiber orientations have observed more resistant than the others. In another important study, Aktas and colleagues [14] have examined impact and post-impact resistance of knitting glass fiber-reinforced composites with epoxy matrix. As a result of the conducted experiments, they have observed that the maximum contact force was occurred in the rib knitting-reinforced composites whereas the minimum contact force was observed in flat knitting reinforced composites. Pandita and Verpoest [15] have investigated the tension-tension fatigue behaviour of knit and woven glass fibers reinforced composites before and after tensile loading. Experimental study is supported by finite

element analysis and Scanning Electron Microscope (SEM). The results showed that the fatigue life of unloading composites higher than the loading composites.

Ma and his colleagues [16] have formed glass fiber and carbon nanotubes reinforced laminated composites. Created composites are in the form of $(90°/0°)_2$/nanotube/$(0°/90°)_2$. Then the layers were interconnected through thickness by sewn. The impact resistance of composites was increased by increasing nanotubes percentage. Consequently, it was also observed that increasing in the impact energy increases the damage area. Yang and colleagues [17] have studied the bending, compression and shear behavior of woven glass fiber reinforced composites. Consequently, the woven glass fiber reinforced composites were exhibited low bending strength. Kim and coworkers [18] have studied the interlaminar fracture behaviour of knitting glass fabric reinforced composites in the case of mode I loading. They have used 1x1 rib milano and interlock as knitting varieties. Fracture surfaces were examined using SEM. Finally, they have observed the highest fracture toughness in the milano knitting-reinforced composites. They have stated that increasing in the tightness of knitting structure increases the fracture toughness of composites. Ramesh and colleagues [19] have produced three different fiber reinforced polyester composites including glass-jute, sisal-glass and jute-sisal-glass and these composites were subjected to mechanical tests. The experimental results showed that the jute-sisal-glass fiber reinforced polyester composites have the best compression and bending strength and glass-jute fiber reinforced polyester composites have the best tensile strength and sisal-glass fiber reinforced polyester composites have the best impact strength.

Arthanarieswaran and colleagues [20] have studied the mechanical properties of hybrid and non-hybrid composites reinforced with glass, bananas and sisal fibers. Test results have been found that the reinforcing glass using natural fibers improves bending, tensile and impact strength. Zhang et al. [21] have investigated the tensile and interfacial strength of linen and glass fiber reinforced hybrid composites. After the experimental samples have been investigated using Scanning Electron Microscope (SEM), they have concluded that the increase in glass density in the hybrid composites was increased the tensile strength. Besides, it was stated that, the stacking sequences of the layers have an

effect on the tensile strength of the composites. Stamenkovic [22] has studied the toughness and the crack propagation of isotropic and orthotropic materials using J-integral method by ANSYS program. The fracture toughness values of the two orbits around the crack tip of isotropic and orthotropic materials were calculated and the fracture toughness values of these two materials were compared to each other. In another recently studied research is conducted in Singapore, Rashedi and his colleagues [23] have proposed a mixed-mode fracture criterion for glass fiber reinforced composite laminates under biaxial loading, numerically and experimentally. The characterization tests were successively performed on uniaxial and cruciform composite specimens to determine the equivalent loaded area, the notch sensitivity behavior and critical fracture toughness properties of cross-ply GFRP laminates. According to the obtained results from this study, a mixed-mode fracture criterion based on the findings from biaxial experimental loading was proposed for cross-ply laminated composites.

Gliesche and colleagues [24] have studied in-plane shear properties of the carbon/epoxy composites, which have 0°/90° textile reinforcing structure with different layer thicknesses, were determined under ±45° tensile loading. Surface deformation of the samples was measured using a whole-field optical method during the tensile loading. As a result, shear strength has been found to be affected by the layer thickness and/or the weight of each reinforcement unit. Optical analysis of surface deformation of the samples has showed the equivalent strain distribution as expected. Besides to that, large deviations were obtained from the calculated average strain values. Elarabi [25] has examined the orientation effects of the carbon/epoxy composites subjected to transverse (BWK) tensile loading. He has also investigated the axial tensile strength of biaxially warp knitted fabrics and unidirectional fibers reinforced carbon/epoxy composites. The values of tensile load and strain percentage of the composites were increased with the increasing BWK ratio. Also, increase in the composite modules was observed with the amount of epoxy. Although, the strain and tensile load were decreased for unidirectional composites, they were increased for BWK composites.

Zhang and Mason [26] have investigated the effects of environmental condition on the mechanical properties of carbon fiber reinforced epoxy composites. In this study, the tap

water, seawater, acid, alkali and organic solvents were used as contaminants and the samples were contaminated before and after curing. Consequently, it was revealed that the contamination disrupt the epoxy matrix. It was also observed that the tap water and seawater conditions reduce the tensile strength and modulus of elasticity. Reis and his colleagues [27] have investigated the effects of delamination on the mechanical behavior of carbon/epoxy composites. In this study, carbon/epoxy composite specimens were produced by vacuum molding method as dog bone shape using 12 balanced bidirectional carbon layers and epoxy resin. Static tests were conducted to examine the effects of the delamination size on the hardness of the layer and strength of specimens. Fatigue tests were also performed in load control for R=0.05 and R=-1 with a loading frequency of 10 Hz at room temperature. The delaminations have an insignificant influence on the fatigue strength for tensile cycle loadings, but produce significant decreases in the strength for R=-1 fatigue loadings.

Suresha and coworkers [28] have investigated the effects of the normal and shear loads rate on the unidirectionally oriented carbon fiber reinforced epoxy composites in the case of friction and dry sliding wear using block-on-roller test. The dry sliding wear was conducted to parallel and anti-parallel surfaces of composite specimens with 0°/90° orientation with respect to the sliding direction. The coefficient of friction and wear of the composites were determined for different loads and velocities. The results showed that the wear resistance was decreased by increasing in sliding velocity and loads. Yang and colleagues [29] have studied copper and carbon fiber knitted fabric reinforced composites (C/C-Cu) fabricated by pressureless infiltration technique. The scanning electron microscope, X-ray diffraction and energy dispersive spectroscopy were used to characterize the microstructure of the composite. The mechanical, electrical and tribological properties of the C/C–Cu composites were compared with the C/Cu contact strip. The C/C–Cu composites were exhibited a high bending strength, excellent impact strength and low electrical resistivity. It was also found that the C/C–Cu composites were exhibited greater wear resistance than the C/Cu contact strip.

Wonderly and his colleagues [30] have compared the mechanical properties of the knitted glass fiber/vinylester and knitted carbon fiber/vinylester composites fabricated using

vacuum infusion. The comparison of the strengths of the knitted glass and knitted carbon specimens in tension, compression, open hole tension, open hole compression, transverse tension, indentation and ballistic impact were done. It was proved that the mechanical properties of carbon fiber/vinylester composites were superior under tensile loading and indentation. The failure was in general more settled in the knitted carbon specimens and the strength in the knitted carbon specimens was more dispersed than in the knitted glass specimens. Deng and Ye [31] have investigated the effects of fiber-matrix adhesion on the mechanical properties of graphite/epoxy composites. It was clearly observed that the interlaminar shear strength and in-plane shear strength of the composites were increased with the improvement of fiber/matrix adhesion by fiber surface treatment. Shan et al. [32] have examined the static and dynamic strain of glass fiber reinforced non-hybrid and glass/carbon fiber reinforced hybrid composites in the aquatic environment. They have concluded that the fatigue life of glass and hybrid composites in the air was less than the fatigue life in water and hybrid composites. In addition, the hybrid structures were showed more resistance than glass composites in the aqueous environment.

Luo and Verpoest [33] have investigated the behavior of a rib and a milano weft knit reinforced composite materials under biaxial tension. Consequently, the ultimate deformation in both wale and course directions were determined at different displacement ratios. Khondker and colleagues [34] have studied the impact resistance and tolerance properties of Milano, 1×1 rib and plain knit fabric of glass fiber reinforced composites. The effect of weft knitted fabric style and knit structural parameters upon the impact and compression after impact properties of the weft-knitted composites was also examined. According to the results, both of the knit style and structural parameters were affected the damage resistance and tolerance of composites. In another study, the fracture strength properties of G550 sheet steel positioned transverse to the rolling direction were investigated by Rogers and Hancock [35]. The mode I fracture resistance of G550 sheet steels was measured in various different temperatures and a numerical study was performed by the authors to investigate the effect of cracks on the structural performance using FRANC2D finite element computer program.

Zappalorto and his colleagues [36] have investigated the effect of nanoclay percentage on the mechanical properties and fracture toughness of nanoclay reinforced composites in the case of mode I and mode II conditions. The toughening effect on the epoxy nanocomposites reinforced with thermally reduced graphene oxide, graphite nanoplatelets, and multiwall carbon nanotubes was examined by Chandrasekaran and his colleagues [37]. The filler dispersion state of the epoxy nanocomposites were observed using scanning electron microscopy According to the studies, a schematic explaining the crack propagation in the graphene/epoxy composites and the interaction of crack front with graphene particles was proposed.

As it can be seen from the above review of the literature, several different types of mechanical behavior of composite was examined. Especially, the number of the studies conducted with knitted reinforced composites is remarkably low. In the experimental study, the hybridization process of the fabric reinforced laminated composite was carried out by superimposition of fabrics with different material structure such as glass or carbon. The originality of this thesis is the formation of laminated hybrid structure from the glass and carbon fabrics and the knitting of the hybrid glass-carbon fabric.

1.3. Scope of Thesis

As it can be seen from the above literature review, the static and dynamic behaviour of the composites reinforced with glass and carbon fibers was investigated by various studies. The mechanical behaviour of the composites was also affected by the form of weaving, knitting, and particulate reinforcement elements. In this context, there have not been found any studies that are particularly working on the fracture toughness of hybrid or non-hybrid knitted carbon-glass fabric reinforced laminated composites. In this thesis, the mechanical properties (E_1, E_2, X_t, Y_t, X_c, Y_c, ν_{12}, G_{12} and S_{12}) and fracture behaviour of non-hybrid and hybrid laminated composites reinforced with 1x1 rib knitted glass and carbon fabrics were determined, experimentally. The fracture behaviour of the knitted non-hybrid and hybrid specimens was also examined by J-integral method with using ANSYS finite element software package.

1.4. Outline of Thesis

This thesis was arranged into eight chapters. In the introduction section, a literature survey has done and sponsors are mentioned. Chapter two includes issue of general information about composite materials, reinforcements and matrix resin systems. In chapter three, the linear elastic fracture mechanics and elastic-plastic fracture mechanics were elucidated. The production process of the composite materials was discussed in the chapter four. The mechanical properties and fracture toughness for non-hybrid and hybrid composites were given in chapter five. The finite element analysis for fracture toughness of non-hybrid and hybrid composites was given in chapter six. In chapter seven, the numerical and experimental results and recommendations for further research were discussed.

1.5. Sponsorship & Material Supply

This thesis was sponsored by The Scientific and Technological Research Council of Turkey (TUBITAK), (Project Number: 115M116).

The carbon and glass fibers were bought from DowAksa incorporated company (The Dow Chemical Company and Aksa Acrylic Chemical Industry Co.) and Pul-Tech FRP, respectively. Matrix materials included DTE 1000 epoxy and DTS 1100 hardener was provided by Duratek Limited Liability Company. Arcan test apparatus was built by Coskunlar Lathe companies. The fabrics which have been used as reinforcement elements had been constructed by me using V-bed semi-automatic knitting machine in Varol Textile. The mechanical properties and fracture toughness specimens were cut with CNC router machine in the mechanical Laboratory at Mechanical Engineering Department of Usak University.

CHAPTER TWO

General Information about Composite materials

Introduction to Composite Materials

Advantages and Disadvantages of Composite Materials

Reinforcement Elements

Resin Systems

2.1. Introduction to Composite Materials

Since the second half of the twentieth century, rapid rise in technology has provided to the development of materials and material science. Scientists working on materials science have begun seeking more different materials due to the limited capacity of the materials found in nature and the inability to respond to the current needs with the existing materials. Thus, materials with superior properties are produced by bringing materials having high properties together in different combinations and macro-structure. As a result of this situation, the importance of composite materials that are consisting of a combination of materials with outstanding engineering properties has increased. Recent technology requires the properties which metal, ceramic and polymer materials cannot provide. For example, high impact and abrasion resistance, high strength and rigidity, light weight, and resistant to corrosion, are being studied in the aerospace industry.

Although when a composite material used for the first time is unknown, it is the scientific reality that composite materials are found in historical artifacts. From the earliest times, fragility feature is trying to resolve by adding vegetal or animal fibers into the brittle material. The best example for this material is adobe. In the adobe production, the embedded straw, ivy branches, herbal stalks and fibers improve strength in the use and the production of the materials. For instance, Israeli was used straw to increase the strength of mud bricks. In the ruins of ancient Egyptian period, the plywood was extensively used for their strength properties, resistance to thermal expansion and ability to absorb moisture. Although the composite materials prepared by conventional methods used in the historical process, the emergence of composite materials as an engineering issues was in the beginning of the 1940's. This means the production of completely artificial material using scientific data and technological opportunities. Figure 2.1 shows the development in each material group between 10000BC and 2020.

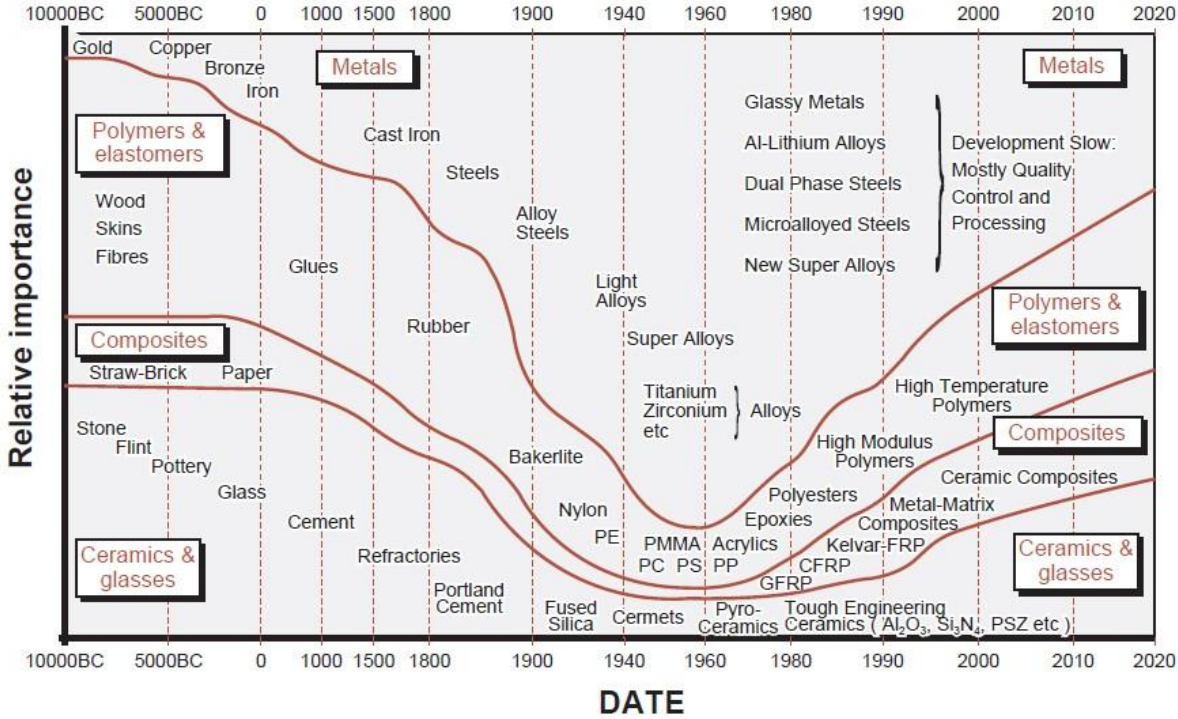

Figure 2.1 The evolution of engineering materials with time [38]

There are many different kinds of materials in our World with rapid technological developments. Each material was highlighted with its specific properties (strength, lightness, strength, manufacture etc.). Composite materials can be found at the center of all kinds of those materials and their importance is increasing day by day. The significance of the composite materials and their place in the engineering materials are shown in Figure 2.2.

A composite material is formed with a combination of two or more materials on the macro scale. This combination consists of reinforcing elements providing strength and load-carrying capability (fibers, particles, etc.) and matrix material that holds reinforcement elements together. The compatibility of these two materials in a composite material determines the resistance. Therefore, reinforcement elements and the matrix material must be appropriately matched to each other when producing a composite material.

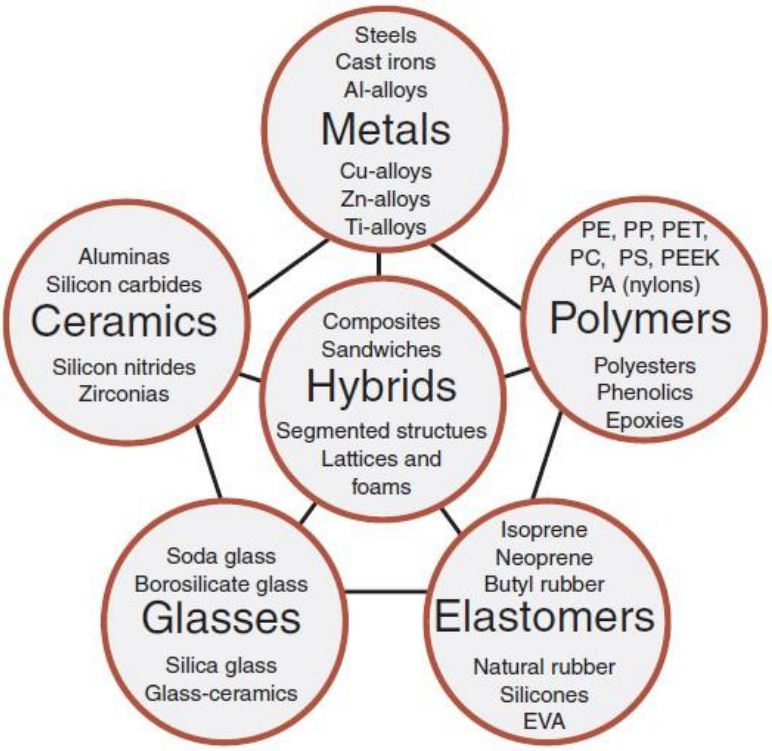

Figure 2.2 The schematic illustration of engineering materials. The basic families of metals, ceramics, glasses, polymers, and elastomers can be combined in various geometries to create hybrids [38]

There are different matrix materials and the composite materials can be classified according to its matrix material such as polymer, metal, carbon, ceramic or cement (e.g., Portland cement). The shape of the filler is another important parameter which can be used for classification of the composite materials. For instance, a composite with particles as the filler is called a particulate composite and concrete can be shown as an example for this type of composite. The concrete composed of cement as the matrix material. Also stones and sands are consisted in concrete as two types of particles together. Fibrous composite is a composite with fibers which are used as filler. Laminate flooring fabrication is done by combining layers of polymer, paper and fiberboard together and this can be shown as an example for the components took the form of the layers in the composite material [39].

2.2. Advantages and Disadvantages of Composites Materials

2.2.1. Advantages of Composites

The composite materials are used in marine, automotive and sports equipment etc. And also these materials are mostly used in aerospace industry. There are so many reasons for choosing this material to use and summary of the advantages of them are described below.

Their advantages include high resistance to fatigue and corrosion degradation. And these features give users opportunity to provide safety in aerospace industry. Also, the composite materials have high 'strength or stiffness to weight' ratio, the light construction can be easily produced by using these materials. Due to composites have greater reliability; there are fewer inspections and structural repairs. To meet the design requirements, composite materials have directional tailoring capabilities. The fiber pattern can be laid in a manner that will tailor the structure to efficiently sustain the applied loads [40]. The usage in automotive industry is mainly because of the improved dent resistance of the material which is normally achieved. Composite panels that are prepared for this industry do not sustain damage as easily as thin gage sheet metals [41]. Another important feature of the composite materials is to be used in aerospace industry, achieving smooth aerodynamic profiles with great drag reduction. Because, manufacturing the complex double-curvature parts with a smooth surface is difficult with other materials, it is possible with composites which can be made in one manufacturing operation [42]. Reduction in overall part count, manufacturing and assembly costs is feasible with composite materials due to their improved torsional stiffness which implies high whirling speeds, reduced number of intermediate bearings and supporting structural elements. As might be expected from the high strength of composites, these materials have high resistance to impact damage [43]. According to their excellent heat sink properties which can be combined with their lightweight, particularly for carbon-carbon composite materials they have extended usage for aircraft brakes [44].

2.2.2. Disadvantages of Composites

Advanced composites have really impressive advantages as described above however, those may have some disadvantages according to their costs, attachment properties or may have some repair properties etc., and you can find the main disadvantages that are defined simply and clearly as below:

- High cost of raw materials and fabrication.
- More brittle than metals, hence, it can be easily damaged.
- Transverse properties may be weak.
- Matrix is weak, therefore, low toughness.
- Reuse and disposal may be difficult.
- Difficult to attach.
- Repair introduces new problems, for the following reasons:
    - Materials require refrigerated transport and storage and have limited shelf life.
    - Hot curing is necessary in many cases.
    - Hot or cold curing takes time.
    - Matrix is subject to environmental degradation [45].

Nevertheless, many of those disadvantages can be circumvented with proper design and material selection. Nowadays, so many types of reinforcing fibers and matrices are defined to be used in composite production and those components of the composites can be combined differently and provide wide range of exceptional properties to the product [46]. Because of these future composites are really innovative materials that might be more frequently used in the near future [47]. Composite materials are capable of providing structural efficiency at lower weights as compared to equivalent metallic structures, so they are preferred in especially aircraft industry, such as floor beams, engine cowlings, flight control surfaces, landing gear doors, wing-to-body fairings, etc. [48]. They provide appropriate usage not only for industries but also for civil infrastructures. The earthquake proof highway supports, power generating wind mills, long span bridges are some examples of them [49].

2.2.3. Comparison with Metals

Requirements which are governing the choice of materials apply to both metals and reinforced plastics. To decide which one is the proper for the required area, there is need to compare main characteristics of them. Some of the comparisons are listed above.

- As we said before, composites offer significant weight saving over existing metals. Thanks to the lower density of the composites, those can provide structures that are 25-45% lighter than the conventional aluminum structures designed to meet the same functional requirements [50]. Depending on material form, composite densities range from 49606 to 71654 kg/m^3 as compared to 110236 kg/m^3 for aluminum [51].
- Unidirectional fiber composites have specific tensile strength and this specific strength is about 4 to 6 times greater than that of steel and aluminum.
- Unidirectional composites have specific modulus about 3 to 5 times greater than that of steel and aluminum.
- Fatigue endurance limit of composites may approach 60% of their ultimate tensile strength. This value is considerably lower for steel and aluminum [52].
- Particularly for aero-elastic loading on the wings and the vertical and horizontal stabilizers of aircraft, the fiber reinforced composites are more versatile than the metals [53].
- Since they are less noisy and provide lower vibration transmission than metals, the fiber reinforced composites can be designed with excellent structural damping features [54].
- High corrosion resistance of fiber composites contributes to reduce cost of the life cycle [55].
- Although, the composites offer lower manufacturing cost by reducing significantly number of detailed parts, the expensive technical joints are needed to form large metal structural components.
- When compared with metals, long term service experience of composite materials is limited [56].

2.3. Reinforcement Elements

Particles, whiskers or fibers can be used as reinforcement for composite materials. As providing reduction in the cost of the material, particles are frequently used as fillers. However, they have no desired orientation and contribute minimal improvements in mechanical properties.

Whiskers can be classified as a particle reinforcement element, they are characterized with their extremely single strong crystal structures, but those single crystals aren't dispersed uniformly in the matrix. When compared with fibers, particle reinforcement elements are small in terms of length and diameter. Fibers have a long axis compared to those elements. They are significantly resistant in the longitudinal direction since; they are normally produced by either drawing or pulling during the manufacturing process (Figure 2.3). Orientation process of the molecules in fibers is provided by drawing. Usage of the fibers as reinforcement element for advanced composites is predominant based on their strength and stiffness. According to their application and manufacturing process, fibers are classified as continuous or discontinuous [57].

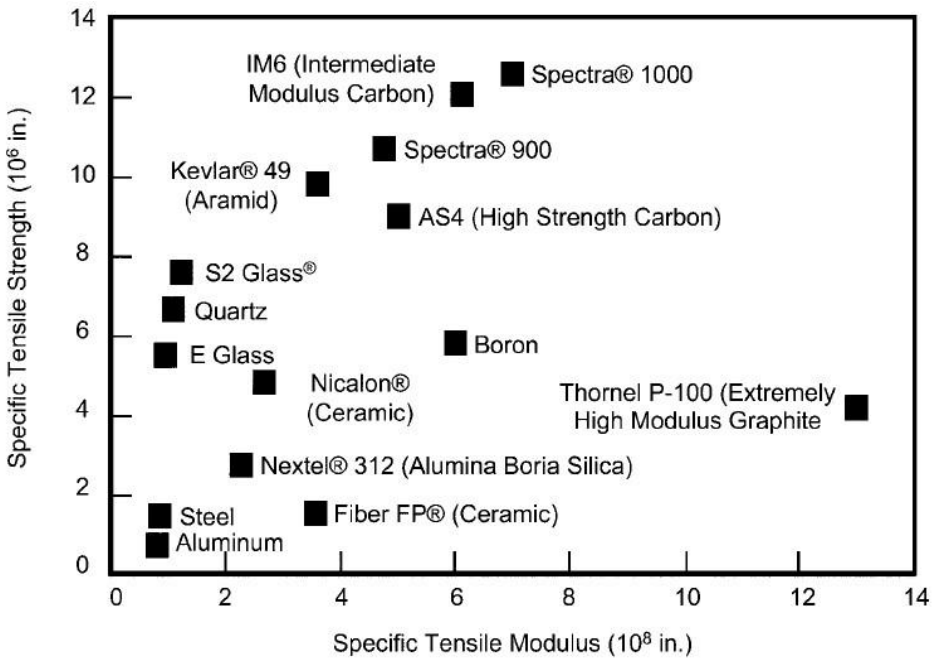

Figure 2.3 Specific strength and modulus of some commercially important fibers [58]

2.3.1. Glass Fibers

Glass fibers have perfect features, which gained them low cost, high tensile strength, high impact resistance, and good chemical resistance to use comprehensively in commercial composite applications. However, different from carbon fibers, which are used in high-performance composite applications, glass fibers have a relatively low modulus and inferior fatigue properties.

Although there are various types of glass fibers, only three types are most commonly used as E-glass, S-2 glass, and quartz (Figure 2.4). E-glass can be said as the most common used one and least expensive and it provides a good combination of tensile strength 3.5 GPa and modulus 70 GPa. With a tensile strength of 4.5 GPa and a modulus of 87 GPa, S-glass is stronger than E-glass in the rate of 40% at high temperatures, it retains a major percentage of its strength. However, when we compared those types according to their costs, S-glass is more expensive than E-glass type. Quartz fiber is another most commonly used glass fiber, which is also quite expensive ultrapure silica glass and used in demanding electrical applications with priority because it is a low dielectric fiber [59].

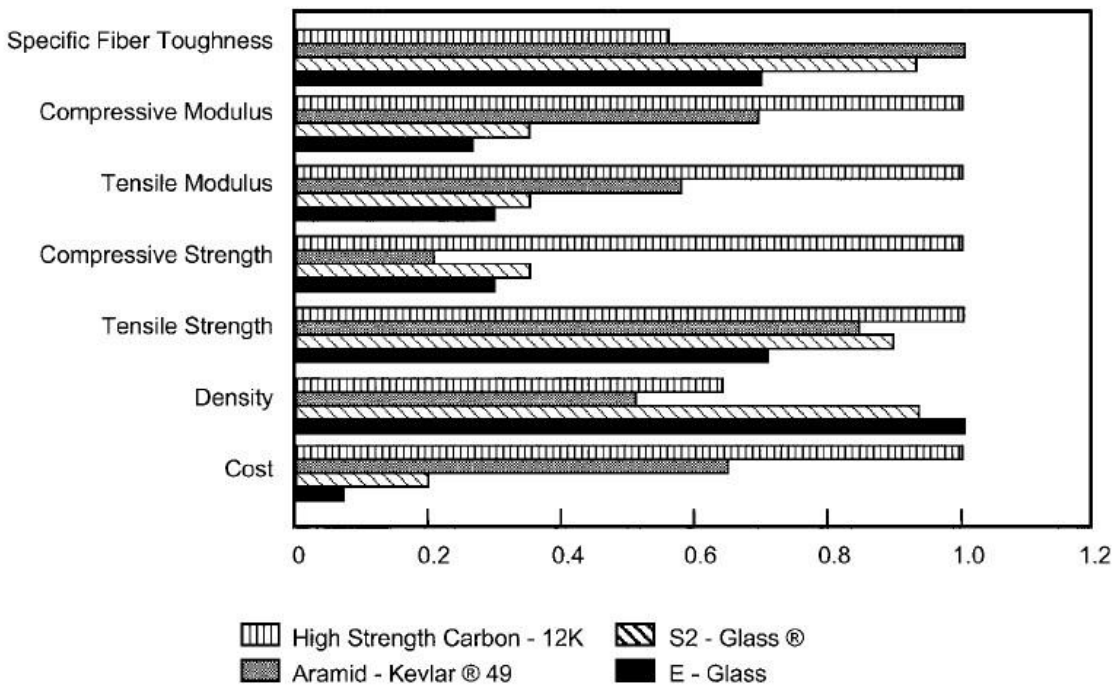

Figure 2.4 Relative fiber cost and performance of some high-strength fibers [58]

Glass fibers are produced by milling and chopping methods. In the production process of the milled fibers, they are milled using a hammer mill and this technic comes up with result of relatively broad length distribution. The diameter is directly related with the filament diameter which becomes in milling process. To produce the chopped fibers, a bundle of glass filaments is chopped into a precise length. According to the length of chopped fibers, their length is majorly larger than the milled fibers. In either case which comes up with those production methods, fibers may or may not contain sizing or surface modification. If sizing is applied, it means that, it is optimized for a certain types of polymers.

Owen Corning milled fibers are produced with a variety of size coatings for different polymers. Recommendation of the different types of milled fibers can be changed according to their characteristic features such as, cationic sized milled fiber is recommended for polyester epoxy, phenolic and thermoplastics. Owen Corning milled fibers are produced with a variety of size coatings for different polymers. Recommendation of the different types of milled fibers can be changed according to their characteristic features such as, cationic sized milled fiber is recommended for polyester epoxy, phenolic and thermoplastics. The glass fibers are extensively used in the industry, according to their reinforcing effect and the improvements in thermal conditions. This preferential usage is due to some features of the glass fibers, for instance, reducing in thermal expansion and also increasing in heat deflection temperature. The incorporation process, which is the most important tasks of fiber application to prevent breakage, to improve matrix fiber adhesion, to prevent fiber corrosion in some environments, and to develop proper fiber orientation, must be designed [60].

2.3.2. Carbon Fibers

According to studies that are conducted to develop features of the carbon fibers, especially for the last 50 years, it can be seen that carbon fibers have been under continuous development. There is an obvious progression of feed stocks of carbon fibers, which is starting with rayon, proceeding to polyacrylonitrile (PAN), on to isotropic and mesophase pitches, to hydrocarbon gases, to ablated graphite and finally back to carbon containing gases. The most commercial production of carbon fibers is PAN-based fiber production,

because of the well development of this production technology. Pitch-based fibers meet the needs of niche markets and with its comparatively low prices; it takes place in mass markets. When looked at the carbon nanotubes, which are though as full of promise for the future, Vapour-grown fibers are the most popular nanotube technology material and entering commercial production.

When comparing the strength and modulus of the PAN with mesophase pitch and isotropic pitch (Figure 2.5). The modest level of strength and modulus belong to the fibers made from isotropic pitch and also it can be called as 'General purpose' fibers. However, they are the least expensive pitch-based fiber, and they are useful according to their enhancing modulus and also conductivity in many applications. The strongest available fibers between those types are thought to be PAN-based fibers, but, studies are showed that, its strength decreased, when they are heat treated to increase modulus. Another type of mesophase pitch fibers might be heat treated to very high modulus values, which is found to be approaching the in-plane modulus of graphite at 1TPa. As can be seen in Figure 2.6 which shows compressive properties of carbon fibers, the Achilles heel of mesophase pitch-based fibers in composite applications is low compressive strength. Also electrical and thermal conductivity are important in many applications with carbon fibers, in Figure 2.7 and 2.8 these features are demonstrated respectively. Mesophase pitch fibers have the highest conductivity and lowest resistivity [58].

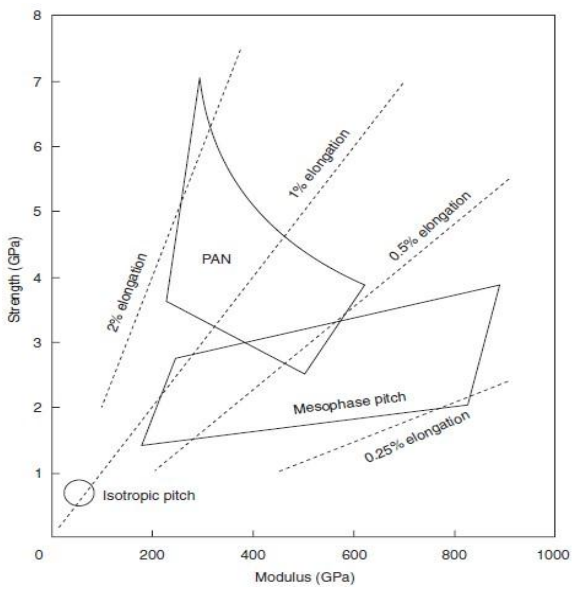

Figure 2.5 Tensile properties of carbon fibers [58]

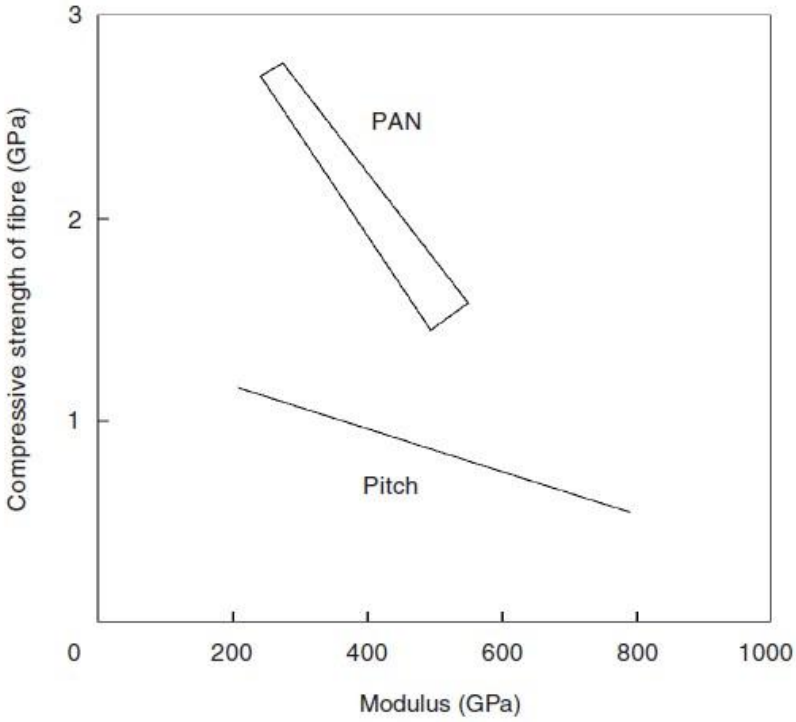

Figure 2.6 Compressive properties of carbon fibers [58]

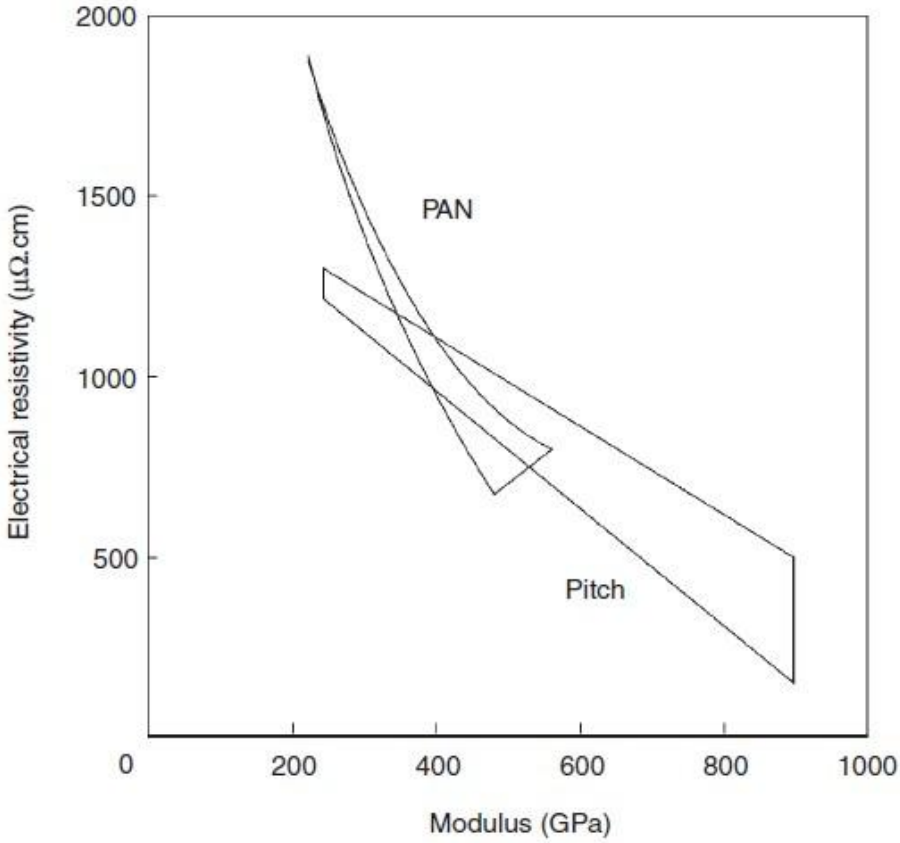

Figure 2.7 Electrical resistivity of carbon fibers [58]

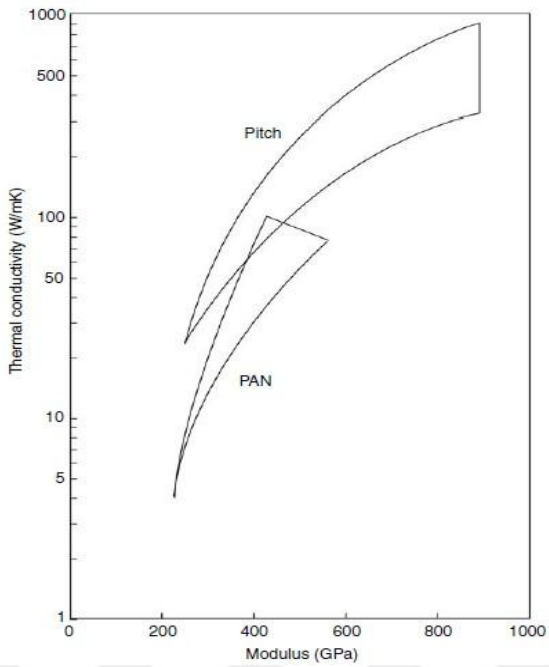

Figure 2.8 Thermal conductivity of carbon fibers [58]

2.3.2.1. Production of Carbon Fibers

Carbon fiber is currently produced in relatively limited quantities and mostly two manufacturing processes are used as: based on pitch (coal tar and petroleum products), and Polyacrylonitrile (PAN) (Figure 2.9). Current global capacity for pitch-based carbon fiber is estimated at about 3500 metric tons per year. Global use for PAN-based carbon fiber increases rapidly however, total production capacity should be increased because; its production capacity does not currently meet the demand. PAN-based carbon fiber is more expensive to produce, hence, limiting its use to high end applications [61].

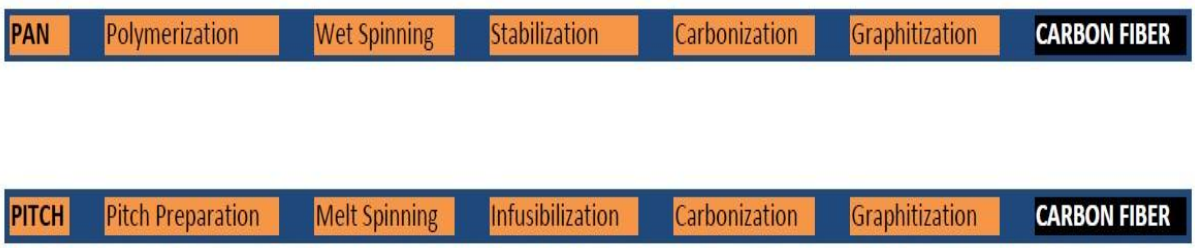

Figure 2.9 PAN and PITCH based carbon fibers [62]

2.3.3. Textile Reinforcements

According to the studies about textile reinforcements, it can be said that various types of textile structures are popular in these studies because those structures are unique based on their combination of light weight and flexibility and their ability to offer a combination of strength and toughness. Also textile structures have been recognized as an attractive reinforcement form for applications ranging from aircraft wings produced by Boeing Aircraft Co. in the 1920s to carbon–carbon nose cones produced by General Electric in the 1950s. With textile usage as reinforcement in composite material production, various fibrous assemblies can be performed with prearranged fiber orientation pre shaped and often pre impregnated with matrix. The microstructural of fibers within a preform, or fiber architecture, specifies the pore geometry, pore distribution and tortuosity of the fiber paths within a composite. Textile preforms translate fiber properties to composite performance and also influence the ease or difficulty in matrix infiltration and consolidation. In addition to that those preforms are the structural backbone for the toughening and net shape manufacturing of composites. The design options for strong and tough structural composites are expanded with the creative use of fiber architecture which is formed from matrices and properly tailored fiber/matrix interfaces with combination of high-performance fibers [63]. You can see some major examples (Figure 2.10) and comparison of the textile reinforcement elements (Table 2.1).

Table 2.1 A comparison of the textile reinforcement elements [64]

Yarn to fabric processes	Basic direction of yarn introduction	Basic formation technique
Weaving	Two (0°/90°)	Interlacing (by selective warp and fill insertion of 90° yarns into 0° yarn system
Braiding	One (machine direction)	Intertwining (position displacement)
Knitting	One (0° or 90°)	Interloping (by drawing warp or fill loops of yarns over previous loops)
Nonwoven	Three or more (orthogonal)	Mutual fiber placement

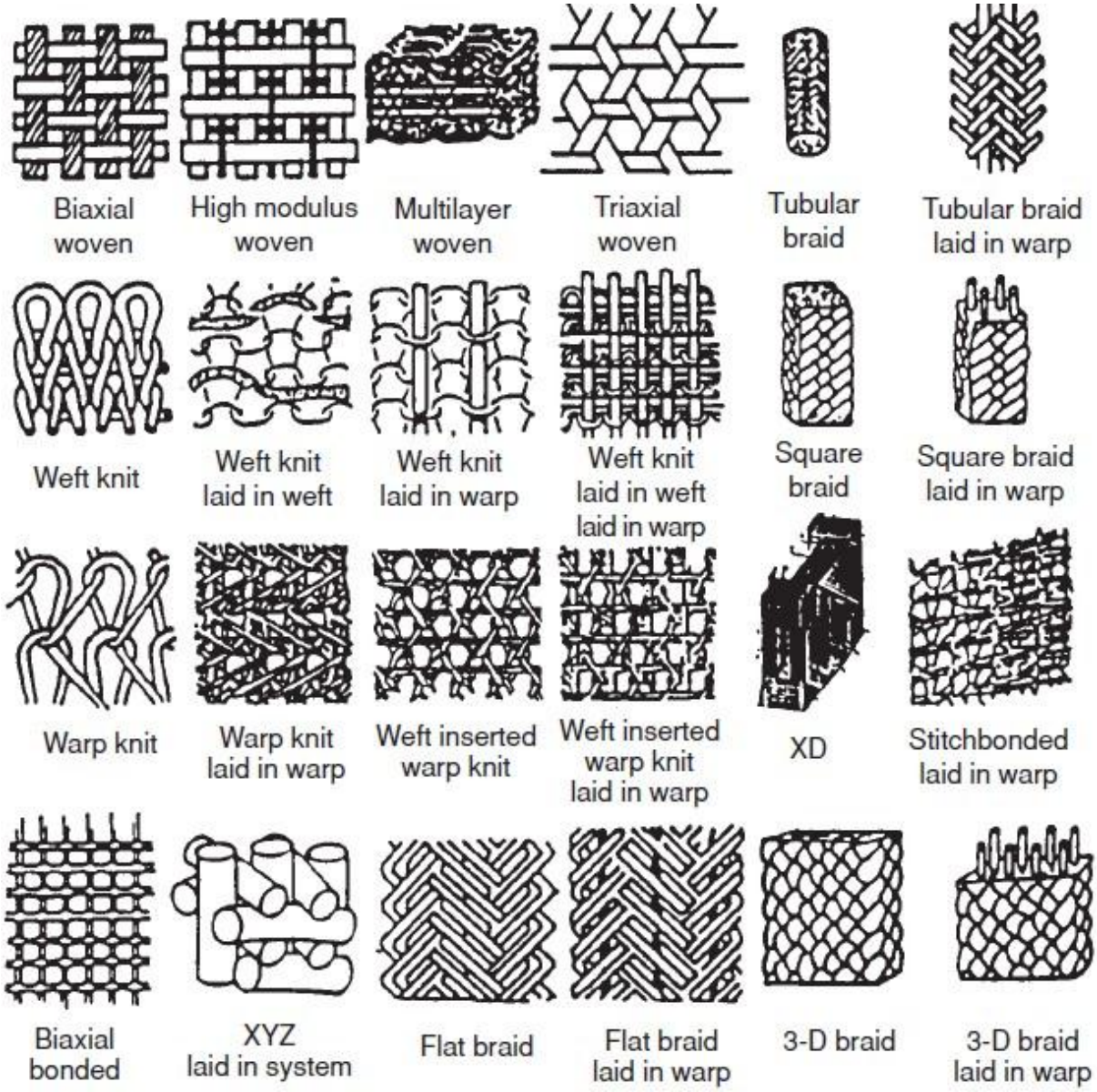

Figure 2.10 Examples of yarn-to-fabric preforms [65]

2.4. Resin Systems

The role of the matrix is binding the fibers together in an orderly array and protecting them from the environment. By transferring loads to the fibers, the matrix is critical in compression loading in preventing premature failure due to fiber micro buckling. Also it was proved with many studies that, the matrix provides the composite with toughness, damage tolerance, and impact and abrasion resistance. In addition to those properties that are provided to composite material by matrix, the maximum usage temperature, resistance to

moisture and fluids, and thermal and oxidative stability can be determined with the properties of the matrix [57].

Polymeric matrices for advanced composites are classified as either thermosets or thermoplastics. Thermosets are known as low molecular weight, low viscosity monomers (≈2000 centipoise) and during curing they are converted into three-dimensional cross-linked structures which are infusible and insoluble. As illustrated in Figure 2.11, crosslinking is resulted from chemical reactions that are driven by heat generated either by the chemical reactions themselves for instance, exothermic heat of reaction, or by externally supplied heat. As curing progresses, the reactions accelerate and the available volume within the molecular arrangement decreases, which results in less mobility of the molecules and cause increase in viscosity. Because this process is depended on chemical reactions, after the resin gels and forms a rubbery solid, it cannot be re-melted. Besides to that, further heating causes additional crosslinking until the resin is fully cured. This progression through cure can be seen in Figure 2.12. Thermosets are characterized as having rather long processing times and this is because of the event which is a thermally driven and requires chemical reactions. In contrast to thermosets, thermoplastics are not chemically cross-linked with heat and by this way, they do not require long cure cycles. Thermoplastics are high molecular weight polymers that can be melted, consolidated, and then cooled. The feature of the thermoplastics, which they do not crosslink, can be used for forming or joining operations, but, due to their inherently high viscosity and high melting points, high temperatures and pressures are normally required for processing [59].

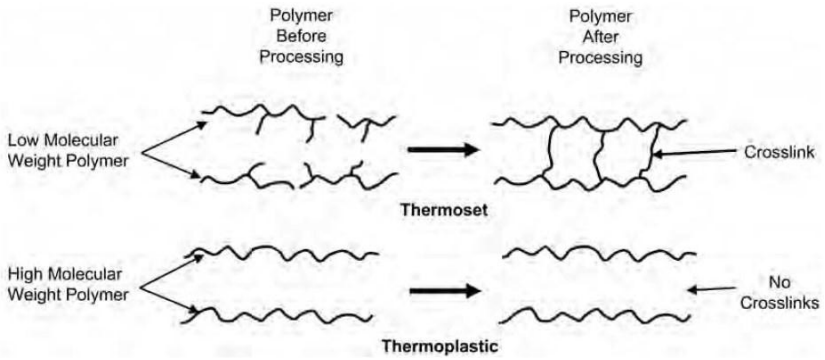

Figure 2.11 Comparison of thermoset and thermoplastic polymer structures [57]

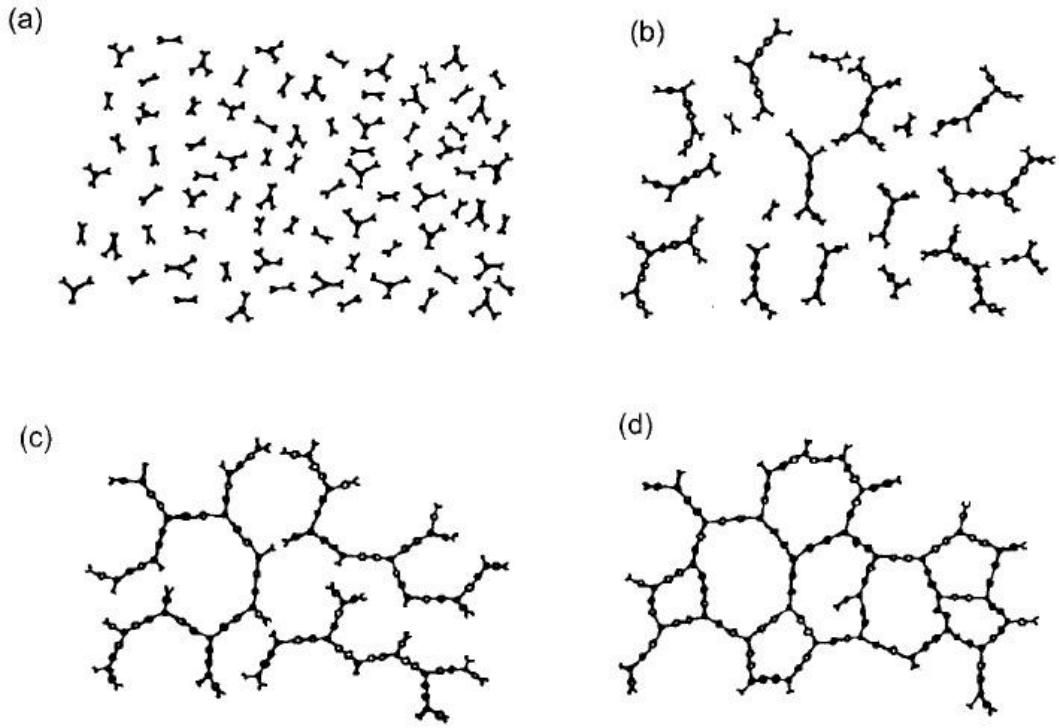

Figure 2.12 Stages of cure for thermoset resin. (a) Polymer and curing agent prior to reaction. (b) Curing initiated with size of molecules increasing. (c) Gelation with full network formed. (d) Full cured and cross-linked [66]

2.4.1. Thermosets

In order to use in low and moderate temperatures (up to 275 °F or 135 °C), epoxies are currently most used resins. The temperature range of Bismaleimides usage is between 275–350 °F (135–175 °C). For very-high temperature applications (up to 550–600 °F or 290–315 °C), polyamides are the material that is most preferred. Due to their lower mechanical properties and also poorer environmental resistance in some cases, polyesters and vinyl esters are infrequently used for high-performance composite matrices. Nevertheless, they can be used approximately at the same temperatures as epoxies, are used extensively for commercial applications. There is a new class of resins, which is designed to compete with both epoxies and bismaleimides. This class is called cyanate esters which offer some advantages in lower moisture absorption and have attractive electrical properties, however, in contrast to other resins, its cost is significantly higher than others. Phenolics are high temperature systems that provide outstanding smoke and fire resistance and they are frequently used for aircraft interior components. Besides to that, thanks to their high char

yield, they can be used as ablators and as precursors for carbon-carbon (C-C) components. All of the polyesters, epoxies, bismaleimides, and cyanate esters are classified as additional curing polymers, however, polyimides and phenolics are classified as condensation-curing systems [59].

Thermoset composite matrices include polyesters, vinyl esters, epoxies, bismaleimides, cyanate esters, polyimides, and phenolics (Table 2.2).

Table 2.2 Relative characteristics of thermoset resin matrices [67]

Polyesters	Used extensively in commercial applications. Relatively inexpensive, with processing flexibility. Used for continuous and discontinuous composites.
Vinyl Esters	Similar to polyesters, but are tougher and have better moisture resistance.
Epoxies	High-performance matrix systems for primary continuous-fiber composites. Can be used at temperatures up to 250–275 °F. Give better high-temperature performance than polyesters and vinyl esters.
Bismaleimides	High-temperature resin matrices for use in the temperature range of 275–350 °F with epoxy like processing. Requires elevated-temperature post cure.
Cyanate Esters	High-temperature resin matrices for use in the temperature range of 275–350 °F with epoxy like processing. Requires elevated-temperature post cure.
Polymides	Very-high-temperature resin systems for use at 550–600 °F. Very difficult to process.
Phenolics	High-temperature resin systems with good smoke and fire resistance. Used extensively for aircraft interiors. Can be difficult to process.

2.4.1.1. Epoxy Resin

A thermosetting resin covers a wide range of cross-linking polymers which includes unsaturated polyester resins, phenol formaldehyde resins, and amino resins. Under the term of thermosetting resins, principal polymers can be found and epoxy resin is belonged to this term. Depend on the formation of a covalently cross-linked and thermally stable network structure; thermosetting polymers can be form an infusible and insoluble mass by heating. They are generally amorphous and possess various desirable properties. To give examples for these properties, high tensile strength and modulus, easy processing, good thermal and

chemical resistance, and dimensional stability can be considered. The epoxy resin term is applied to both pre polymers and to cured resins; the former is characterized with a three-membered ring which is known as the epoxy, epoxide, oxirane, or ethoxyline group [68].

2.4.1.2. Cure Reactions

All reactive groups have potential to react and as having those groups, all reactive groups may have reacted in the cured resin and so that, they may no longer contain epoxy groups. However, this situation does not affect the term and the cured resins are still called *epoxy resins*. Commercial epoxy resins contain aliphatic, cycloaliphatic, or aromatic backbones. Epoxy ring has the capability to react with a variety of substrates. Treatment with curing agents gives thermoset polymers which are insoluble and intractable. Fillers, solvents, diluents, plasticizers, and accelerators may be included in the composition to facilitate processing and modify cured resin properties [69].

2.4.1.3. Catalytic Cure

During epoxy resin homopolymerization process, the function of the catalytic curing agents is known as initiation. Lewis acids and bases such as boron trihalides (Lewis acid) and tertiary amines (Lewis base) initiate the catalytic cures. The usage of catalytic curing agents for homopolymerization can be as supplemental curing agents with polyamines, or as accelerators for anhydrides-cured systems. These catalytic curing agents have long pot lives and high-temperature resistance capacity. But, they have long cure cycles at high temperature, due to the reasons that are explained in Matrix Resin System part. The materials are also used as adhesives and for electrical encapsulation purposes [70].

2.4.1.4. Co-reactive Cure

The co-reactive curing agents act as a comonomer during the polymerization step of the whole process. Among these, a wide variety of compounds can be found such as amines (both primary and secondary), mercaptans, isocyanates, carboxylic acids, acid anhydrides, and etc [70].

2.4.2. Thermoplastics

The molecules in thermoplastic polymers contain rigid aromatic rings and these rings give them a relatively high glass transition temperature and a superior dimensional stability at high temperatures [71].

Thermoplastic polymers have the following advantages over their counter-part thermoset polymers. Their advantages are:

- High impact strength and fracture resistance
- Higher strain-to-failure, therefore better resistance to matrix micro-cracking
- Unlimited storage life at room temperature (25°C)
- Shorter fabrication time
- Easy joining and repair by welding, solvent bonding etc.
- Easy handling
- Can be reprocessed and recycled

However, there are also some disadvantages of them. They have lower creep resistance and lower thermal stability [72].

2.4.3. The Comparison of Thermosets and Thermoplastics

A thermoset polymer can be identified as a large cross-linked molecule which is held together with strong covalent bonds. If thermoset was heated, the cross-links that are found in polymer, would prevent displacement of the chains and the material would degrade. As a result, thermosets cannot be reshaped like thermoplastics after curing, and also repairs require a liquid state catalyzer for cross-linking the repair material into the cured material. Epoxy, polyester, silicone, and bismaleimides are included as commonly used thermoset materials [73].

In general, thermoplastics show increased toughness when compared with thermosets. But, it is important that the increased addition of fillers or fibers to thermoplastics reduces its impact strength to levels when compared to thermosets [74]. The comparison between thermoplastics and thermosets according to their characteristic features is given in Table 2.3.

Table 2.3 The comparison of thermosets and thermoplastics [75]

Characteristic	Thermosets	Thermoplastics
Tensile Properties	Excellent	Excellent
Stiffness Properties	Excellent	Excellent
Compression	Good	Excellent
Compression Strength After Impact	Good to excellent	Fair to excellent
Bolted Joint Properties	Fair	Good
Fatigue Resistance	Good	Excellent
Damage Tolerance	Excellent	Fair to excellent
Durability	Excellent	Good to excellent
Maintainability	Fair to poor	Good
Service Temperature	Good	Good
Dielectric Properties	Good to excellent	Fair to good
Environmental Weakness	None, or hydraulic fluid	Moisture
NBS Smoke Test Performance	Good to excellent	Fair to good
Processing Temperatures, C(F)	343-425 (600-800)	121-315 (250-600)
Processing Pressure, MPa (psi)	1.38-2.07 (200-300)	0.59-0.69 (85-100)
Lay-up Characteristics	Dry, boardy, difficult	Tack, drape, easy
Debulking, Fussing, or Heat Tacking	Every ply if part is not flat	Typically, every 3 or more plies
In-process Joining Options	Co-fusion	Co-cure, Co-bond
Postprocess Joining Options	Fastening, bonding, fusion	Fastening, bonding
Manufacturing Scrap Rates	Low	Low
Ease of Prepregging	Fair to poor	Good to excellent
Volatile-free Prepreg	Excellent	Excellent
Prepreg Shelf Life and Out Time	Excellent	Good
Health/Safety	Excellent	Excellent

CHAPTER THREE

Fracture Mechanics

Introduction to Facture Mechanics

The Importance of Fracture Mechanics

Linear Elastic Fracture Mechanics

Elastic-Plastic Fracture Mechanics

3.1. Introduction to Fracture Mechanics

Fracture mechanics is a field in mechanics that deals with the crack propagation, crack growth, or crack extension. The components, which may frequently found in the material, contain cracks, microcracks, or defects. Machining flaws, manufacturing defects or crack formation during service might have role in these types of crack formations. In Figure 3.1, an image captured the cracks, which may initiate by different types of particles like precipitates, can be seen. Besides to that, the particules often appear with an unfavorable geometry such as, being plate-like or sharp-edged. Also they can fail easily by detaching from the matrix or by breaking. Designing the components against the yield strength is not dealing way in order to prevent the failure by crack propagation because this situation can occur at much smaller loads. However, using fracture mechanics is the best choice to deal with such problems.

The main purpose in the fracture mechanics is to determine the load which starts to the crack for making a safety design. Cracks are characterized as extremely sharp notches. The methods, which are used for assessing the notches, are not considered as applicable because when the stress field at the crack tip calculates, the value becomes infinite. The tools used in fracture mechanics are able to deal with these infinites [76].

Fracture toughness denotes the resistance of the material under the load against the crack propagation, numerically. So the material that has more fracture toughness will be more resistant to crack propagation. Figure 3.2 shows fracture toughness and strength of the different engineering materials. It can be easily seen from this chart; the fracture toughness of composites is higher than the fracture toughness of the other materials.

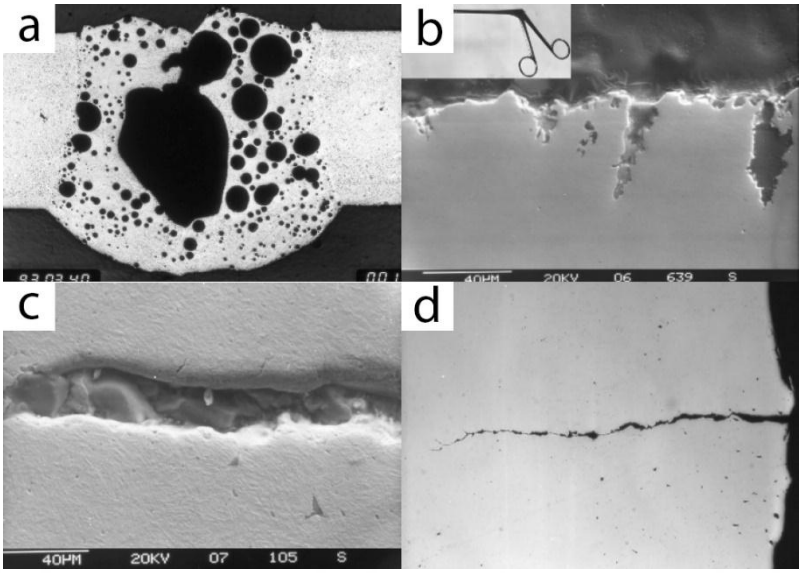

Figure 3.1 The examples of initial cracks and other damage phenomena, (a) welding line in pressure die cast aluminum, (b) corrosion attack on a rongeur forceps made of a martensitic stainless steel, (c) slag inclusion in a forged casing, and (d) crack in a connection rod [76]

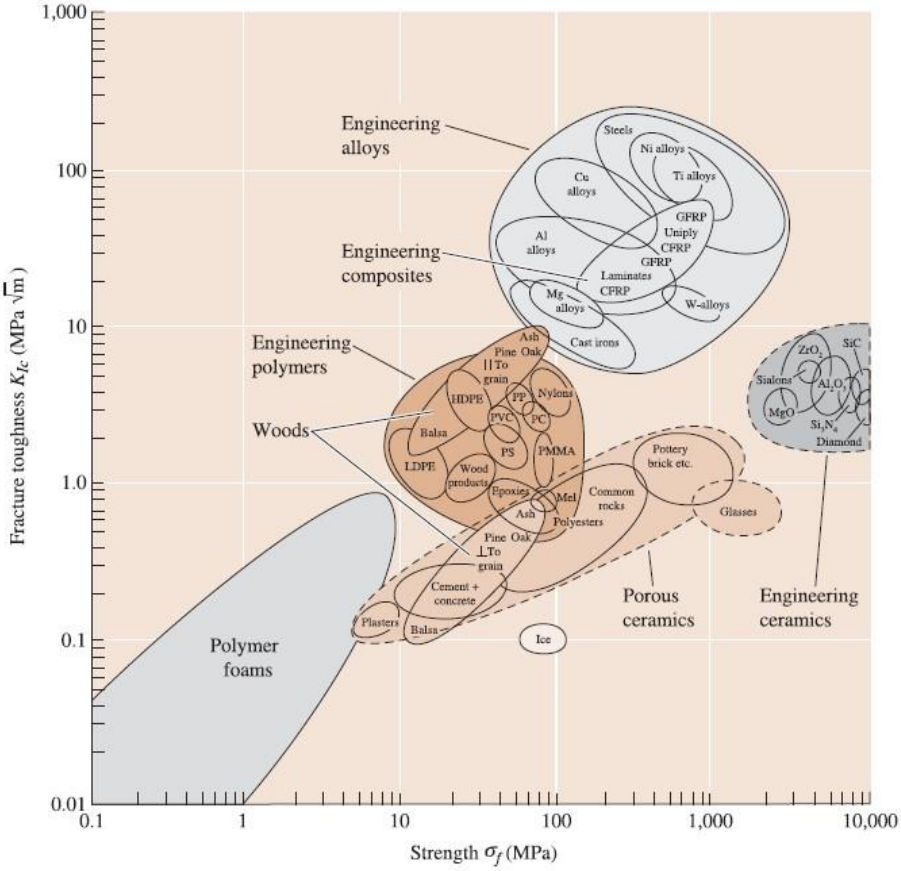

Figure 3.2 Fracture toughness versus strength of different engineering materials [77]

3.2. The Importance of Fracture Mechanics

One of the important properties of fracture mechanics is allowing us to design and select the materials without ignoring the inevitable presence of flaws. Three variables should be considered; the property of the material (K_c or K_{Ic}), the stress σ that the material must withstand, and the size of the flaw a.

Selection of material: In this issue, if the maximum size of flaws in the material and the magnitude of the applied stress were determined, the material, which has a fracture toughness K_C or K_{IC} large enough to prevent the flaw from growing, can be selected.

Design of a component: If the maximum size of any flaw and the material (it's KC or KIC has already been selected) were certain, the maximum stress that the component can withstand would be calculated. After that, the appropriate size of the part can be designed in order to assure that the maximum stress is not exceeded.

Design of a manufacturing or testing method: The maximum size of a flaw which can be tolerated can be calculated, if the material has been selected, the applied stress is known, and the size of the component is fixed. To detect any flaw greater than this critical size, a technique as nondestructive testing can help. Also by selecting the correct manufacturing process, the size of the flaws can be limited to be smaller than this critical size [78].

3.3. Linear Elastic Fracture Mechanics

To load a plate containing a crack, there are three ways and each load orientation has its own destination. These three different loading configurations has associated problems to

them and they are called as modes I, II, and III. Mode I occurs when tensile forces, which are applied perpendicularly to the plane of the crack, separate two surfaces of a crack. And this type of principal mode of fracture can be seen in Figure 3.3a. Mode II, which can be sometimes called as sliding mode of fracture, occurs when in-plane shear forces are applied to a body containing a crack and this can be seen in Figure 3.3b. Mode III mode of fracture, which can be also known as the tearing mode of fracture or the antiplane crack problem, has out-of-plane shear forces acting on a plate. And mode III is shown in Figure 3.3c [79].

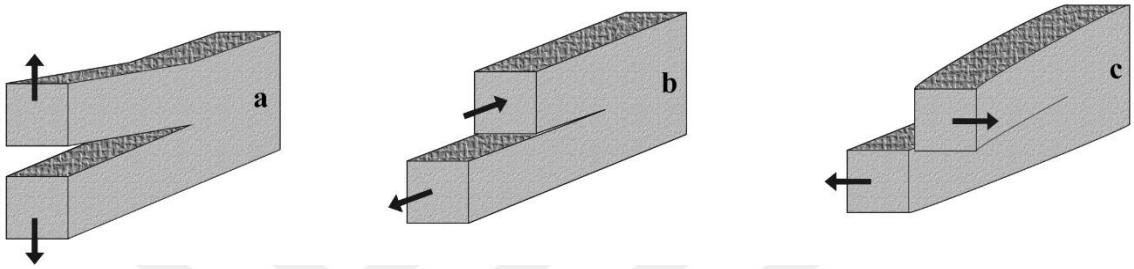

(a) (b) (c)

Figure 3.3 The modes of fracture crack separation a) Mode I: opening, b) Mode II: in-plane shear, c) Mode III: out of-plane shear

3.3.1. Plane Stress and Plane Strain Conditions

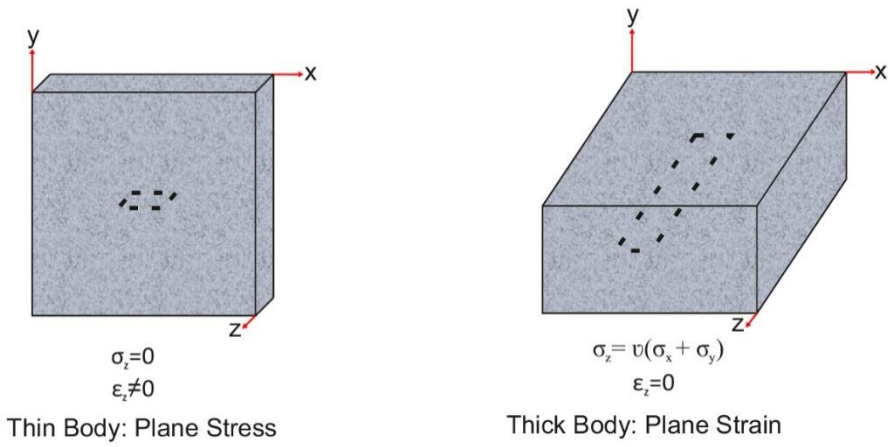

Figure 3.4 Plane stress and plane strain conditions for plates under biaxial positive tensile stresses

When the sample with crack in its structure exposed to tensile stress, triaxial tensiles occur due to the geometry of cracks. If samples exposed to tensile stresses were very thin, there would be stresses formed at x and y directions, but, the formed stress at the z-direction

is considered to be zero ($\sigma_{zz} = 0$) (Figure 3.4). In this case the plane stress state is concerned (Figure 3.5).

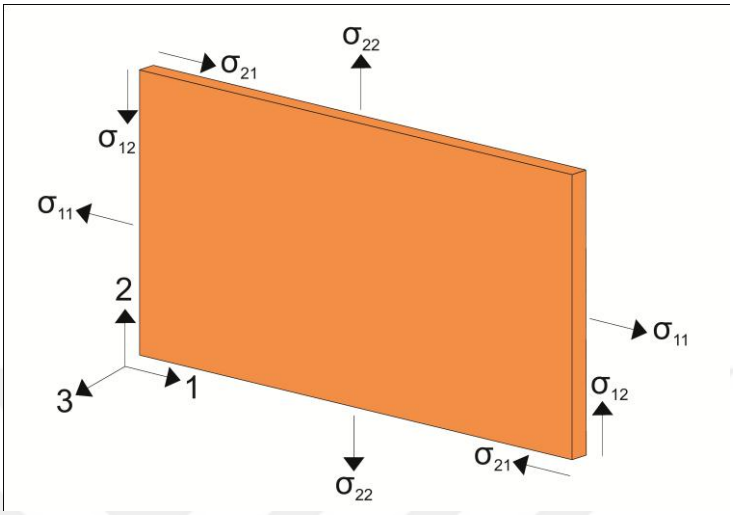

Figure 3.5 Thin body (plane stress condition)

In the thick samples, plane stress occurs at the sample surface and the sample is deformed in three dimensions. But the deformations occur in x and y dimensions (ε_{zz}=0). In this case, the plane strain state is considered (Figure 3.6).

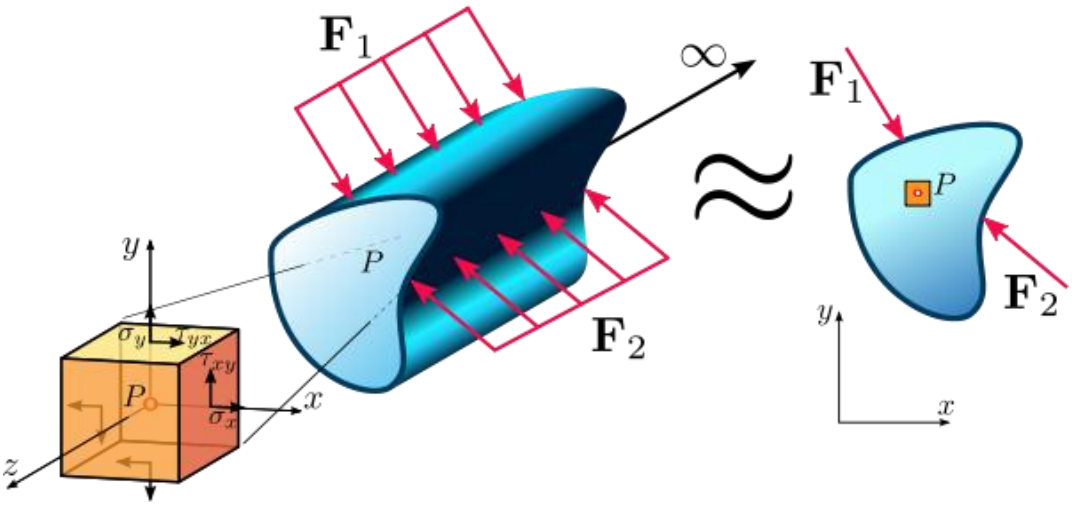

Figure 3.6 Thin body (plane strain condition) [80]

3.3.2. Crack Tip Stress and Displacement Components

Isotropic and linear elastic materials for stress at the crack tip (Figure 3.7) and the displacement components for all failure modes can be expressed as follows.

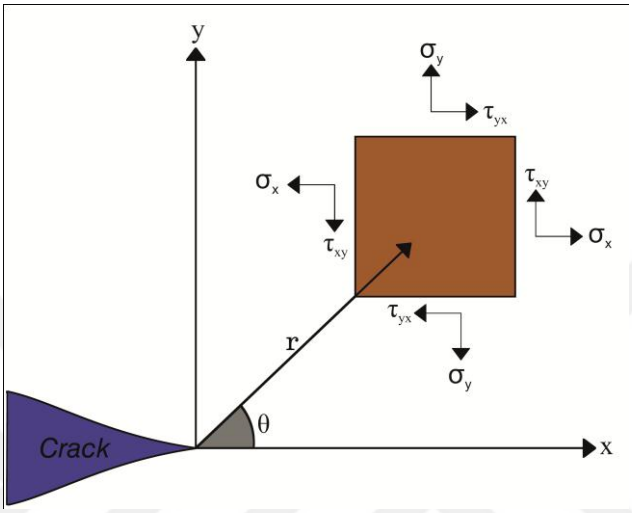

Figure 3.7 Location of local stresses near a crack tip

Crack tip stress components of mode I:

$$\sigma_{xx} = \frac{K_I}{\sqrt{2\pi r}} cos\left(\frac{\theta}{2}\right)\left(1 - sin\left(\frac{\theta}{2}\right) sin\left(\frac{3\theta}{2}\right)\right)$$

$$\sigma_{yy} = \frac{K_I}{\sqrt{2\pi r}} cos\frac{\theta}{2}\left(1 + sin\left(\frac{\theta}{2}\right) sin\left(\frac{3\theta}{2}\right)\right)$$

$$\tau_{xy} = \frac{K_I}{\sqrt{2\pi r}}\left(cos\left(\frac{\theta}{2}\right) cos\left(\frac{3\theta}{2}\right) sin\left(\frac{\theta}{2}\right)\right) \tag{3.1}$$

$$\sigma_{zz} = \begin{cases} 0 & \text{(Plane stress)} \\ v(\sigma_{xx} + \sigma_{yy}) & \text{(Plane strain)} \end{cases}$$

$$\tau_{xz} = \tau_{yz} = 0$$

Crack tip displacement components of mode I:

$$u_x = \frac{K_I}{\sqrt{2\mu}}\sqrt{\frac{r}{2\pi}}cos\frac{\theta}{2}\left(\kappa - 1 + 2sin^2\frac{\theta}{2}\right)$$

$$u_y = \frac{K_I}{\sqrt{2\mu}}\sqrt{\frac{r}{2\pi}}sin\frac{\theta}{2}\left(\kappa + 1 - 2cos^2\frac{\theta}{2}\right)$$

$$u_z = \begin{cases} -\frac{vz}{E}\left(\sigma_{xx} + \sigma_{yy}\right) & \text{(Plane stress)} \\ 0 & \text{(Plane strain)} \end{cases} \tag{3.2}$$

$$\kappa = \begin{cases} (3 - v)/(1 + v) & (Plane\ stress) \\ 3 - 4v & (Plane\ strain) \end{cases}$$

Crack tip stress components of mode II:

$$\sigma_{xx} = \frac{K_{II}}{\sqrt{2\pi r}}sin\left(\frac{\theta}{2}\right)\left(2 + cos\left(\frac{\theta}{2}\right)cos\left(\frac{3\theta}{2}\right)\right)$$

$$\sigma_{yy} = \frac{K_{II}}{\sqrt{2\pi r}}sin\left(\frac{\theta}{2}\right)cos\left(\frac{\theta}{2}\right)cos\left(\frac{3\theta}{2}\right)$$

$$\tau_{xy} = \frac{K_{II}}{\sqrt{2\pi r}}cos\left(\frac{\theta}{2}\right)\left(1 - sin\left(\frac{\theta}{2}\right)sin\left(\frac{3\theta}{2}\right)\right) \tag{3.3}$$

$$\sigma_{zz} = \begin{cases} 0 & \text{(Plane stress)} \\ v\left(\sigma_{xx} + \sigma_{yy}\right) & \text{(Plane strain)} \end{cases}$$

$$\tau_{xz} = \tau_{yz} = 0$$

Crack tip displacement components of mode II:

$$u_x = \frac{K_{II}}{\sqrt{2G}}\sqrt{\frac{r}{2\pi}}\,sin\frac{\theta}{2}\left(\kappa + 1 + 2cos^2\frac{\theta}{2}\right)$$

$$u_y = \frac{K_{II}}{\sqrt{2G}}\sqrt{\frac{r}{2\pi}}\,cos\frac{\theta}{2}\left(\kappa - 1 - 2sin^2\frac{\theta}{2}\right) \tag{3.4}$$

$$u_z = \begin{cases} -\frac{vz}{E}\left(\sigma_{xx} + \sigma_{yy}\right) & \text{(Plane stress)} \\ 0 & \text{(Plane strain)} \end{cases}$$

$$\kappa = \begin{cases} (3 - v)/(1 + v) & (Plane\ stress) \\ 3 - 4v & (Plane\ strain) \end{cases}$$

Crack tip stress components of mode III:

$$\sigma_{xx} = 0$$

$$\sigma_{yy} = 0$$

$$\sigma_{zz} = 0$$

$$\tau_{xy} = 0 \tag{3.5}$$

$$\tau_{yz} = \left(\frac{K_{III}}{\sqrt{2\pi r}}\right)cos\frac{\theta}{2}$$

$$\tau_{zx} = \left(-\frac{K_{III}}{\sqrt{2\pi r}}\right)sin\frac{\theta}{2}$$

Crack tip displacement components of mode III [81]:

$$u_x = 0$$

$$u_y = 0 \tag{3.6}$$

$$u_z = \left(\frac{K_{II}}{\sqrt{2G}}\right)\left(\sqrt{\frac{r}{2\pi}}\right)\left(sin\frac{\theta}{2}\right)$$

3.4. Elastic-Plastic Fracture Mechanics

Linear fracture mechanics generally applied to brittle materials. If the stress applied to a substrate material is low, the maximum stress occurring in the crack tip does not exceed the yield strength of the material. In this case, the material allows the presence of cracks. Plastic deformed areas are formed around the cracks in metallic materials. This region is called the crack tip plastic zone. High stress at the crack tip will show the new distribution by spreading over a wider area [82].

3.4.1. Crack Tip Plastic Zone

A region undergone plastic deformation occurs at the crack tip in which the stress exceeds the limit of the material yield. This region is called the crack tip plastic zone. When calculating the crack tip plastic zone, the yield of plastic material in that zone is taken as a bases [82].

3.4.2. Calculation of Crack Tip Plastic Zone

According to von misses yield criterion, the formation of the yield in terms of the principal stresses depends on the following equation 3.7 [82].

$$(\sigma_1 - \sigma_2)^2 + (\sigma_2 - \sigma_3)^2 + (\sigma_3 - \sigma_1)^2 = 2{\sigma_{yield}}^2 \tag{3.7}$$

The σ_1, σ_2 and σ_3 principal stresses in this equation 3.8;

$$\sigma_1 = \frac{K_I}{\sqrt{2\pi r}} cos\left(\frac{\theta}{2}\right)\left(1 - sin\left(\frac{\theta}{2}\right) sin\left(\frac{3\theta}{2}\right)\right)$$

$$\sigma_2 = \frac{K_I}{\sqrt{2\pi r}} cos\frac{\theta}{2}\left(1 + sin\left(\frac{\theta}{2}\right) sin\left(\frac{3\theta}{2}\right)\right) \tag{3.8}$$

For the plane stress condition, σ_3 is zero.

For the plane strain condition, σ_3;

$$v\left[\frac{K_I}{\sqrt{2\pi r}}cos\left(\frac{\theta}{2}\right)\left(1-sin\left(\frac{\theta}{2}\right)sin\left(\frac{3\theta}{2}\right)\right)\right] + v\left[\frac{K_I}{\sqrt{2\pi r}}cos\frac{\theta}{2}\left(1+sin\left(\frac{\theta}{2}\right)sin\left(\frac{3\theta}{2}\right)\right)\right] \tag{3.9}$$

Substituting this equation 3.10 and equation 3.11;

Plane stress;

$$\frac{K_I^2}{4\pi r}\left(1+\frac{3}{2}sin^2\theta+cos\theta\right)={\sigma_{yield}}^2$$
$$r(\theta)=\left(\frac{1}{4\pi}\right)\left(\frac{K_I}{\sigma_{yield}}\right)^2\left[1+\frac{3}{2}sin^2\theta+cos\theta\right] \tag{3.10}$$

Plane strain:

$$\frac{K_I^2}{4\pi r}\left(\frac{3}{2}sin^2\theta+(1-2v)^2(1+cos\theta)\right)={\sigma_{yield}}^2$$
$$r(\theta)=\left(\frac{1}{4\pi}\right)\left(\frac{K_I}{\sigma_{yield}}\right)^2\left[\frac{3}{2}sin^2\theta+(1-2v)^2(1+cos\theta)\right] \tag{3.11}$$

The code array and graphic (Figure 3.8) that I prepared for the shape of the plastic zone using this formula with MATLAB R2012b program for the Ti-6Al-4V (ELI) R (Titanium Alloy) material were given below:

```
clc
clear all
%Yalcind
%11.Oct.2015
%Elected Material=Ti-6Al-4V(ELI)RA Titanium alloy
%KIC,YS and v values for material
KIC=2606;
YS=827;
v=0.33;
```

```
%Angle sequence
Q=1:361;
%Matrix size
Qmatrix(:,1)=Q ;
%Degree calculation
degree=(pi/180)*Qmatrix ;
cos=cos(degree) ;
sin=sin(degree) ;
sinsquare=sin.*sin ;
% Formulation
stress=((1/(4*pi))*((KIC/YS)^2)*(1+(3/2)*(sinsquare)+cos)) ;
stressx=stress.*cos ;
stressy=stress.*sin ;
strain=((1/(4*pi))*((KIC/YS)^2)*((3/2)*(sinsquare)+((1-2*v)^2)*cos)) ;
strainx=strain.*cos ;
strainy=strain.*sin ;
%Gösterim
plot(stressx,stressy,strainx,strainy)
```

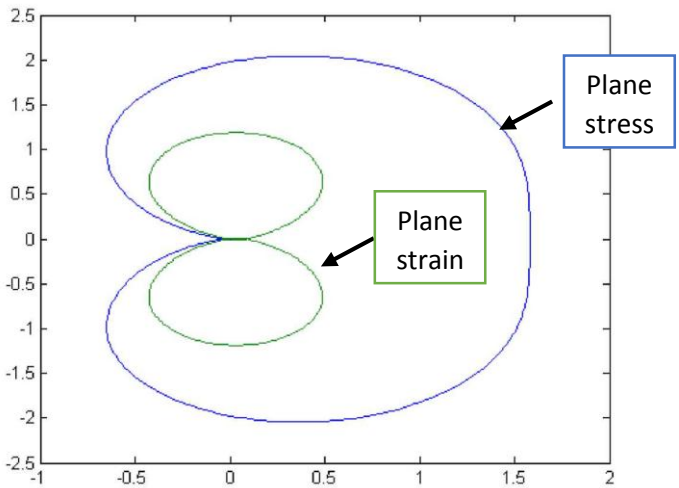

Figure 3.8 The shape of plastic zone for Ti-6Al-4V(ELI)RA (Titanium alloy)

3.4.3. J-Integral

The *J*-integral can be explained as a change of potential energy of the body with an increment of crack extension. The general expression for *J*, as defined by Rice, is given by:

$$J = \int_{\Gamma} W dy - \vec{T}.U \frac{\delta \vec{u}}{\delta x} ds \tag{3.12}$$

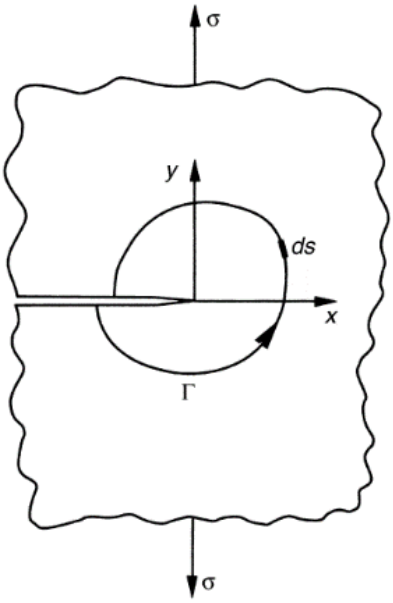

Figure 3.9 Definition of the J-integral [83]

where $\vec{T}$ is the traction vector, acting on a segment *ds* of contour Γ, $\vec{u}$ is a displacement vector r*u* (the displacement on an element along arc *s*), and Γ is any contour in the *X*-*Y* plane that encircles the crack tip. Γ is taken in a counterclockwise direction, starting from one crack face, ending on the opposite face, and closing the crack tip (Figure 3.9) [83]. *W* is the strain energy density, given by:

$$W = \int_0^{\varepsilon_{ij}} \sigma_{ij}.d(\varepsilon_{ij}) \tag{3.13}$$

That is,

$$W = \int \left(\sigma_x d\varepsilon_x + \tau_{xy} d\gamma_{xy} + \tau_{xz} d\gamma_{xz} + \sigma_y d\varepsilon_y + \tau_{yz} d\gamma_{yz} + \sigma_z d\varepsilon_z\right) \tag{3.14}$$

For generalized plane stress, W is reduced to:

$$W = \int \left(\sigma_x d\varepsilon_x + \tau_{xy} d\gamma_{xy} + \sigma_y d\varepsilon_y\right) \tag{3.15}$$

CHAPTER FOUR

Production of Composite Materials

Reinforcement Elements

Matrix Material

Production of Composite Materials

Preparation of Test Samples

Preparation of Arcan Test Apparatus

4.1. Reinforcement Elements

4.1.1. The Fibers Used in Knitting Reinforcement

4.1.1.1. Carbon and Glass Fibers

Carbon fibers used for the knitting reinforcement element were obtained from Dowaks Company. 3K carbon fibers were used as a knitting reinforcement element in this dissertation. The carbon fibers were named with the number of filaments. Hence, 3K carbon fibers have 3000 carbon filaments. 3K carbon fibers are the most popular and most widely used carbon fibers. Their major features are relatively stiff, easy to get and make. Also, 3K carbon fibers have got higher elongation and ultimate strength than 6K, 9K, and 12K [84]. The following table includes the properties of 3K carbon fibers.

Table 4.1 The properties of the 3K carbon fibers [85]

Properties	English		Metric	Tolerancess	Unit	Test Method
Tensile Strength	610	ksi	4200	Min.3906	MPa	ISO 10618
Tensile Modulus	35.6	Msi	245	230-270	GPa	ISO 10618
Strain	1.8	%	1.8	Min.1.5	%	ISO 10618
Density	0.065	Ibs/in^3	1.79	1.78-1.81	g/cm^3	ISO 10119
Yield	7448	ft/Ibs	200	194-206	g/1000 m	ISO 1889
Sizing Type & Amount	Epoxy Compatible		1.2	0.8 - 1.6	%	ISO 10548
Twist	Never twisted					

Glass fibers used for knitting reinforcement element were supplied from the Pul-Tech FRP Composites Inc. There are different glass fiber types such as, A (Alkali), C (Corresion), S (Strength) and E (Electric). In this study, E-glass fibers were used as a knştting reinforcement element. E type glass fibers are very good compared to other types of glass due to their electrical resistivity, low alkali ratio, quite high resistance, and very well qualified water resistance. E type glass fibers are especially used in the composite materials exposed to humid environment. The mechanical properties of E glass fibers were given in Table 4.2.

Table 4.2 The properties of the E glass fibers [86]

Properties	Unit	Values
Tensile strength	MPa	3445
Compressive strength	MPa	1080
Density	g/cm3	2.58
Thermal expansion	µm/m·°C	5.4
Softening	°C	846

4.1.2. The Production of Knitting Reinforcement Elements

The fabrics were formed by using pure glass (100%), pure carbon (100%) non-hybrid fabrics and also glass-carbon (50%-50%) hybrid fabrics knitted with carbon and glass fibers. The hiybrid and non-hybrid knitting fabrics had been constructed by me in V-bed semi-automatic knitting machine (Figure 4.1), which was provided by Varol Textile located in Samsun.

Figure 4.1 V-bed semi-automatic knitting machine

During the knitting process for reducing the friction coefficient between the fibers and the V-bed semi-automatic knitting machine and also to prevent the separation of carbon

and glass fibers, waxing was performed (Figure 4.2). The most basic definition of the waxing is the process to provide lubricity to the thread.

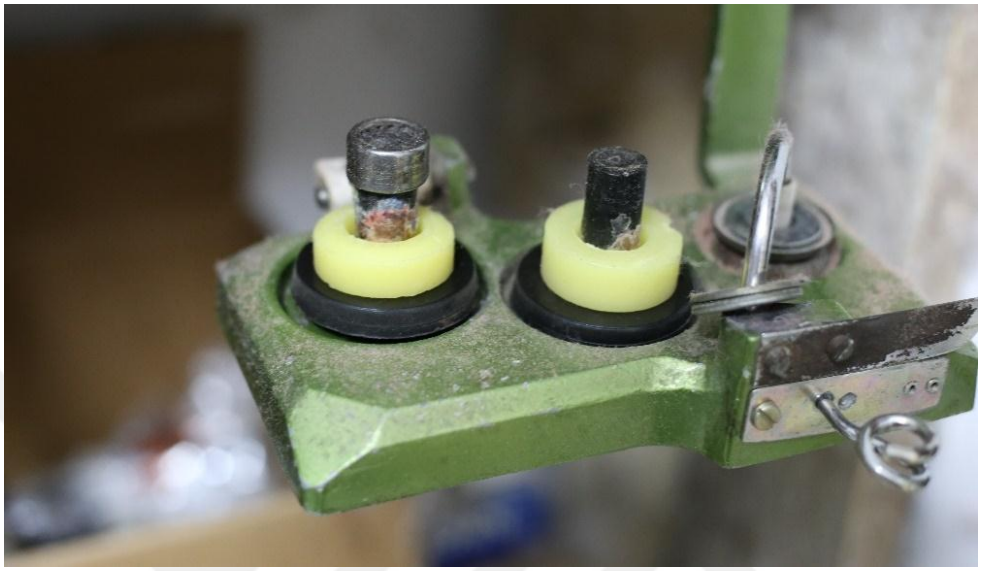

Figure 4.2 The waxing apparatus

Before starting to the knitting process, the fibers must be passed through the guide (Figure 4.3) in order to fibers come to the needles in a certain direction. Wherein the guides should be smooth and the thread accumulator must be fine-tuned. Otherwise, the thread causes to damage on the fabric edge.

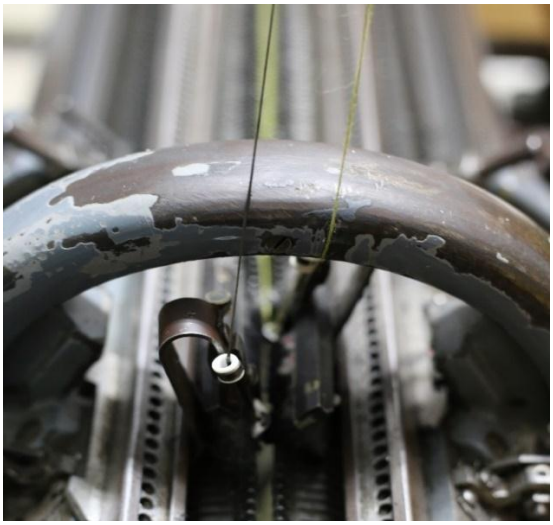

Figure 4.3 Passing fibers through the guides

It is required to pull the knitting threads in the direction of gravity otherwise, there would not been jump to loop formation in the needle and this might cause damage in the fabrics. After a series of knitting, a comb was passed to loop and the concentric weights were attached to this comb. This system was illustrated in Figure 4.4.

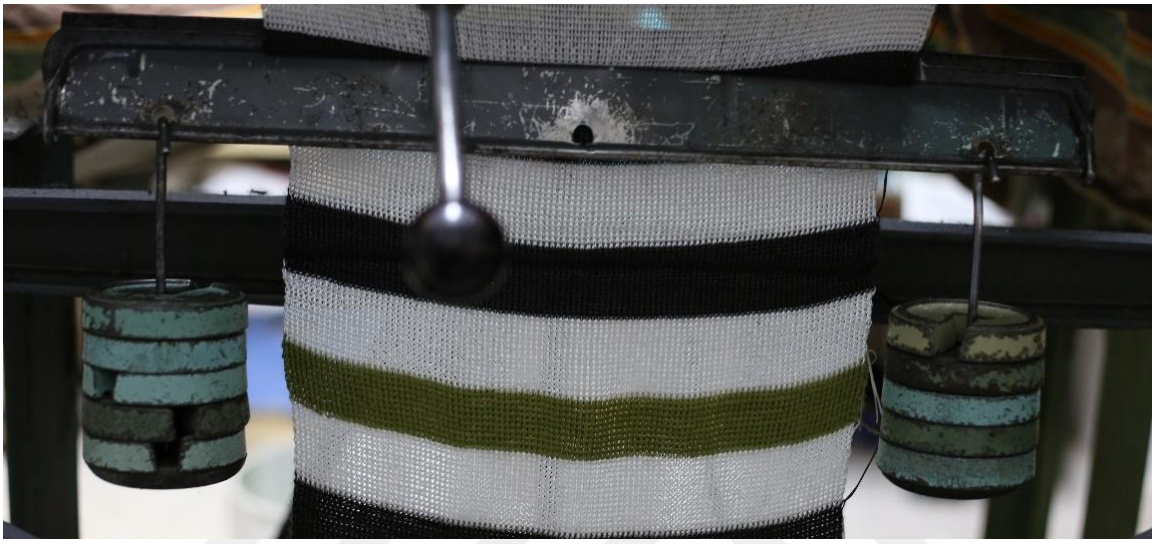

Figure 4.4 The withdrawal of the knitted fabrics with concentric weights

Knitting needles were located as diagonally in the V-bed knitting machines. This is because; the needles on both sides must be going out to take the thread at the same time. The process of knitting was performed by a cam-rail system fixed on V-bed knitting machine. Cam system determines how much will be the needle height and a variety of knitting can be obtained by this way. A section of a loop was shown in Figure 4.5 and movements of a needle for loop formation can be seen in Figure 4.6. The horizontal row of loops is called course and the vertical column of loops is called wale as seen in Figure 4.7.

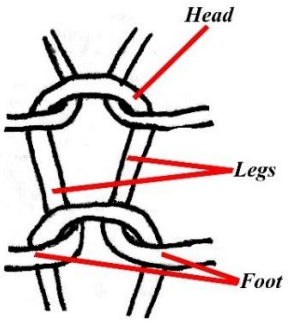

Figure 4.5 A knitted loop

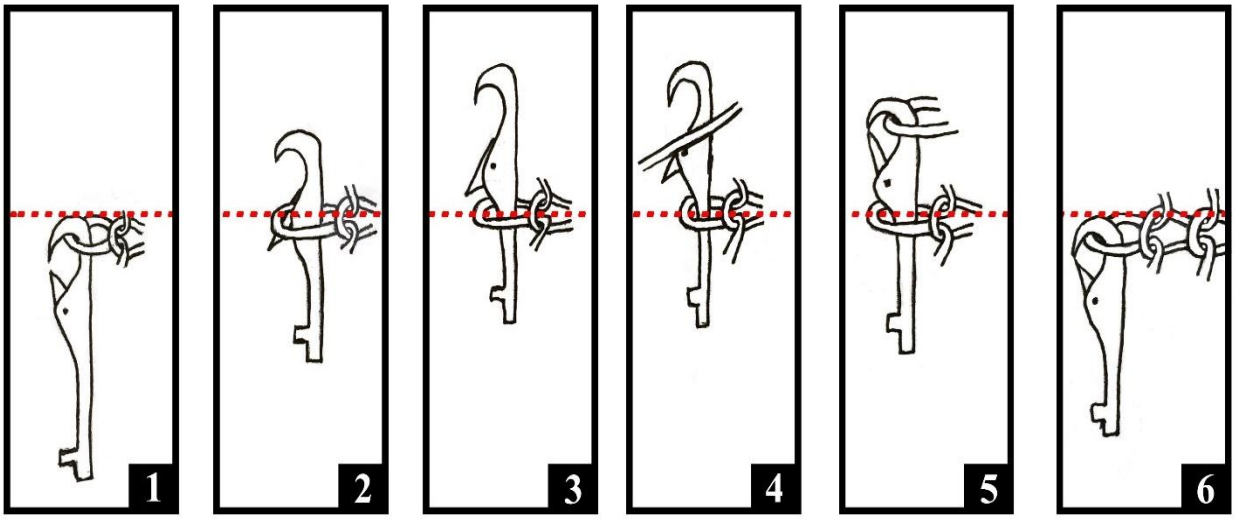

Figure 4.6 A needle movement for loop formation; (1) starting position, (2) half of the movement of the needle, (3) the highest position of the needle, (4) thread depositing, (5) "cast on" for new loop formation, and (6) new loop length setting

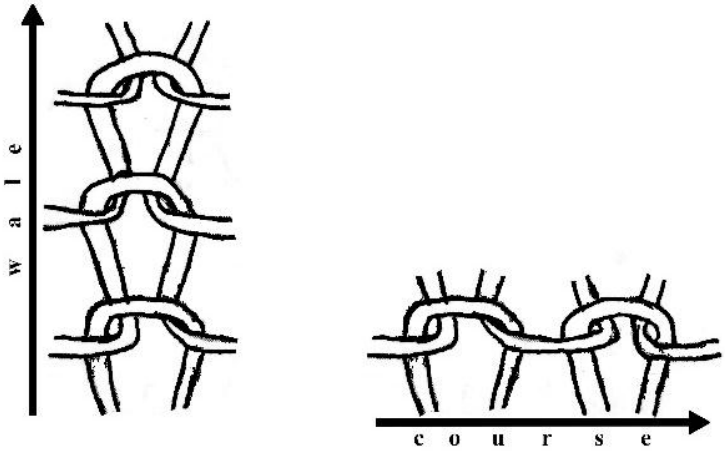

Figure 4.7 The wale and course directions of loops

The flat knitting machines were classified and called in between 3 and 18 numbers, commercially. V-bed semi-automatic knitting machines are named according to the number of needles in 1 inch in length. In this thesis, 5 number machine was used for hybrid and non-hybrid rib knitted fabrics. There are 3 different frequency settings in this machine. The fibers were knitted in the low frequency settings. The rib fabrics produced in this machine are schematically shown in Figure 4.8.

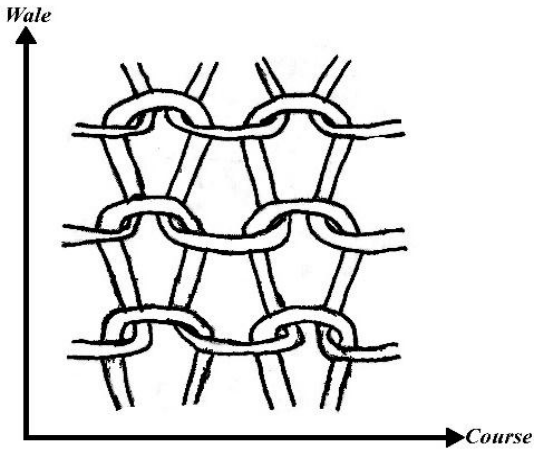

Figure 4.8 Schematic representation of rib fabric

1x1 rib knitted fabrics were produced as pure glass (100%) and pure carbon (100%) non-hybrid fabrics and also glass-carbon (50%-50%) hybrid fabrics. The image of the 100% glass knitted fabrics and 100% carbon knitted fabrics on the V-bed machine were given in Figure 4.9 and 4.10. The glass-carbon (50%-50%) hybrid fabrics were knitted in height of the Arcan samples in order to provide easy production. To save time in production, instead to start knitted again at the end of each part, 5 additional rows were built with another thread in order to cut both end of knitted structures. The image of the glass-carbon (50%-50%) knitted hybrid fabrics were shown in Figure 4.11.

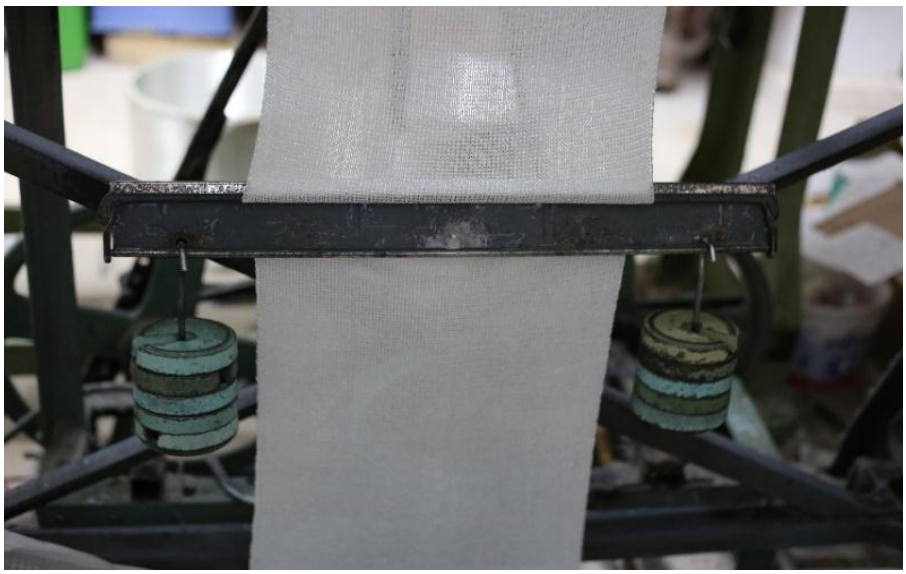

Figure 4.9 The production of 1x1 rib glass knitted non-hybrid fabric

Figure 4.10 The production of 1x1 rib carbon knitted non-hybrid fabric

Figure 4.11 The glass-carbon (50%-50%) knitted hybrid fabrics with 5 additional rows

In the knitted form, the modulus of elasticity in the course direction of carbon and glass fibers used to knitting fabrics is different. It can be said that, the modulus of elasticity of the carbon fiber is higher than the glass fibers. This difference can not be seen in small-sized fabric, but when fabric size grows, this difference can be clearly seen. The modulus of elasticity difference was depending on the knitting rows is required to achieve the desired length. The row numbers of glass and carbon corresponding to the desired length were shown in Table 4.3.

Table 4.3 The row numbers of glass and carbon fibers for desired pattern widths

Fiber	Pattern width (mm)	Row	Pattern width (mm)	Row	Pattern width (mm)	Row
Pure glass	12.5	4	25	8	50	15
Pure carbon	12.5	4	25	9	50	17

4.2. Matrix Material

The epoxy resin used for production of composite material was obtained from the Duratek Company. Cross-link density has the major effect on the properties of cured epoxy resin. Therfore, increasing in cross-link density leads to improvement in the tensile modulus, glass transition temperature, thermal stability and chemical resistance; however, it causes reduction in strain to failure and fracture toughness [87-89]. Epoxy resin is very commonly used in aerospace structures. Epoxy has two components and found in liquid form in general. DTE 1000 epoxy and DTS 1100 hardener were obtained from Duratek Company as given in Figure 4.12.

Figure 4.12 DTE 1000 epoxy and DTS 1100 hardener

4.3. Production of Composite Materials

In this thesis, non-hybrid and hybrid laminated composite materials based on knitted glass and carbon fabrics were produced by hand lay-up methods in composite manufacturing laboratory, Usak University. Hand layup method is known as one of the oldest and simplest method. The most suitable resins for this method are polyester and epoxy resins.

4.3.1. Production Parameters and Matters to Consider

As a reinforcing element in laminated composites, textile fabrics are utilized and particularly woven fabrics are used. The fibers are usually positioned in 0° and 90° in woven fabrics. Therefore, during the manufacture, there won't be any difficulty in impregnating the matrix material. However, if you working with knitted fabrics, you will most probably have difficulty in impregnating the resin. There is no specific fiber direction in the knitted fabrics and this situation makes the knitted fabrics with a higher volume than the woven fabrics. As volume gained fabric will have really flexible structure, the matrix material must be carefully and equally distributed to all surfaces. Otherwise, the knitted fabrics, which are in the flexible structure, form different stresses under pressures and shifts on the loop rows may occur. And because of this, a rigid composite material cannot be obtained. In this study, the production was done particularly in the sample size by considering the flexibility and the volume size of the knitted fabrics. In this way, epoxy was distributed equivalently in each field and also the slipping in loop rows were minimized which may occur because of the difference between pressure and epoxy. In Figure 4.13, the prepared knitted fabrics that in sample size were shown.

Figure 4.13 The knitted fabrics that in sample size

Another important element in the production of knitted reinforced composite materials is the well adjustments of the density of the matrix material. Due to the structure of the knitting having a three-dimensional configuration, the prepared material for the production of the laminated composite contains more resins. According to the production that is carried out in this study, 80 g epoxy and 40 g hardener were used for 100 g knitted reinforcement elements.

The ideal curing temperature for the used matrix material is 100°C. Another factor that should be considered for the composite to be produced in this temperature is pressure. If the pressure is not adjusted properly, the pressure cause shifts on the loop rows of the knitted fabrics, which are in a three-dimensional configuration and having flexible structure, with the effect of epoxy and pressure. Again according to the production experiments, 8 MPa pressure has been found to be appropriate for 1x1rib knitted fabrics. Under all these parameters, the knitted composite materials were cured for 120 minutes in a hydraulic press then cooled with the same pressure deu to prevent warping effect. The produced knitted hybrid composites and the schematic representation of knitted composite production were shown in Figure 4.14 and Figure 4.15, respectively.

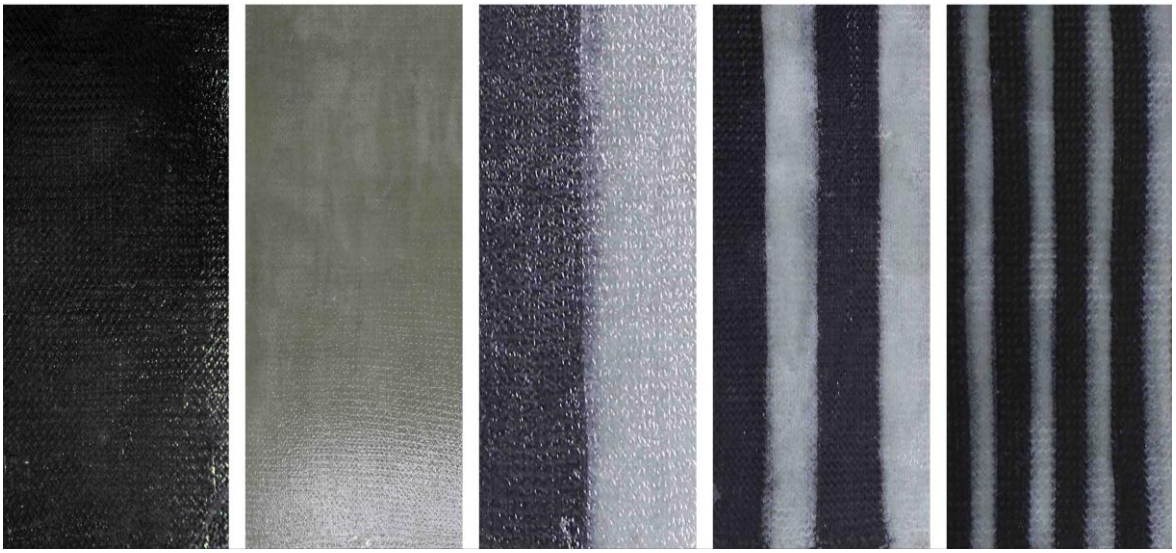

(a) (b) (c) (d) (e)

Figure 4.14 The produced composites: a) pure carbon and b) pure glass non-hybrid knitted composites, and glass-carbon hybrid knitted composites with c) 50mm, d) 25mm, and e)12.5mm pattern widths

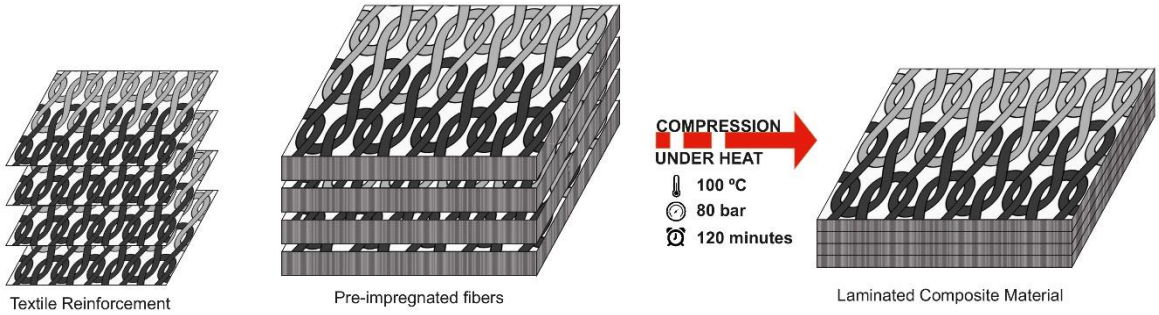

Figure 4.15 The schematic representation of knitted composite production

4.4. Preparation of Test Samples

The modulus of elasticity in the wale direction of knitted samples (E_W) and in the course direction (E_C), tensile strength in the wale (W_T) and course direction (C_T), shear modulus (G_{WC}), and in plane shear strength (S_{WC}) of the knitted hybrid and non-hybrid laminated composites reinforced with glass and carbon knitting fabrics were determined according to ASTM standards. Poisson's ratio (ν_{WC}) of the knitted laminated composites was accepted as 0.3 agreeing to literature. The fracture toughness of knitted laminated composites were also determined for mode I (0°), mode I-II (30°, 45°, and 60°) and mode II (90°) by using modified Arcan test apparatus. The coordinate system which can be seen in Figure 4.16 was considered in the preparation of the test sample. In the figure, the notation of W, C, and T were represented the wale direction, course direction, and out of plane direction, respectively.

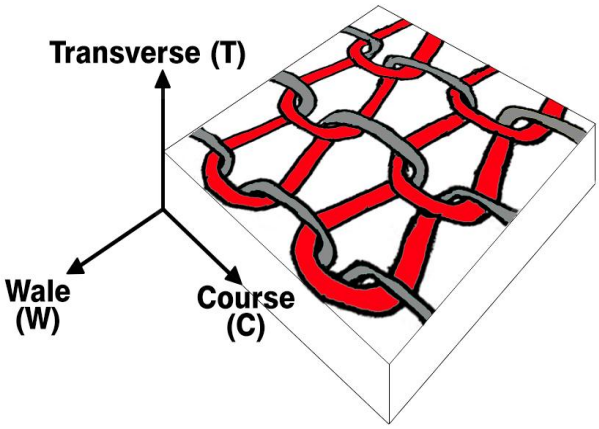

Figure 4.16 The coordinate system for the knitted composite samples

In this context, the samples were cut with CNC router machine which was bought from SHT Machine Company. The modulus of elasticity and tensile strength in the wale direction were determined according to ASTM 3039-76. The modulus of elasticity and the compressive strength in the course direction were determined with regard to ASTM 3410-87. ASTM 3519-76 standard was used for the determination of shear modulus and shear strength of knitted composite samples. Each of the mechanical properties was obtained for five specimens, which were cut for each type of materials. The mechanical and fracture toughness samples were cut by using a 3mm-diameter medium-density fiberboard (mdf) tip CNC router with the speed of 700 rev/min (Figure 4.17).

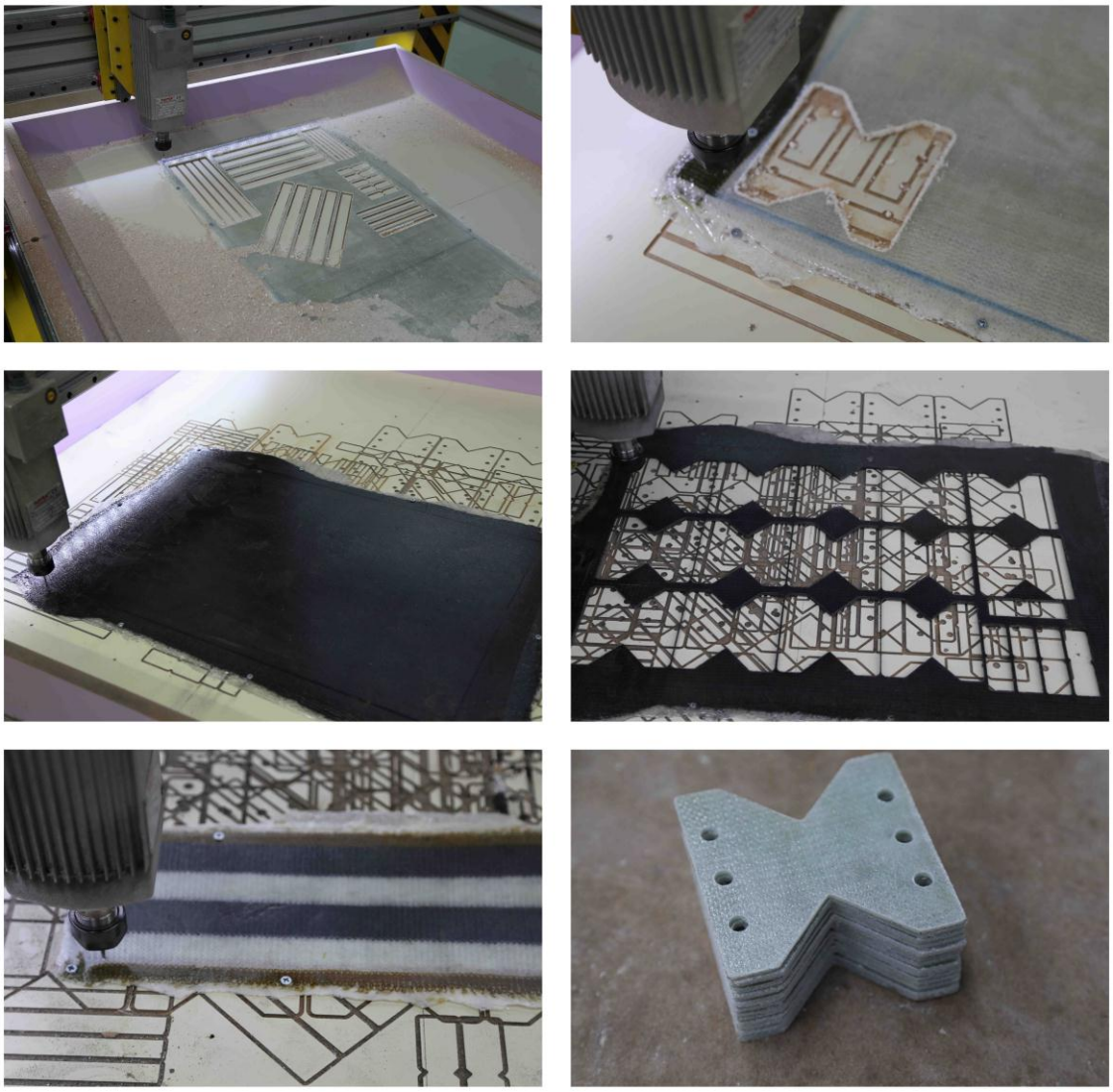

Figure 4.17 The cutting process with the CNC router

Five test samples for fracture toughness tests were cut by CNC router. The geometry of the fracture toughness test samples was given in Figure 4.18. The geometry of the mechanical test samples, which were determined according to ASTM standards, was also shown in Figure 4.19.

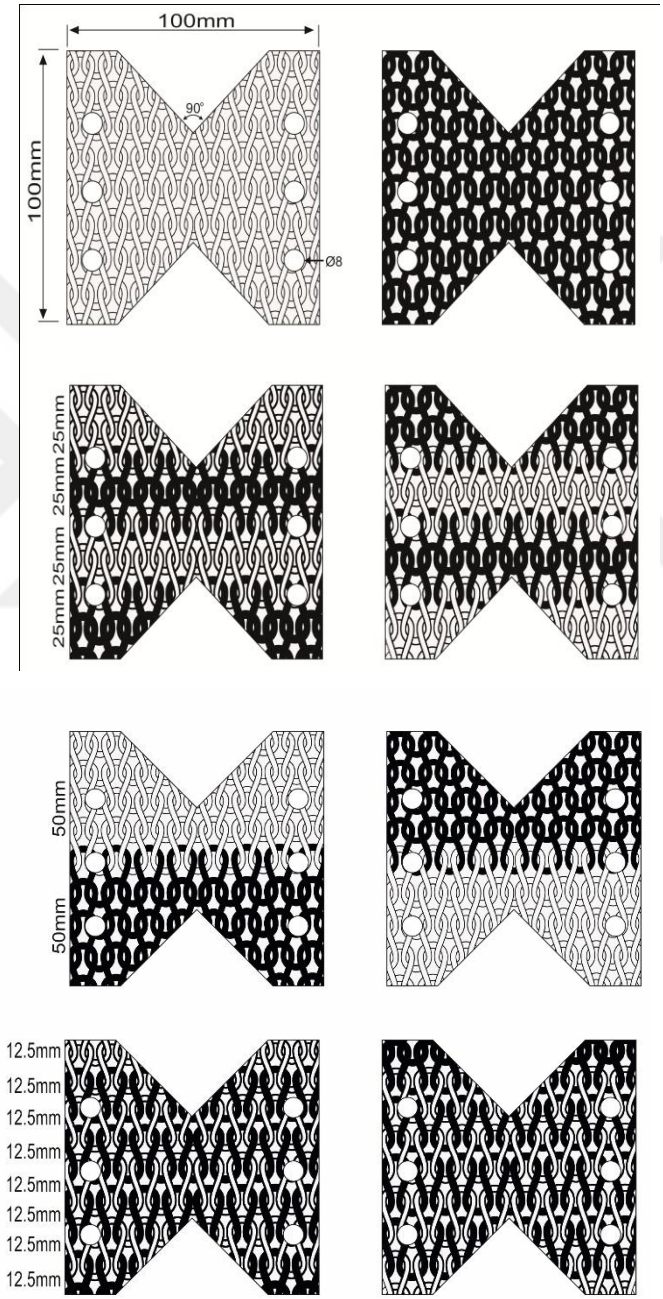

Figure 4.18 The geometry of the fracture toughness test samples

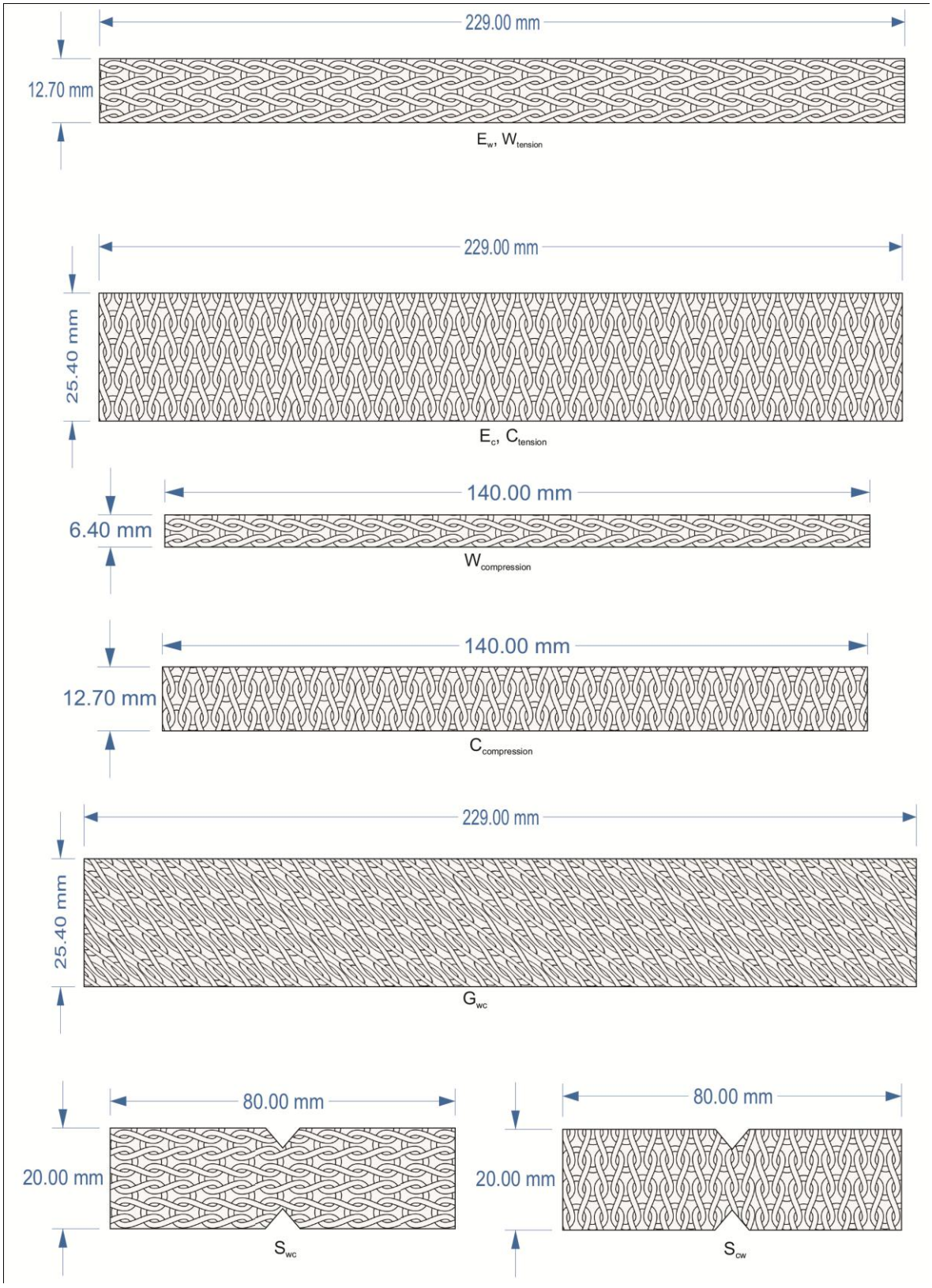

Figure 4.19 The geometry of the mechanical test samples

4.5. Preparation of Arcan Test Apparatus

Arcan test apparatus that will be used to determine the fracture toughness of knitted composites on the mode I (0°), mode I-II (30°, 45°, and 60°), and mode II (90°) installation conditions, had built in Coskunlar Lathe Inc. The dimensions and the image of arcan test apparatus can be seen in Figure 4.20 and Figure 4.21, respectively.

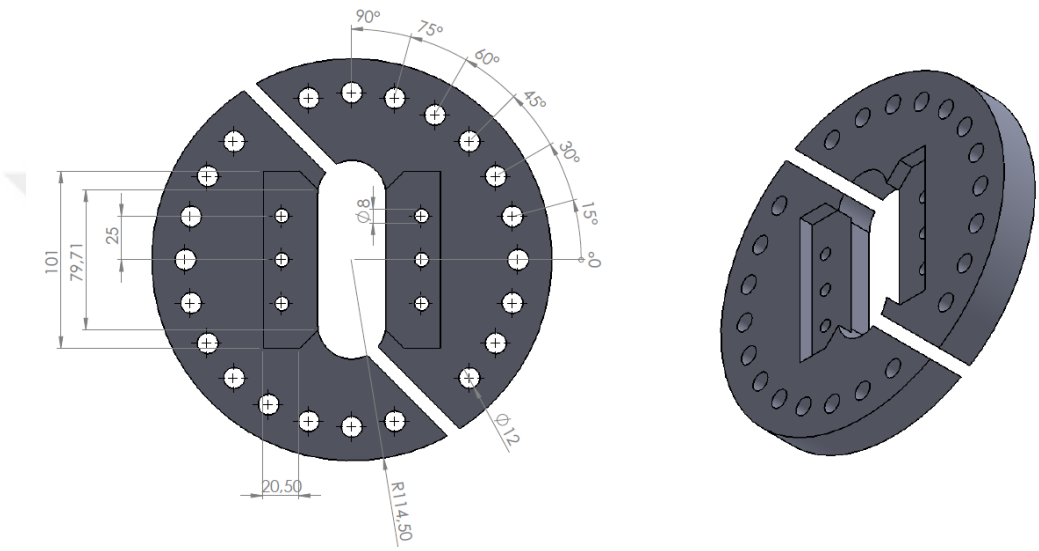

Figure 4.20 The dimensions of arcan test apparatus

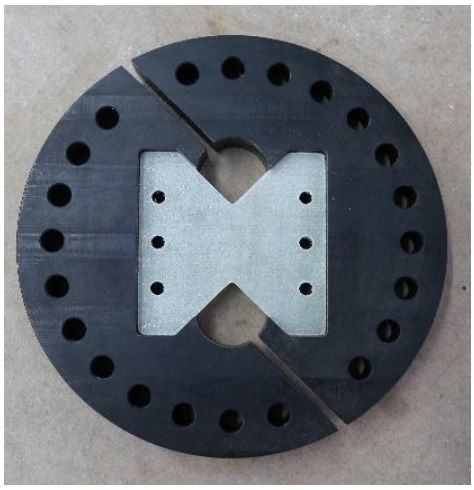

Figure 4.21 The image of arcan test apparatus

CHAPTER FIVE

Experimental Studies

Determination of Tensile Properties

Determination of Compressive Properties

Determination of Shear Properties

Determination of Fracture Toughness

5.1. Introduction

The preparation of the non-hybrid carbon (100%) and glass (100%) knitted laminated composite samples, and also the hybrid glass-carbon (50%-50%) knitted laminated composites with different pattern widths (50mm, 25mm, and 12.5mm) was mentioned in the Chapter 4. Universal U-TEST tension and compression machine with 50kN capacity found in Usak University was used for the mechanical properties and fracture toughness tests. All of the tests were carried out at room temperature with 1 mm/min cross-head speed and were repeated 5 times for each type of material.

5.1.1. Determination of Tensile Properties

The E_W, E_C, W_T and C_T properties of produced samples from 100% carbon and 100% glass composite samples were determined according to ASTM 3039-76 standard (Figure 5.1). In the numerical study, the tensile properties of 100% carbon and 100% glass composite samples were used to anlyze the fracture toughness of hybrid composite Arcan test samples.

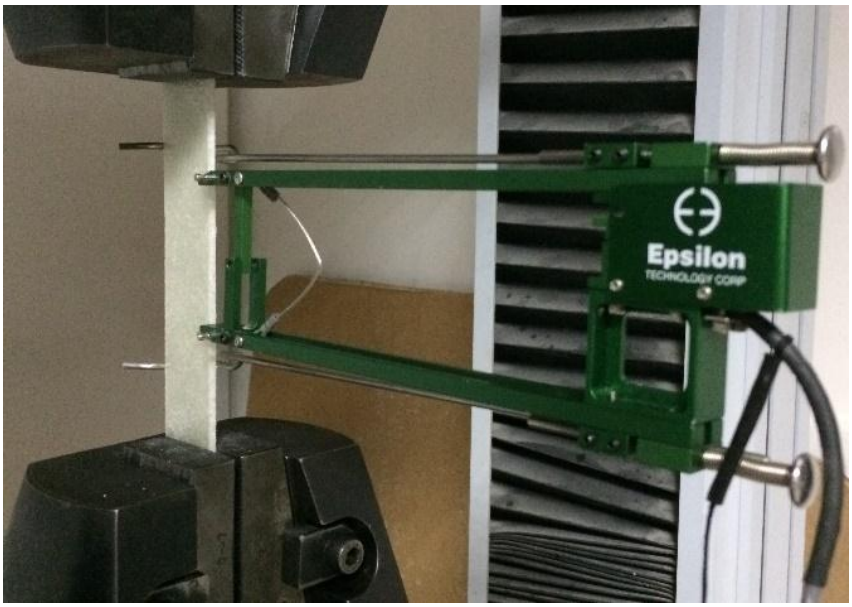

Figure 5.1 Tensile test and the extensometer connected to the composite samples

In the experiments conducted at room temperature, a mechanical extensometer and an indicator were used to determine the mechanical properties of knitted hybrid and non-hybrid composite samples. Extensometer, connected to the composite samples, determine and reflect the amount of strain to the indicator during tensile of knitted composite samples. According to the read load-elongation from the computer, E_W and E_C were determined. Besides, W_t and C_t were calculated by the maximum load divided by the cross sectional area of the samples. The mechanical properties tests were repeated 5 times for pure carbon and pure glass knitted composite structures and the values in Table 5.1 were obtained by averaging the found results from the tests.

Table 5.1 The tensile properties of non-hybrid carbon and glass knitted composite samples

Tensile properties	Carbon	Glass	Unit
The modulus of elasticity in wale direction, E_W	40463.557	27496.450	MPa
The modulus of elasticity in course direction, E_C	19803.811	21895.165	MPa
The tensile strength in wale direction, W_t	143.172	74.952	MPa
The tensile strength in course direction, C_t	118.856	65.026	MPa

It can be clearly seen from Table 5.1; the carbon knitted composite samples have better tensile properties than the glass knitted composite samples. While there was a difference of 20.37% in the modulus of elasticity for the glass knitted composite samples between the wale direction and course direction, this difference was increased to 51.06% for the carbon knitted composite samples. The differences in tensile strength between the wale and course direction for glass and carbon knitted composite samples were obtained as 13.24% and 16.98%, respectively. The loss of properties for the carbon knitted composite samples was higher than for the carbon knitted composite samples due to fragility of carbon and ductility of glass fabrics.

5.1.2. Determination of Compressive Properties

The compressive strength in the wale direction (W_C) and in the course direction (C_C) of 100% carbon and 100% glass knitted laminated composites were determined according

to ASTM 3410-87 standard (Figure 5.2). The W_C and C_C properties were calculated by dividing the maximum load values with cross-sectional area of knitted composite samples. The compressive tests were repeated 5 times for glass and carbon knitted composites samples and the values in Table 5.2 were obtained.

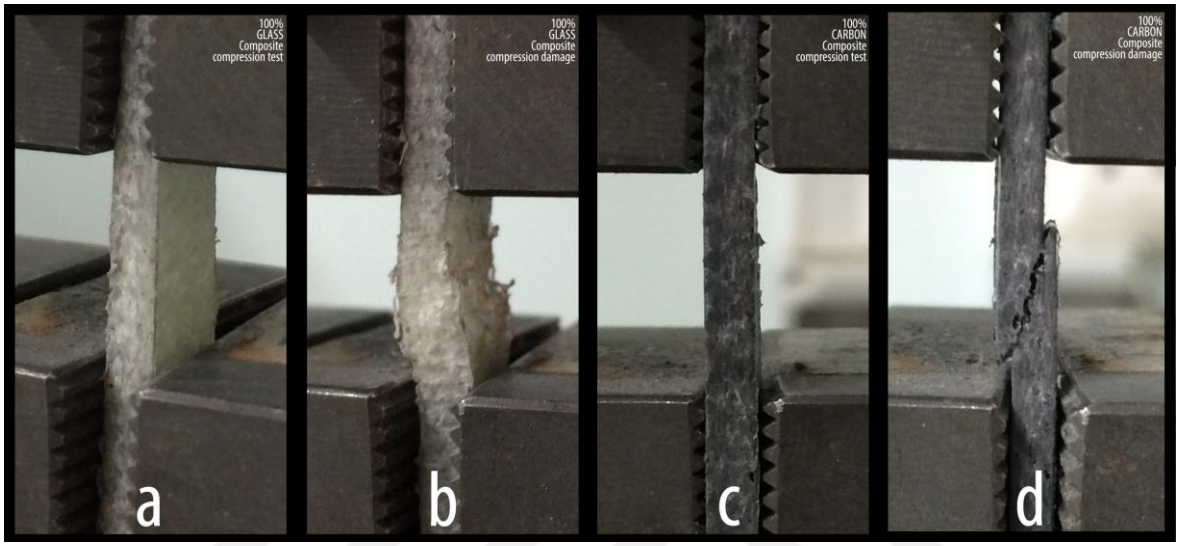

Figure 5.2 The images of glass knitted composite samples (a) before and (b) after compression tests and of carbon knitted composite samples (c) before and (d) after compression tests

Table 5.2 The compressive properties of non-hybrid carbon and glass knitted composite samples

Compressive properties	Carbon	Glass	Unit
The compressive strength in wale direction, W_C	103.349	99.476	MPa
The compressive strength in course direction, C_C	84.476	80.762	MPa

As can be seen in the Table 5.2, the compressive strength of carbon knitted composite samples in the wale direction and in the course direction was found to be higher than the glass knitted composite samples. The compressive strength between the wale and course direction for carbon and glass knitted composite samples were decreased as 18.26% and 18.81%, respectively.

5.1.3. Determination of Shear Properties

For determining the shear modulus (G_{WC}), firstly it is necessary to determine the modulus of elasticity of the samples in 45° direction according to the wale direction. The shear modulus test samples were prepared according to the ASTM 3519-76 standard. The shear test samples were loaded up to catastrophic failure. The damage of glass and carbon knitted shear modulus test samples after catastrophic failure was illustrated in Figure 5.3. G_{WC} was calculated depending on the value of E_W, E_C, E_{45} and ν_{WC} using the following equation 5.1.

$$G_{WC} = \frac{1}{\left(\frac{4}{E_{45}} + \frac{1}{E_W} - \frac{1}{E_C} + \frac{2\vartheta_{WC}}{E_W}\right)} \tag{5.1}$$

where, E_W represents the modulus of elasticity in the wale direction, E_C is modulus of elasticity in the course direction, E_{45} in 45° direction relative to the wale direction and ν_{WC} represents the Poisson's ratio. The shear modulus of knitted glass and carbon non-hybrid composite samples were calculated by accepting ν_{WC} = 0.3 [90].

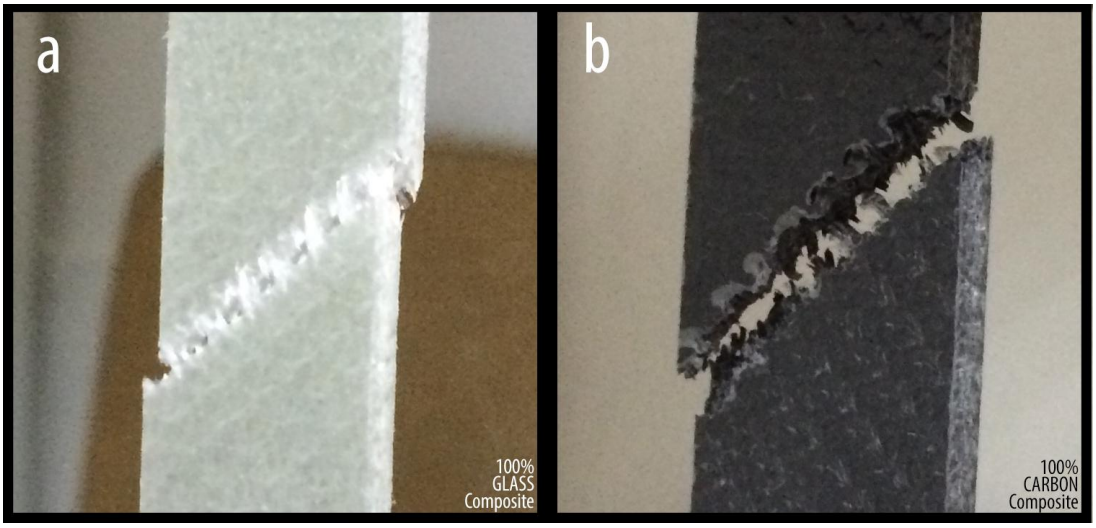

Figure 5.3 E_{45} knitted samples after the shear modulus tests (a) glass (b) carbon knitted composite samples

Shear modulus of the 100% carbon and 100% glass knitted composites were given in Table 5.3. The shear modulus of the carbon knitted composites was found to be higher than the shear modulus of glass knitted composites.

ASTM D 5379 standard was used to determine the shear properties in the wale direction (S_{WC}) and in the course direction (S_{CW}) of carbon and glass knitted composites. The S_{WC} and S_{CW} have been found with the dividing of maximum load by the cross-sectional area of the samples. The shear tests (Figure 5.4) were repeated 5 times for glass and carbon knitted composite samples and the average results were given in Table 5.3. As can be understood from the Table 5.3, the shear modulus of the carbon knitted composites in the wale direction and in the course direction were higher than the glass knitted composites. While the shear strength of carbon knitted composites in the wale direction was higher than the glass knitted composites, the shear strength of glass knitted composites in the course direction was found to be higher than the carbon knitted composites. This situation can be explained with the different behavior and geometrical effects of carbon and glass knitted composites in the wale and course directions.

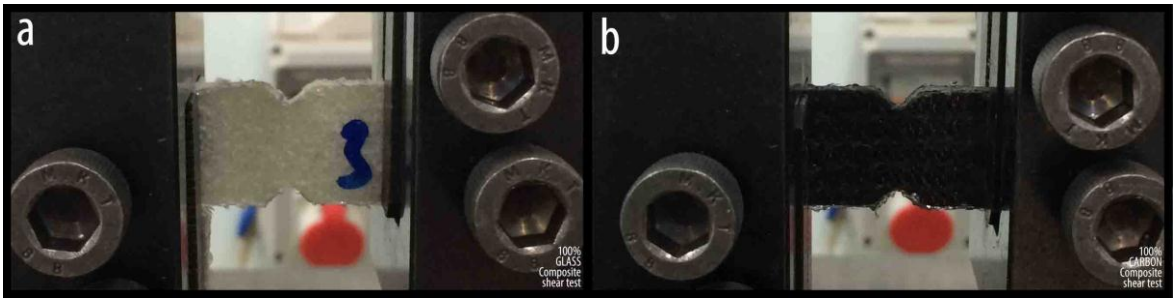

Figure 5.4 The shear test samples for (a) glass and (b) carbon knitted composites

Table 5.3 The shear properties of glass and carbon knitted composite samples

Shear properties	Carbon	Glass	Unit
In plane shear modulus, G_{WC}	4383.452	4278.197	MPa
In plane shear strength in the wale direction, S_{WC}	51.943	40.332	MPa
In plane shear strength in the course direction, S_{CW}	46.229	36.213	MPa

5.1.4. Determination of Fracture Toughness

Fracture toughness tests (Figure 5.5) has been implemented using Arcan test apparatus to pure carbon and pure glass (100%) knitted non-hybrid composite samples and glass-carbon knitted (50%-50%) hybrid composite samples with different pattern widths as 50 mm, 25 mm and 12.5 mm at 0°, 30°, 45°, 60°, and 90° loading angle. Universal U-TEST tension and compression machine with 50kN capacity found in Usak University was used for the fracture toughness tests and experiments were carried out at room temperature with 1 mm/min cross-head speed.

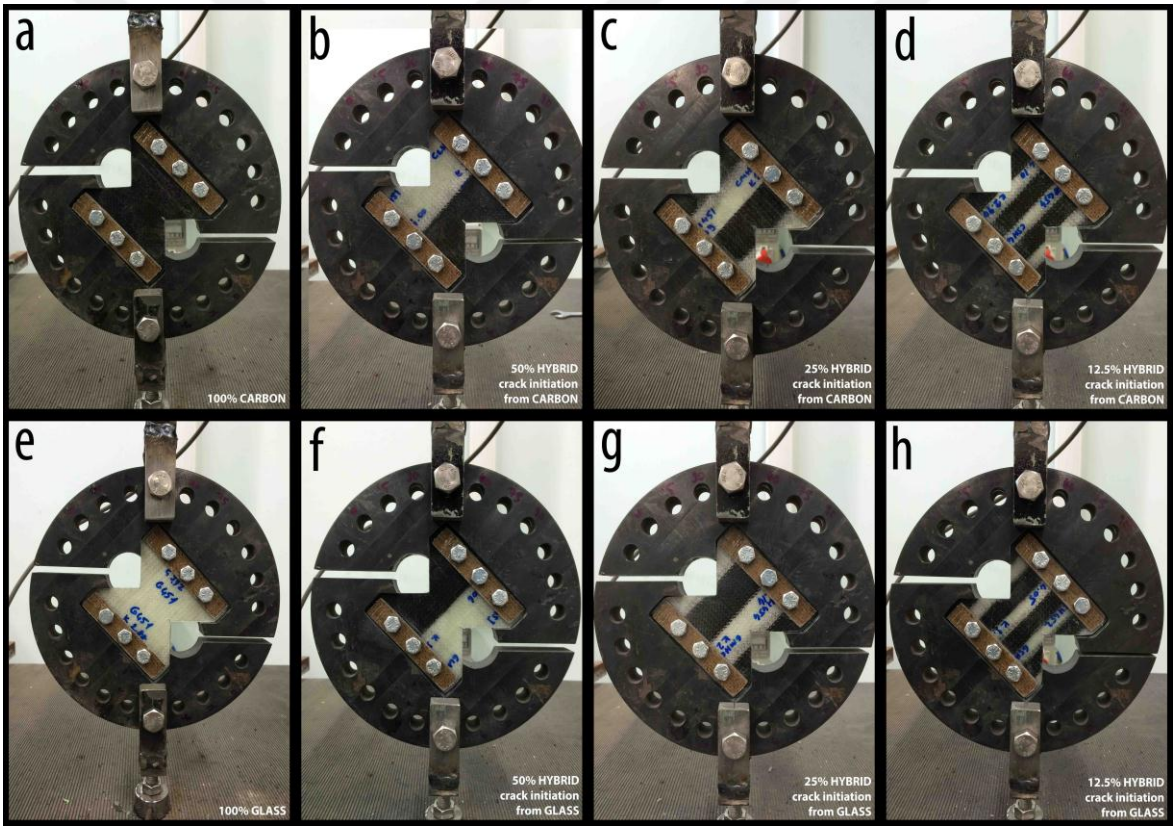

Figure 5.5 The fracture toughness test samples and located in the arcan apparatus in 45° loading angle; a) non-hybrid carbon sample and hybrid glass-carbon samples with crack initiation from carbon side b) 50mm, c) 25mm, and d) 12.5mm pattern width and e) non-hybrid glass sample and hybrid glass-carbon samples with crack initiation from glass side f) 50mm, g) 25mm, and h) 12.5mm pattern widths

The values of fracture toughness for the opening mode (mode I) and shearing mode (mode II) were found using the following formulas. The strees intensity factor, K_C, at the tip of the crack for the Arcan test tension specimens is given by;

$$K_C = \frac{P_{max}\sqrt{\pi a}}{wt} f\left(\frac{a}{w}\right) \tag{5.2}$$

In this equation 5.2, P_{max} is referred to the maximum load values in the stress-strength curve, a is represent the crack length, w is the specimen width, t is the specimen thickness, and f (a/w) is geometrical factor. The primary requirements are linear elastic fracture mechanics and plane strain conditions. The layers of the composite samples contain weak planes and presence of those planes oftenly cause subjection of interlaminar fracture to a mixed-mode stress field. The stress intensity factors ahead of the crack tip for arcan test sample were calculated by using the following equations 5.3:

$$K_I = \frac{P_{max}\sqrt{\pi a}}{wt} f_I\left(\frac{a}{w}\right), \qquad K_{II} = \frac{P_{max}\sqrt{\pi a}}{wt} f_{II}\left(\frac{a}{w}\right) \tag{5.3}$$

The geometric factor formulas f_I (a/w) and f_{II} (a/w) used to calculate the K_I and K_{II} were provided below [91].

$$f_I\left(\frac{a}{w}\right)(\alpha = 0°) = 182.12\left(\frac{a}{w}\right)^4 - 293.81\left(\frac{a}{w}\right)^3 + 187.87\left(\frac{a}{w}\right)^2 - 51.492\left(\frac{a}{w}\right) + 6.1137$$

(5.4)

$$f_{II}\left(\frac{a}{w}\right)(\alpha = 90°) = -18.622\left(\frac{a}{w}\right)^4 + 36.753\left(\frac{a}{w}\right)^3 - 25.182\left(\frac{a}{w}\right)^2 + 7.759\left(\frac{a}{w}\right) + 0.0944$$

The fracture toughness values calculated as a result of experiments conducted using arcan test apparatus at 0°, 30°, 45°, 60° and 90° were given in the Table 5.4 and results were schematically shown in Figure 5.6.

Table 5.4 The fracture toughness values of non-hybrid and hybrid samples

Non-hybrid samples			Hybrid samples					
Loading Angle (°)	**Pure carbon**	**Pure glass**	**crack initiation from carbon side Pattern width (mm)**			**crack initiation from glass side Pattern width (mm)**		
			50	**25**	**12.5**	**50**	**25**	**12.5**
0	756.721	508.484	535.066	677.246	692.886	515.518	557.984	652.178
30	570.504	431.082	491.149	522.013	541.157	458.289	499.189	534.788
45	505.456	353.545	437.049	443.622	453.799	401.241	429.620	436.881
60	398.244	255.106	311.794	318.965	339.607	294.930	310.871	329.759
90	215.920	110.971	166.848	178.829	210.289	132.823	145.567	162.961

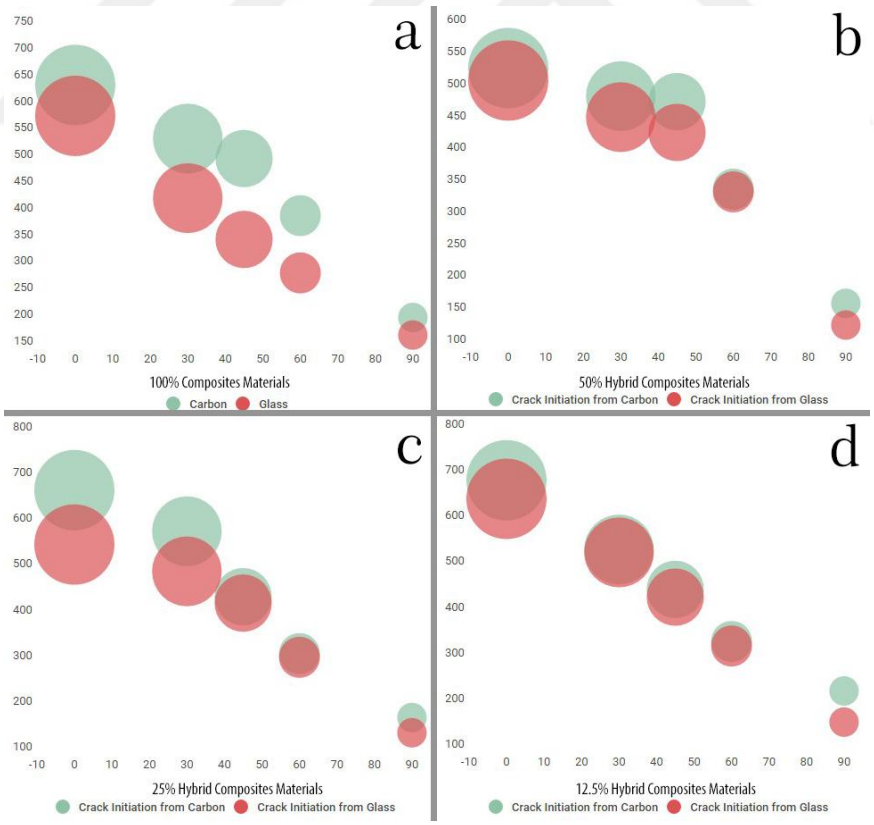

Figure 5.6 The average fracture toughness values (a) pure carbon and pure glass knitted samples and glass-carbon hybrid knitted samples with (b) 50mm, (c) 25mm and (d) 12.5mm pattern widths

CHAPTER SIX

Finite Element Analysis

Program Overview: ANSYS 17.0

Fracture Analysis

Calculation of Fracture Toughness

6.1. Introduction

Fracture toughness values of the pure glass (100%) and pure carbon (100%) knitted composites and also with 12.5mm, 25mm and 50mm pattern widths hybrid glass-carbon composite materials were determined by using ANSYS 17.0 software. In this chapter, the analysis of composite materials will be explained as an example.

6.2. Program Overview: ANSYS 17.0

ANSYS 17.0 software allows us to determine the mechanical properties of a material under certain operating conditions. This program can also work with many drawing programs in an integrated manner and gives you an opportunity to design the material that will be analyzed, with other programs. During the analysis with this program, many analyses can be studied in an integrated way with each other simultaneously. The desktop image which is come with the start of the program, is shown in Figure 6.1. Project can be created with double click on the desired type of analysis from the **Analysis Systems** section. Then, by following the necessary steps and make the required analysis the mechanical properties of the material can be determined. We should not forget that the finite element analysis does not reflect reality, but it enables us to obtain realistic data.

6.3. Fracture Analysis

6.3.1. Defining the Material Properties

After opening the ANSYS 17.0 program, Static Structural was selected from the Analysis Systems section. **Engineering Data** was selected from the Analysis scheme. By selecting the orthotropic material from incoming window, experimentally obtained properties of the material was entered as shown in Figure 6.2.

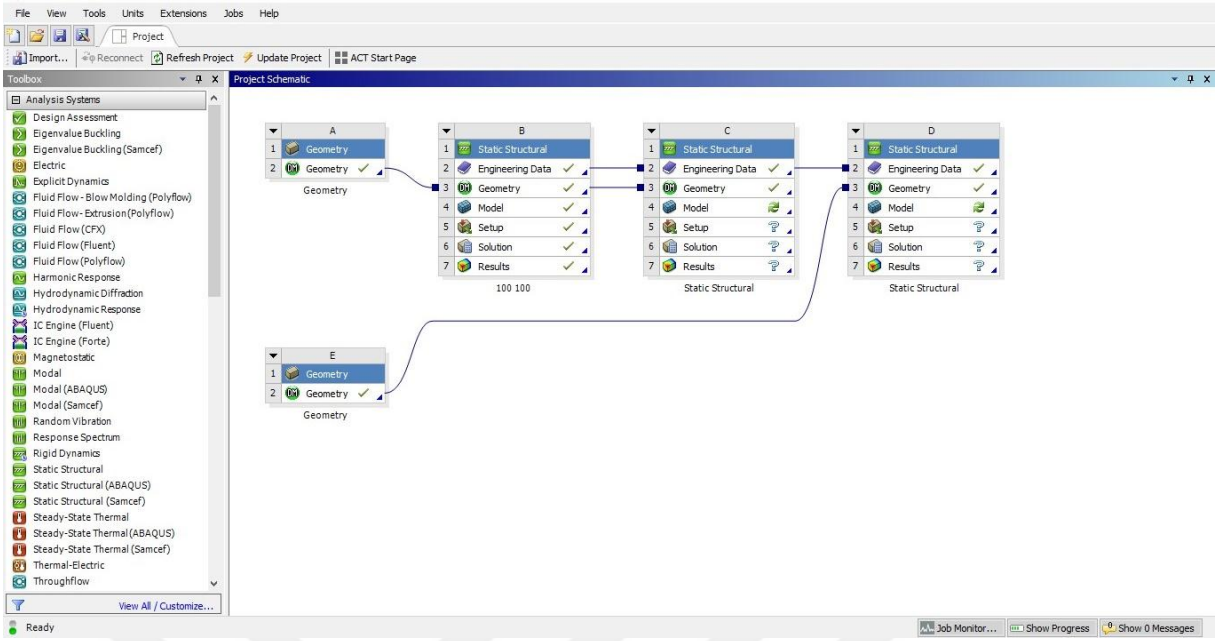

Figure 6.1 Desktop image of ANSYS 17.0

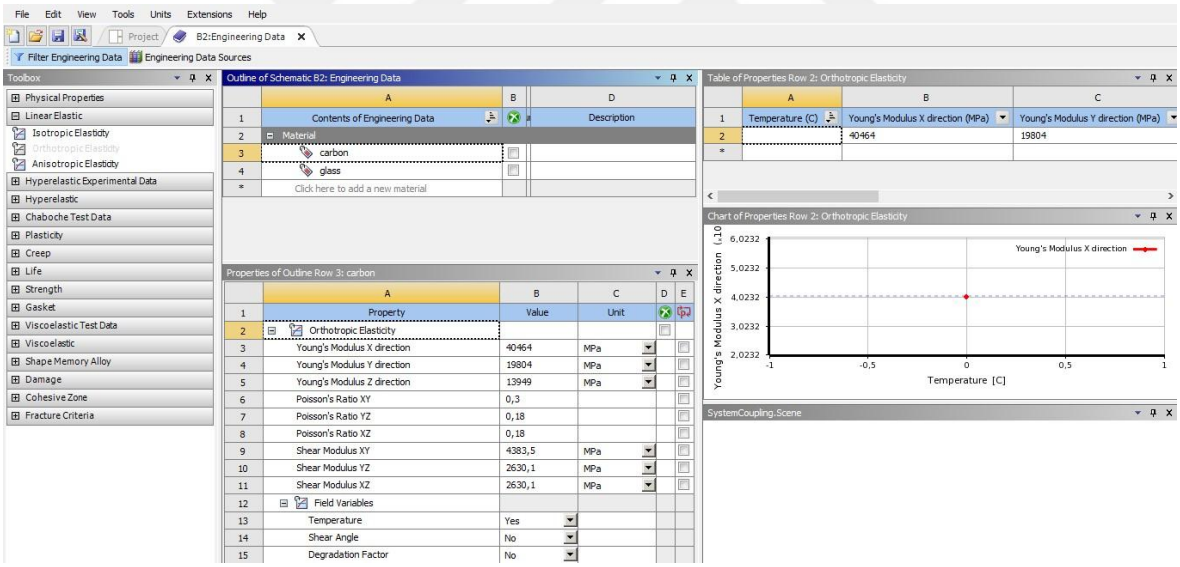

Figure 6.2 Defining the material properties

The experimental properties of the pure glass and pure carbon knitted composites were shown in Table 6.1. In this table, E_T, G_{WT}, G_{CT}, ν_{WC}, ν_{WT} and ν_{CT} values could not be determined, hence these properties were assumed according to literature [92-96].

$$E_T = 0.6E_C$$

$$G_{WT} = G_{CT} = 0.6G_{WC} \tag{6.1}$$

$$v_{WT} = v_{CT} = 0.6v_{WC}$$

Table 6.1 Mechanical properties of carbon and glass composites

Properties	Pure Carbon	Pure Glass	unit
E_W	40463.557	27496.450	MPa
E_C	19803.811	21895.165	MPa
E_T	11882.287	13137.099	MPa
G_{WC}	4383.452	4278.197	MPa
G_{WT}=G_{CT}	2630.071	2566.918	MPa
ν_{WC}	0.300	0.300	-
ν_{WT}=ν_{CT}	0.180	0.180	-
W_t	143.172	74.952	MPa
C_t	118.856	65.026	MPa
W_C	103.349	99.476	MPa
C_C	84.476	80.762	MPa
S_{WC}	51.943	40.332	MPa
S_{CW}	46.229	36.213	MPa

6.3.2. Modelling of the Test Sample

By selecting the Geometry from the project scheme the arcan test sample can be modelled in desired sizes (Figure 6.3).

6.3.3. Appointment of the Material Properties

By selecting the **Model** from the project scheme, data entry can be started. As shown in Figure 6.4 previously made data inputs were called for each material at this stage. In this analysis, for the 12.5mm pattern width of hybrid composite materials with a crack initiation from carbon side, appointment was made from top to bottom as C-G-C-G-C-G-C-G (C: Pure carbon pattern and G: Pure glass pattern).

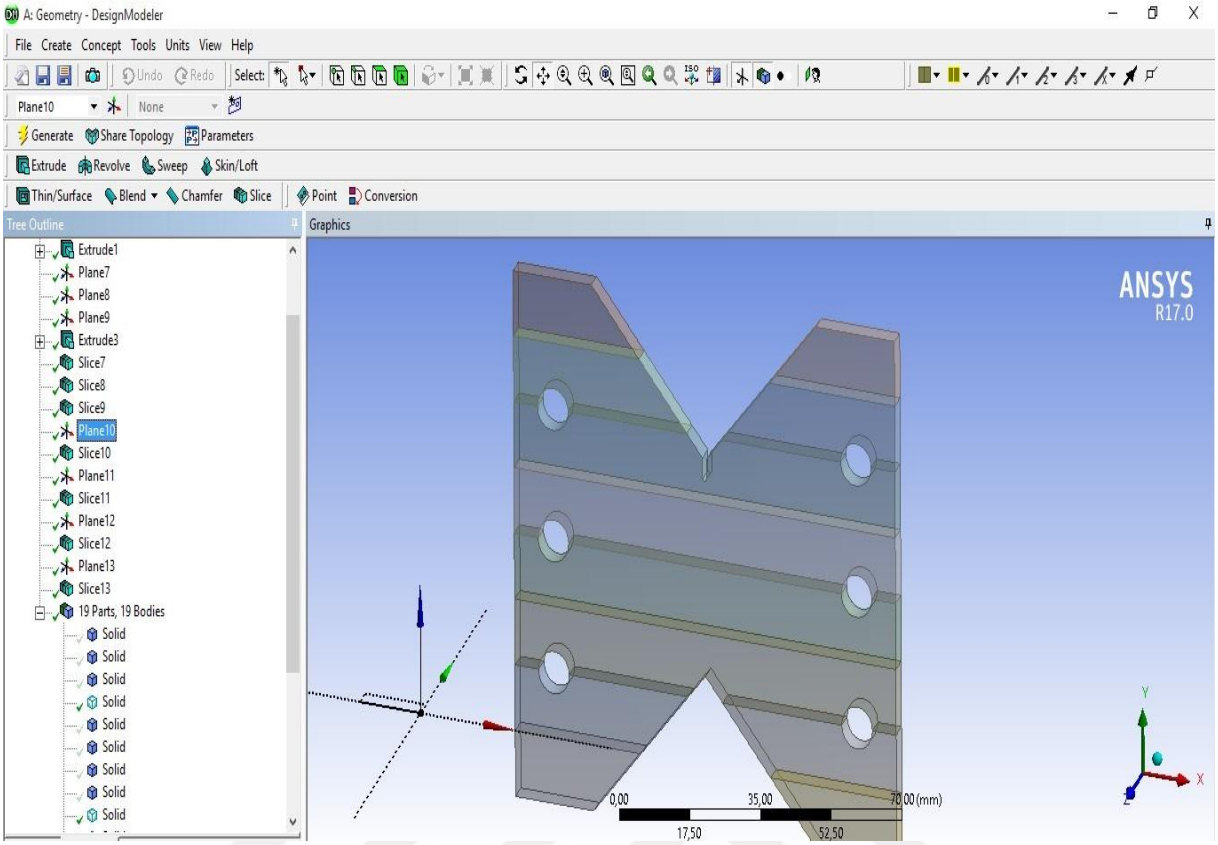

Figure 6.3 The solid model of the arcan test sample

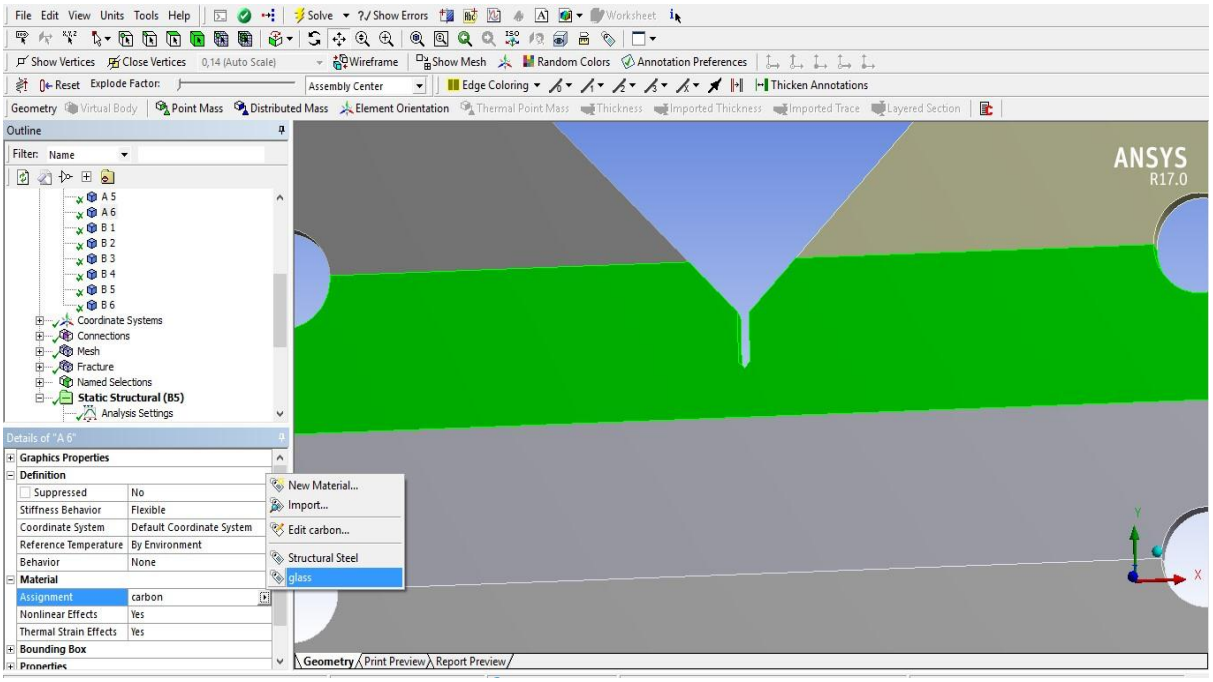

Figure 6.4 Entering material properties

6.3.4. Creation of the Coordinate System

Coordinates were generated to the crack tip as shown in the Figure 6.5 to identify the beginning of the crack.

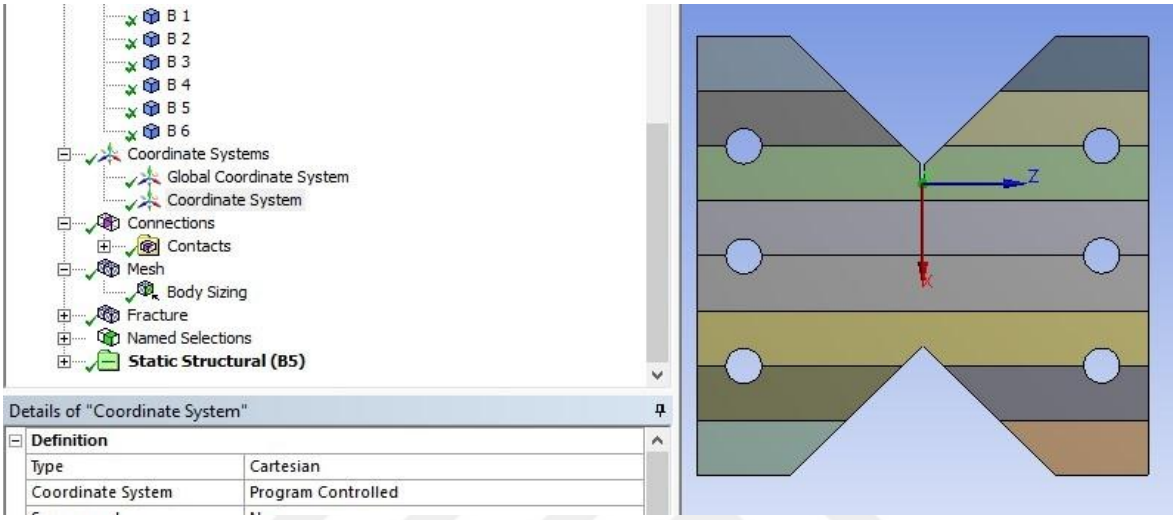

Figure 6.5 Creating a coordinate system of arcan test sample

6.3.5. Meshing Procedure

Finite elements method works by reducing the infinite number of points to finite numbers on the material. This method is called as **meshing**. With this method, the infinite points on the part of a car can be made finite. This reduced points are called the as **node**. With combining the nodes 1, 2 or 3 dimensional shapes can be created. Each of these created shapes is called as **element**. Thus, the design would have become the finite element model. Figure 6.6 shows the finite element model which was established for hybrid glass-carbon composite samples. In meshing, the error rate in the transition region between the mesh and refinement is minimized.

6.3.6. Identification of Crack Zone

To define the crack zone, "model/insert/named selection" was selected from Outline and crack is indicated as seen in the Figure 6.7. After that the crack was brought to nodal form by right-clicking.

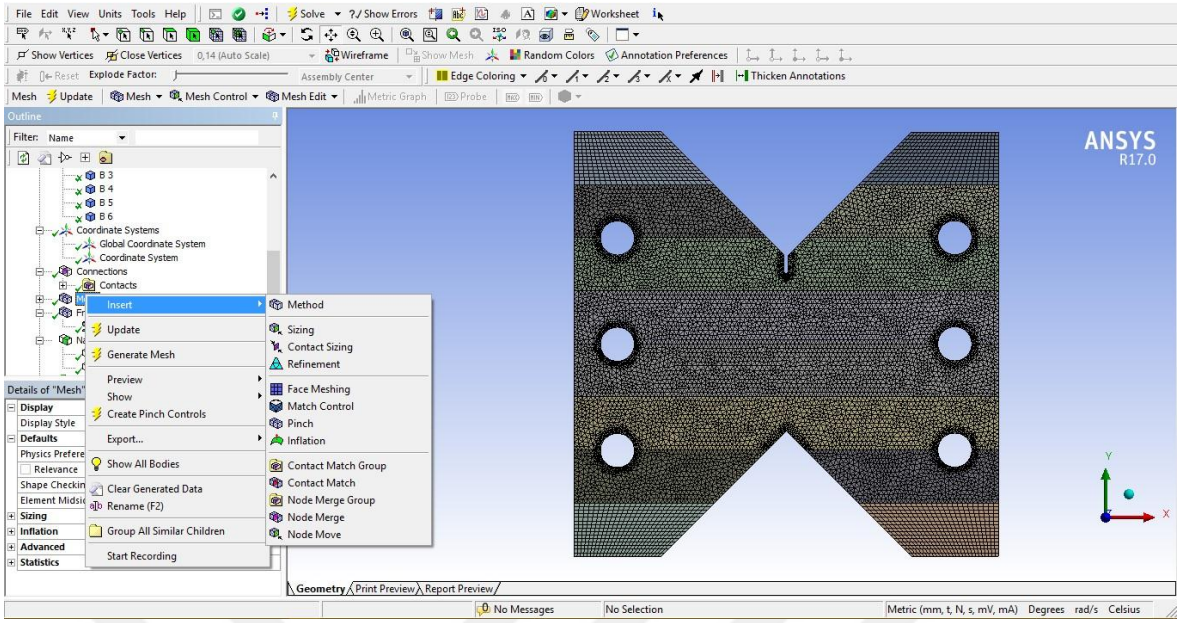

Figure 6.6 Meshing of arcan test sample

Figure 6.7 Defining the crack zone

6.3.7. Identification of Fracture Contour

To determine the fracture contours, "model/insert/fracture" was selected from **Outline** and defined selection was selected by right clicking on the fracture and selecting pre-meshed crack, as shown in Figure 6.8.

6.3.8. Loading and Boundary Conditions

As shown on the model in Figure 6.9, boundary conditions were entered. You can perform this procedure by right clicking on the static structural from Outline.

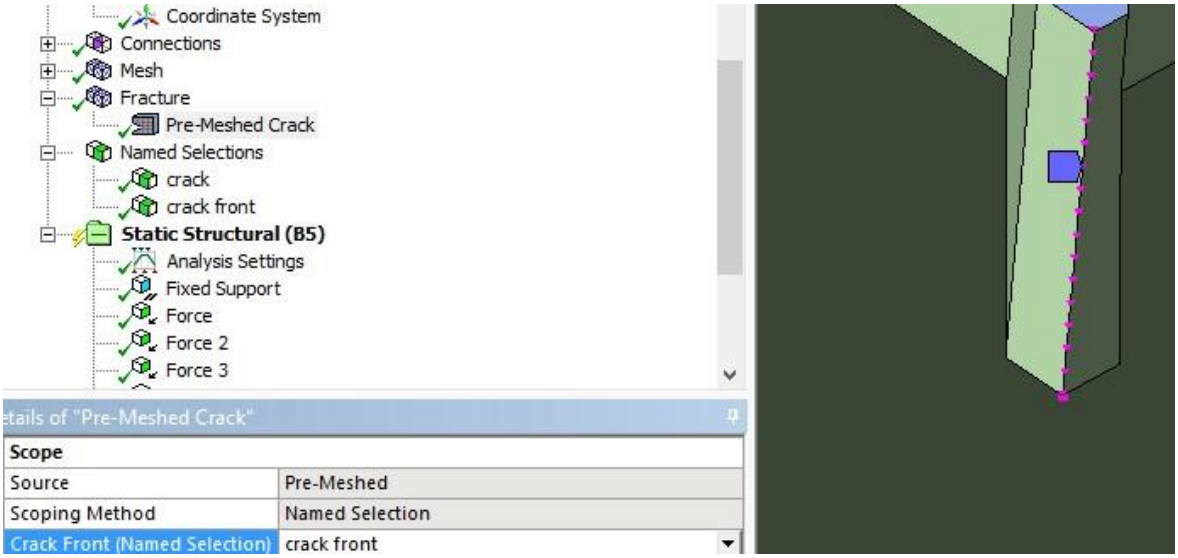

Figure 6.8 Illustration of Fracture Contours

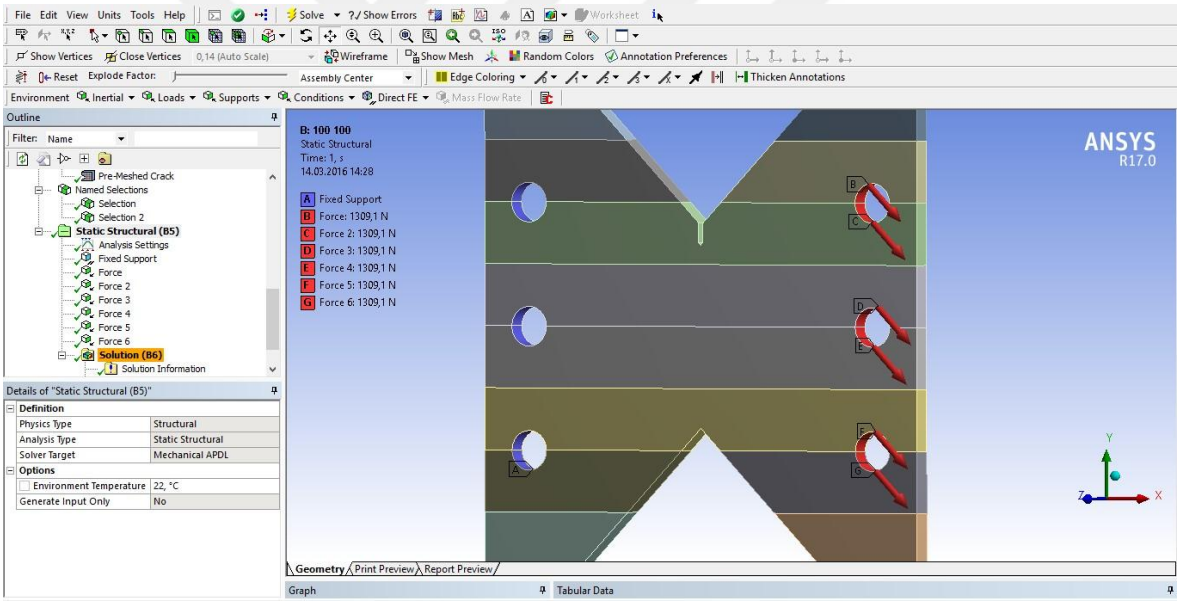

Figure 6.9 Entering the boundary conditions

6.3.9. Identification of the Output Results

The output results were defined by right-clicking on solution from Outline. To make fracture analysis, fracture tool was selected and then pre-mesh crack was selected from crack selection. After these processes, results can be gotten by clicking on solve.

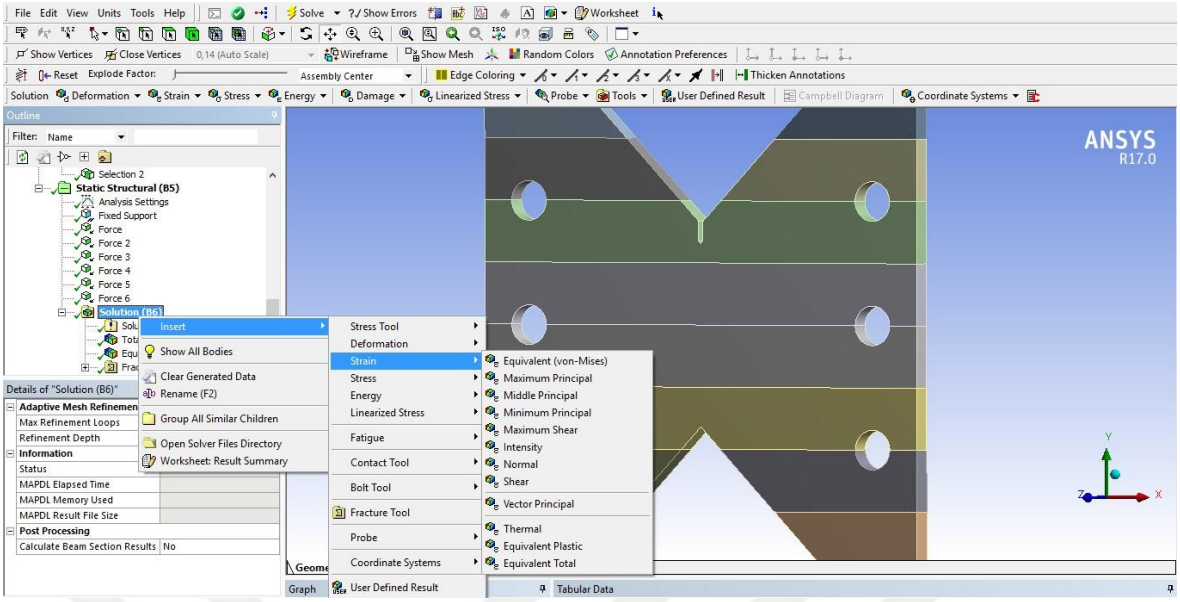

Figure 6.10 Determination of the output results

6.3.10. Reading the Results

After solution, the composed damage on the crack tip can be seen in Figure 6.11. J-integral values were calculated for each contour in the crack tip. Convergence to the actual value can be made based on the value of the concentrated contour frequency. The distribution of J-integral values thought the crack tip can be seen Figure 6.12.

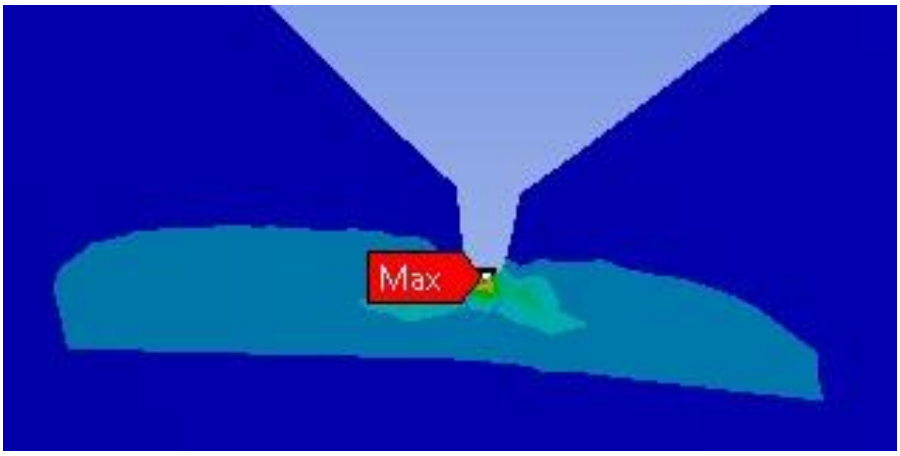

Figure 6.11 Stresses at the crack tip

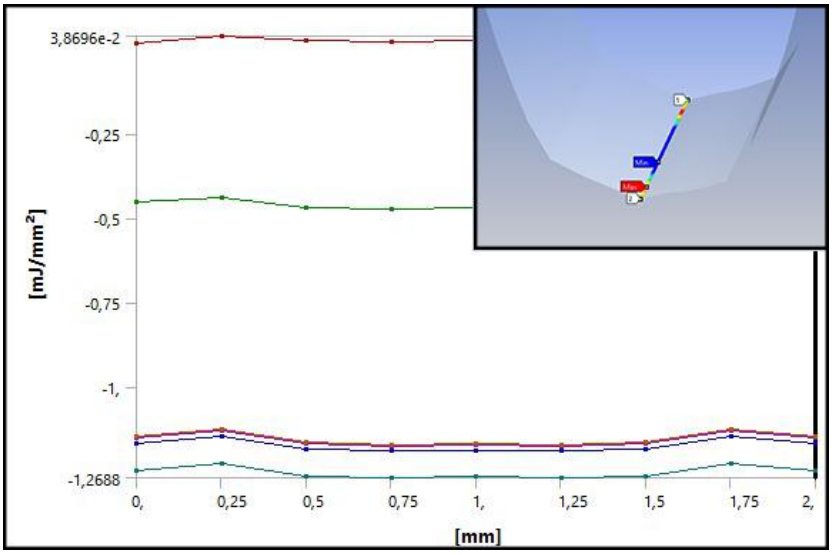

Figure 6.12 Distribution of J-integral values through the crack tip

6.4. Calculation of Fracture Toughness

In linear elastic fracture mechanics, the following equation 6.2 is valid between the fracture stress intensity factor (K) and the J-integral value for plane stress and plane strain cases. During the analysis, if the thickness of the material is neglected, plane stress condition is applicable and if it is included in the solution, the plane strain condition is applicable. Depending on the J-integral value obtained from finite element numerical analysis, fracture toughness was determined according to equation 6.2 for plane strain condition [97-100].

$$K_I = \begin{cases} \sqrt{JE} & (Plane\ stress) \\ \sqrt{\dfrac{JE}{1-v^2}} & (Plane\ strain) \end{cases} \tag{6.2}$$

The J-integral values obtained from finite element methods were given in Table 6.2, and calculated fracture toughness values can be seen in Table 6.3. As can be understood from the table, when going towards 0° to 90° a reduction has occurred in the J-integral and toughness values.

Table 6.2 J-integral values obtained from ANSYS finite element software

Non-hybrid samples			Hybrid samples					
Loading Angle (°)	**Pure carbon**	**Pure glass**	**crack initiation from carbon side Pattern width (mm)**			**crack initiation from glass side Pattern width (mm)**		
			50	**25**	**12.5**	**50**	**25**	**12.5**
0	24.860	9.830	13.010	21.510	19.240	11.800	14.300	19.370
30	14.160	8.210	11.630	11.920	11.510	8.030	10.830	12.651
45	12.300	5.790	8.130	8.630	8.630	6.910	8.440	9.160
60	7.920	2.470	4.090	4.840	4.930	3.110	4.330	4.980
90	2.260	0.470	1.320	1.410	1.901	0.660	0.910	1.210

Table 6.3 Calculated fracture toughness values

Non-hybrid samples			Hybrid samples					
Loading Angle (°)	**Pure carbon**	**Pure glass**	**crack initiation from carbon side Pattern width (mm)**			**crack initiation from glass side Pattern width (mm)**		
			50	**25**	**12.5**	**50**	**25**	**12.5**
0	735.540	486.329	532.099	684.186	647.077	532.837	586.572	682.682
30	555.118	444.452	503.088	509.321	500.485	439.553	510.467	551.707
45	517.376	373.244	420.629	433.370	433.370	407.749	450.635	469.463
60	415.161	243.782	298.343	324.546	327.550	273.548	322.773	346.153
90	221.770	106.341	169.489	175.171	203.344	126.016	147.970	170.768

CHAPTER SEVEN

Results and Discussion

Evaluation of Test Results

Pure Carbon Knitted Composites

Hybrid Knitted Composites with 50mm Pattern Width (Crack Initiation from Carbon Side)

Hybrid Knitted Composites with 25mm Pattern Width (Crack Initiation from Carbon Side)

Hybrid Knitted Composites with 12.5mm Pattern Width (Crack Initiation from Carbon Side)

Pure Glass Composites

Hybrid Knitted Composites with 50mm Pattern Width (Crack Initiation from Glass Side)

Hybrid Knitted Composites with 25mm Pattern Width (Crack Initiation from Glass Side)

Hybrid Knitted Composites with 12.5mm Pattern Width (Crack Initiation from Glass Side)

General evaluation of results

Evaluation of Scanning Electron Microscopy Images

Discussion

7.1. Introduction

In this chapter, the results of this thesis, which was supported by TUBITAK, will be discussed. The fracture values and fracture images, which were obtained by experiments and by calculating with ANSYS 17.0 program at different loading angles, were also compared. The experimental study was conducted at 0°, 30°, 45°, 60°, and 90° loading angles. However, the fracture toughness values of the non-hybrid and hybrid composite samples, which placed in the 15° and 75° angles, were not experimentally determined. The stress values for 15° and 75° angles were obtained via regression analysis by using the stress obtained from 0°, 30°, 45°, 60°, and 90° loading angles. And then these stresses were used in ANSYS finite element program and as a result, the fracture toughness values and the damaged images were numerically obtained for 15° and 75° loading angles. In the illustration in Figure 7.1, the fracture test angle and the loading direction were shown. The cross-head speed was selected as 1 mm/min for the Arcan fracture tests. The fracture toughness values were obtained experimentally and numerically for all angles and J-integral values were also given in tables and graphs and comparisons were made between each other.

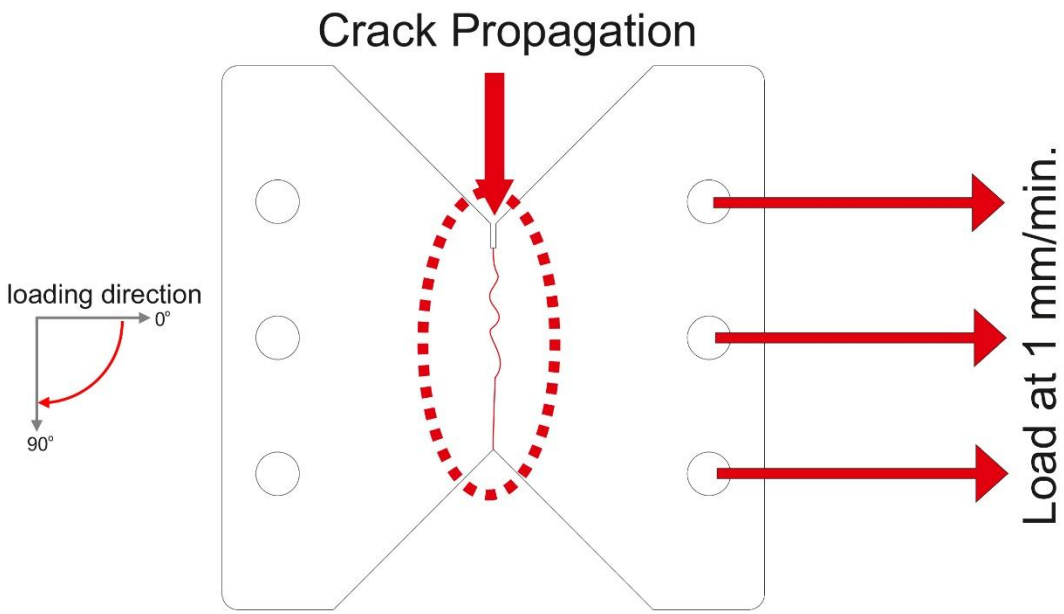

Figure 7.1 The illustration of crack propagation and the loading direction of arcan fracture test

7.2. Evaluation of the Test Results

7.2.1. Pure Carbon Knitted Composites

The fracture tests were carried out using arcan test apparatus for 0°, 30°, 45°, 60°, and 90° loading angles to obtain the fracture toughness values of pure carbon knitting composites, which have four layers and have produced by hand lay-up method. A numerical study was also performed by using ANSYS finite element program for all loading angles. The experimental and numerical fracture images were given in Figure 7.2. It is seen that the stress concentration was increased from 0° to 90°. In the ANSYS 17.0 program, to determine the fracture toughness for 15° and 75° angles, the stress values corresponding to these angles must be known. For this purpose, a regression approach was used and Figure 7.3 were drawn. The stresses for 15° and 75° angles were calculated according to Figure 7.3 with 1% error and the fracture toughness values were calculated using ANSYS finite element program for the mentioned angles.

The fracture toughness and J-integral values obtained from finite element analysis and experimental study were given in Table 7.1 and Figure 7.4 The errors between these values were also given for comparison. The fracture toughness tests were repeated 5 times for each material and the fracture toughness values were obtained by averaging the found results. When the Table 7.1 and Figure 7.4 were examined, it was obviously seen that J-integral values, which were determined from experimental and numerical fracture toughness values, decrease from 0° to 90° loading angles. So the most suitable angle for the fracture toughness can be stated as 90°. The highest and lowest error values between the experimental and numerical fracture toughness values (without taking into account the 15° and 75° loading angles) were obtained from the pure carbon knitted composite samples with 60° loading angles and with 45° loading angles, respectively. The maximum and minimum errors in J-integral were also obtained in the samples with 60° and with 45° loading angles depending on these results.

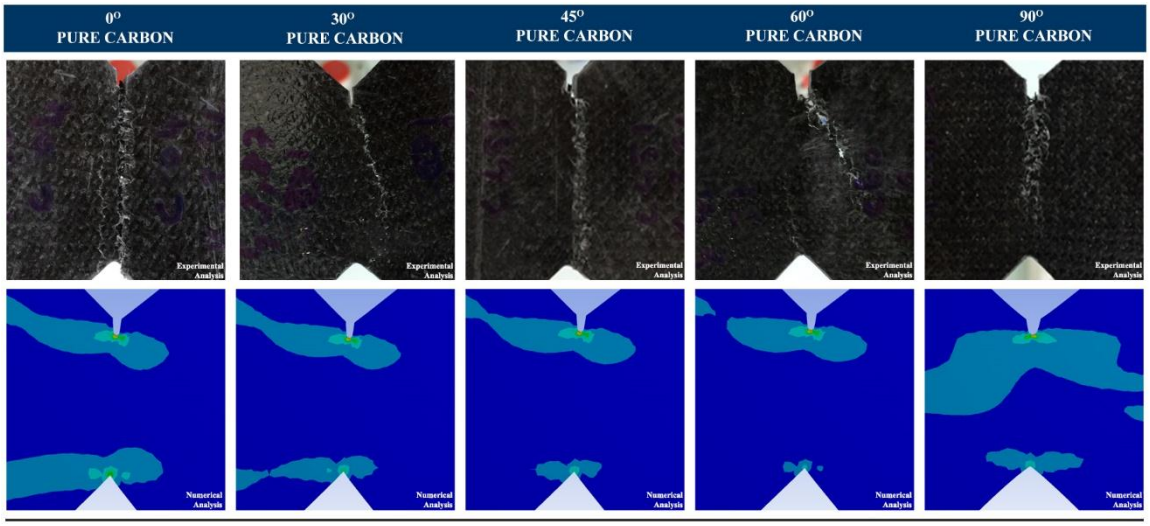

Figure 7.2 The experimental and numerical damage images of pure carbon knitted composite samples

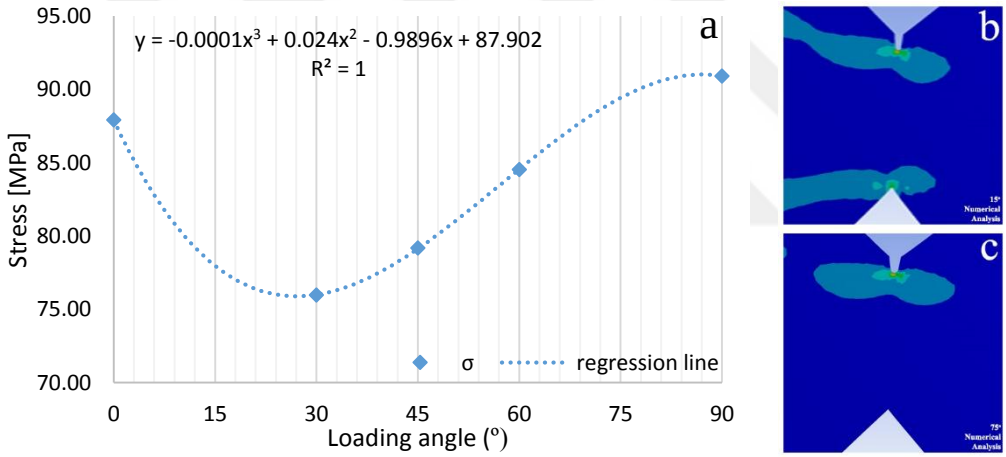

Figure 7.3 The stress-loading angles curve for pure carbon knitted composite samples (a) and numerical damage images for 15° (b) and 75° (c) loading angles

Table 7.1 The fracture toughness and J-integral values of the pure carbon knitted composite samples

Loading angles (°)	$(K_{EFF})_{EXP}$ (Mpa.mm$^{0.5}$)	$(K_{EFF})_{NUM}$ (Mpa.mm$^{0.5}$)	Error (%)	$(J_{EFF})_{EXP}$ (Mpa.mm)	$(J_{EFF})_{NUM}$ (Mpa.mm)	Error (%)
0	756.721	735.541	2.80	26.313	24.860	5.52
15	728.853	710.552	2.51	24.407	23.200	4.95
30	570.504	555.125	2.70	14.956	14.160	5.32
45	505.456	517.383	2.36	11.740	12.300	4.77
60	398.244	415.166	4.25	7.288	7.920	8.68
75	278.607	270.811	2.80	3.566	3.370	5.51
90	215.920	221.774	2.71	2.142	2.260	5.49

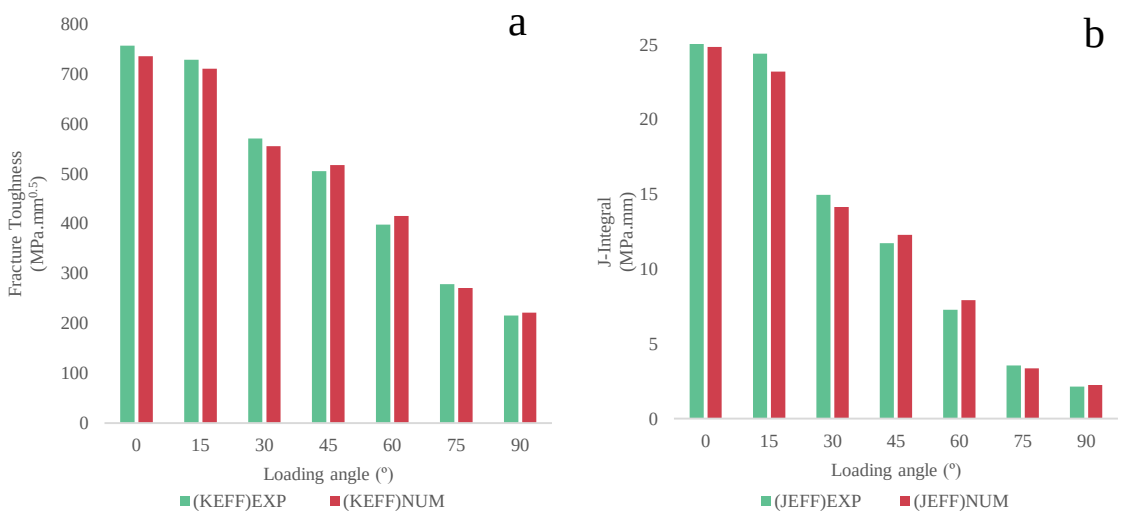

Figure 7.4 The fracture toughness (a) and J-integral (b) variation depending on the loading angles of the pure carbon knitted composite samples

7.2.2. Hybrid Knitted Composites with 50mm Pattern Width (Crack Initiation from Carbon Side)

The experimental and numerical damage images of hybrid glass-carbon knitted composite samples with 50mm pattern width (crack initiation from carbon side) were shown in Figure 7.5. It can be seen from this figure that the carbon part of hybrid knitted composite samples were carried loads from the fulcrum point and because the carbon fiber is more brittle than the glass fiber, a momentary fracture was occurred. When the crack reached to the glass part, the propagation of the crack has slowed due to the ductility of glass part and fracture was occurred at the end. The stress-loading angles curve for hybrid glass-carbon knitted composite samples with 50mm pattern width (crack initiation from carbon side) was shown in Figure 7.6a. The regression approach was applied in this figure for the 15° and 75° loading angles. As a result, the stresses for the 15° and 75° loading angles were obtained with 16.35% error and then the numerical fracture toughness values were determined for the 15° and 75° loading angles using ANSYS finite element program.

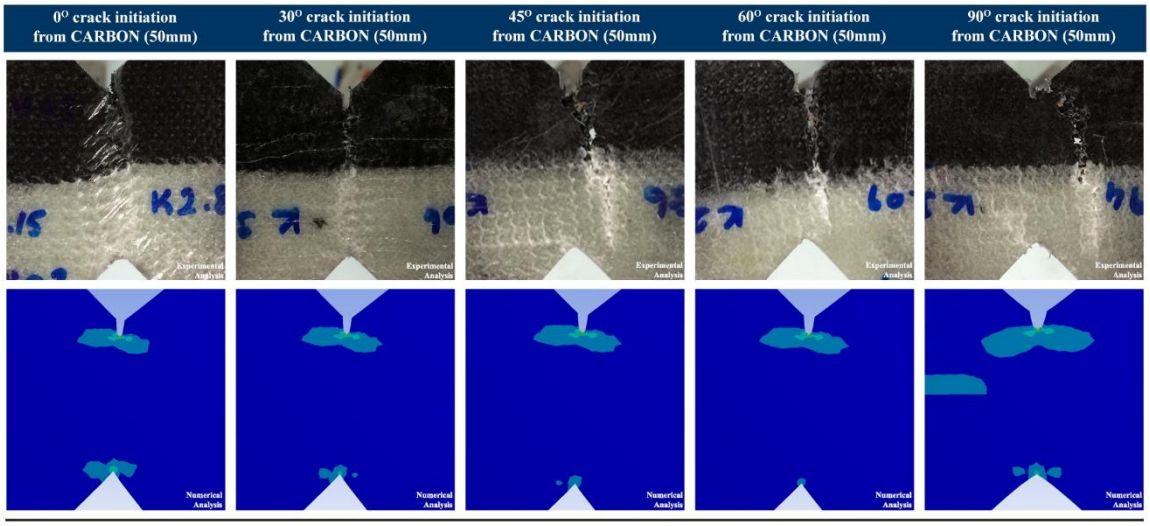

Figure 7.5 The experimental and numerical damage images of hybrid glass-carbon knitted composite samples with 50mm pattern width (crack initiation from carbon side)

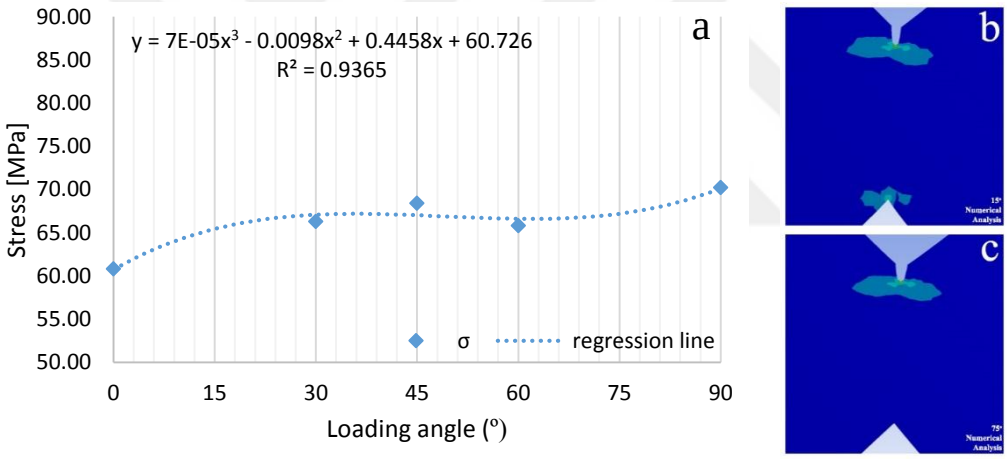

Figure 7.6 The stress-loading angles curve for hybrid glass-carbon knitted composite samples with 50mm pattern width (crack initiation from carbon side) (a) and numerical damage images for 15° (b) and 75° (c) loading angles

The experimental fracture toughness and the J-integral values of hybrid glass-carbon knitted composite samples with 50mm pattern width (crack initiation from carbon side) were given in Table 7.2 and Figure 7.7 by taking the average of five experimental data's. The numerical fracture toughness and the J-integral values of hybrid glass-carbon knitted composite samples with 50mm pattern width (crack initiation from carbon side) were also given in these table and figure. It can be seen from obtained figure and table that there is a

decrease in the fracture toughness and the J-integral values when the loading angles is going towards 0° to 90°. As a result of error between experimental and numerical fracture toughness values, the lowest error was observed as 0.55% for the sample subjected to 0° loading angle and the highest error was obtained as 4.31% in the sample with 60° loading angle. The highest and lowest error in the J-integral values were also occurred in the samples with 60° as 8.44% and in the samples with 0° as 1.11% depending on the fracture toughness values.

Table 7.2 The fracture toughness and the J-integral values of hybrid glass-carbon knitted composite samples with 50mm pattern width (crack initiation from carbon side)

Loading angles (°)	$(K_{EFF})_{EXP}$ (Mpa.mm$^{0.5}$)	$(K_{EFF})_{NUM}$ (Mpa.mm$^{0.5}$)	Error (%)	$(J_{EFF})_{EXP}$ (Mpa.mm)	$(J_{EFF})_{NUM}$ (Mpa.mm)	Error (%)
0	535.066	532.099	0.55	13.156	13.010	1.11
15	498.415	506.966	1.72	11.415	11.810	3.46
30	491.149	503.088	2.43	11.085	11.630	4.92
45	437.049	420.629	3.76	8.777	8.130	7.37
60	311.794	298.343	4.31	4.467	4.090	8.44
75	196.144	192.344	1.94	1.768	1.700	3.84
90	166.848	169.489	1.58	1.279	1.320	3.19

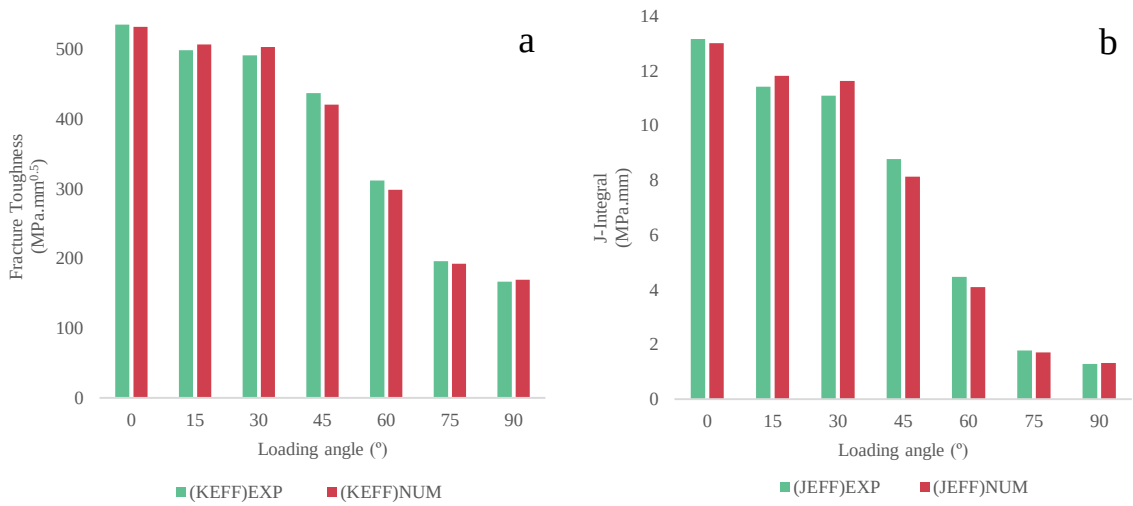

Figure 7.7 The fracture toughness (a) and J-integral (b) variation depending on the loading angles of hybrid glass-carbon knitted composite samples with 50mm pattern width (crack initiation from carbon side)

7.2.3. Hybrid Knitted Composites with 25mm Pattern Width (Crack Initiation from Carbon Side)

The experimental and numerical damage images of hybrid glass-carbon knitted composite samples with 25mm pattern width (crack initiation from carbon side) were shown in Figure 7.8. Although, the crack propagation was straight for the 0° and 90° loading angles, the propagation was not found straight for 30°, 45°, and 60° loading angles. The stress versus loading angles curve for hybrid glass-carbon knitted composite samples with 25mm pattern width (crack initiation from carbon side) was shown in Figure 7.9a. The stresses, which cannot be calculated as experimentally, for the 15° and 75° loading angles were obtained with 13.25% error by using regression approach. As a result, the numerical fracture toughness values were determined for the 15° and 75° loading angles using ANSYS finite element program. The stress concentration at the crack tip were illustrated for the 15° and 75° loading angles in Figure 7.9b and Figure 7.9c, respectively.

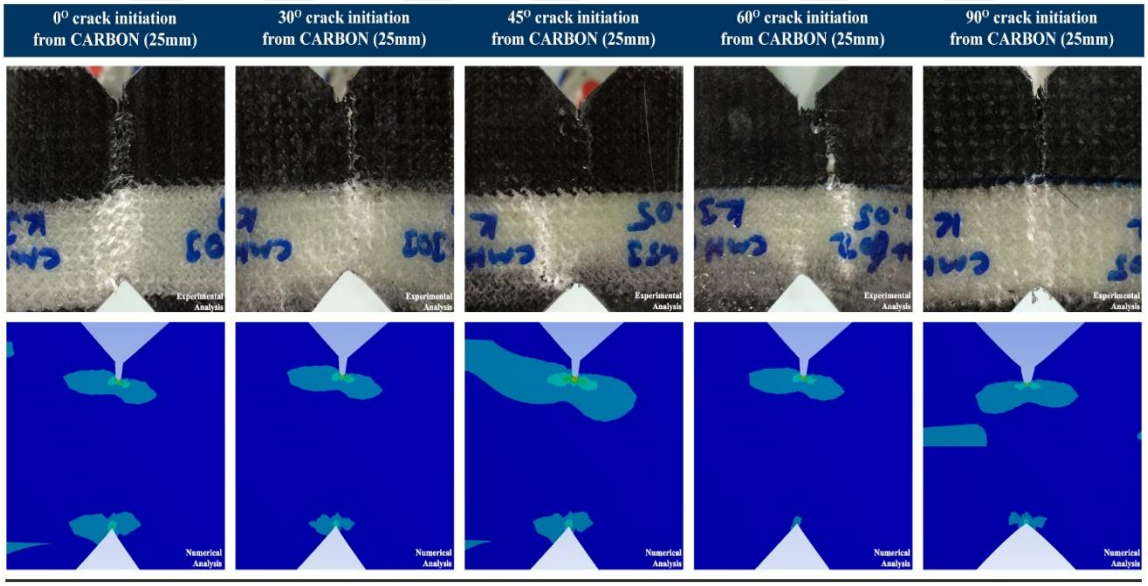

Figure 7.8 The experimental and numerical damage images of hybrid glass-carbon knitted composite samples with 25mm pattern width (crack initiation from carbon side)

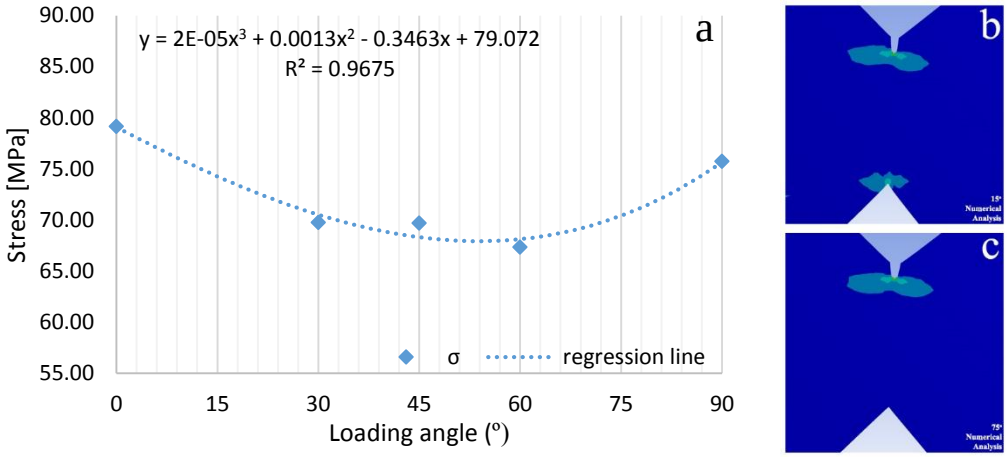

Figure 7.9 The stress-loading angles curve for hybrid glass-carbon knitted composite samples with 25mm pattern width (crack initiation from carbon side) (a) and numerical damage images for 15° (b) and 75° (c) loading angles

The experimental and numerical fracture toughness and the J-integral variation of hybrid glass-carbon knitted composite samples with 25mm pattern width (crack initiation from carbon side) were given in Table 7.3 and Figure 7.10. The data's, which were obtained by experimental study, were calculated by taking the average of five fracture toughness tests. When the Figure 7.10 and Table 7.3 for the hybrid glass-carbon knitted composite samples with 25mm pattern width were examined, it can be observed that the J-integral values with experimental and numerical fracture toughness values decrease towards 0° to 90° loading angles. The numerical and experimental fracture toughness values support one another in the range of 1.02% and 3.27% errors. While, the best fracture toughness value was found at 0° with 677.246 MPa.mm$^{0.5}$, the minimum fracture toughness values was observed at 90° with 178.829 MPa.mm$^{0.5}$.

Table 7.3 The fracture toughness and the J-integral values of hybrid glass-carbon knitted composite samples with 25mm pattern width (crack initiation from carbon side)

Loading angles (°)	$(K_{EFF})_{EXP}$ (Mpa.mm$^{0.5}$)	$(K_{EFF})_{NUM}$ (Mpa.mm$^{0.5}$)	Error (%)	$(J_{EFF})_{EXP}$ (Mpa.mm)	$(J_{EFF})_{NUM}$ (Mpa.mm)	Error (%)
0	677.246	684.186	1.02	21.076	21.510	2.06
15	653.835	632.45	3.27	19.644	18.380	6.43
30	522.013	509.321	2.43	12.521	11.920	4.80
45	443.622	433.37	2.31	9.043	8.630	4.57
60	318.965	324.546	1.75	4.675	4.840	3.53
75	250.600	246.409	1.67	2.886	2.790	3.32
90	178.829	175.171	2.05	1.470	1.410	4.05

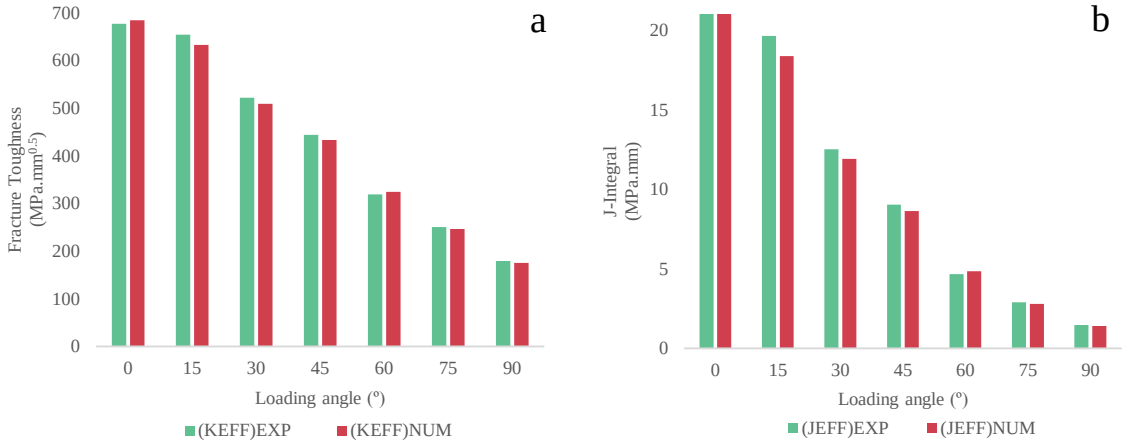

Figure 7.10 The fracture toughness (a) and J-integral (b) variation depending on the loading angles of hybrid glass-carbon knitted composite samples with 25mm pattern width (crack initiation from carbon side)

7.2.4. Hybrid Knitted Composites with 12.5mm Pattern Width (Crack Initiation from Carbon Side)

The experimental and numerical damage images of hybrid glass-carbon knitted composite samples with 12.5mm pattern width (crack initiation from carbon side) were shown in Figure 7.11. The difference crack propagation was occurred in the carbon and glass parts for 0°, 30°, 45°, 60°, and 90° loading angles. While the crack propagation was quick in the carbon reinforced regions due to fragility of carbon fabric, it was slower in glass reinforced regions than the carbon reinforced parts of the hybrid knitted composites due to ductility of glass fabrics. When the five different loading angles were examined carefully, the deviations were observed in the crack propagation, especially, for 30°, 45°, and 60° loading angles. The regression approach was applied (7.12a) to obtain the stress occurred for 15° and 75° loading angles which cannot calculated by experimentally. As seen in Figure 7.12, the stresses for 15° and 75° loading angles were calculated with 0.15% error (Figure 7.12a) and the damages for samples subjected to 15° and 75° loading angles were determined as illustrated in Figure 7.12b and Figure 7.12c using ANSYS finite element program.

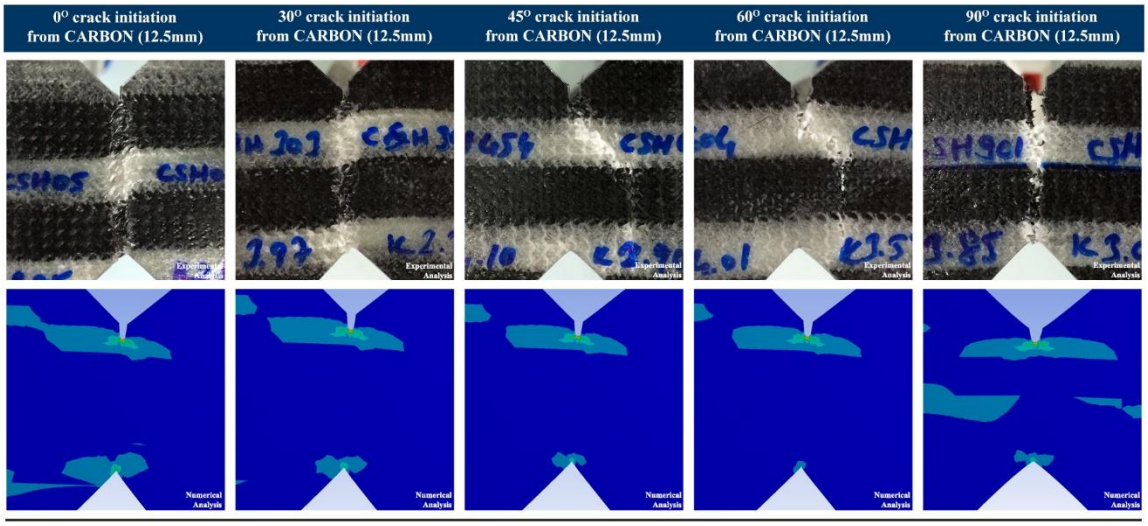

Figure 7.11 The experimental and numerical damage images of hybrid glass-carbon knitted composite samples with 12.5mm pattern width (crack initiation from carbon side)

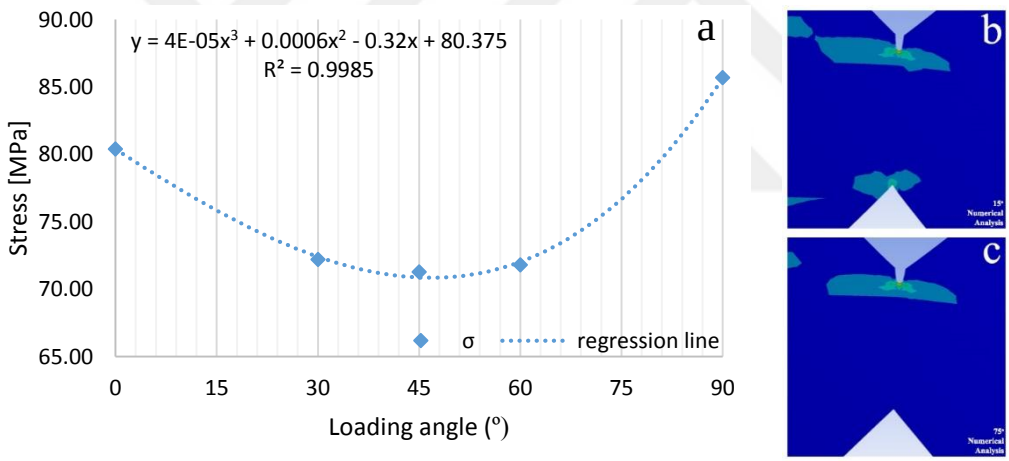

Figure 7.12 The stress-loading angles curve for hybrid glass-carbon knitted composite samples with 12.5mm pattern width (crack initiation from carbon side) (a) and numerical damage images for 15° (b) and 75° (c) loading angles

In Table 7.4 and Figure 7.13, after a series of experiments were conducted, the fracture toughness values of hybrid glass-carbon knitted composite samples with 12.5mm pattern width (crack initiation from carbon side) were calculated by taking the average of five experiments. When looking at the Table 7.4 and Figure 7.13, the highest fracture toughness and J-integral values were found at 0° loading angle. The fracture toughness and

J-integral values were decreased from 0° to 90° loading angles and the lowest fracture toughness value was found at 90° loading angle. The same trend was found for numerical fracture toughness and numerical J-integral values. When numerical and experimental fracture toughness values were compared to each other, the highest error was found for 30° loading angle as 7.52%, however, the best result was found as 3.30% for 90° loading angle.

Table 7.4 The fracture toughness and the J-integral values of hybrid glass-carbon knitted composite samples with 12.5mm pattern width (crack initiation from carbon side)

Loading angles (°)	$(K_{EFF})_{EXP}$ (Mpa.mm$^{0.5}$)	$(K_{EFF})_{NUM}$ (Mpa.mm$^{0.5}$)	Error (%)	$(J_{EFF})_{EXP}$ (Mpa.mm)	$(J_{EFF})_{NUM}$ (Mpa.mm)	Error (%)
0	692.886	647.077	6.61	22.061	19.240	12.79
15	667.356	637.079	4.54	20.465	18.650	8.87
30	541.157	500.485	7.52	13.457	11.510	14.47
45	453.799	433.37	4.50	9.463	8.630	8.80
60	339.607	327.55	3.55	5.300	4.930	6.97
75	257.543	240.599	6.58	3.048	2.660	12.73
90	210.289	203.344	3.30	2.032	1.901	6.45

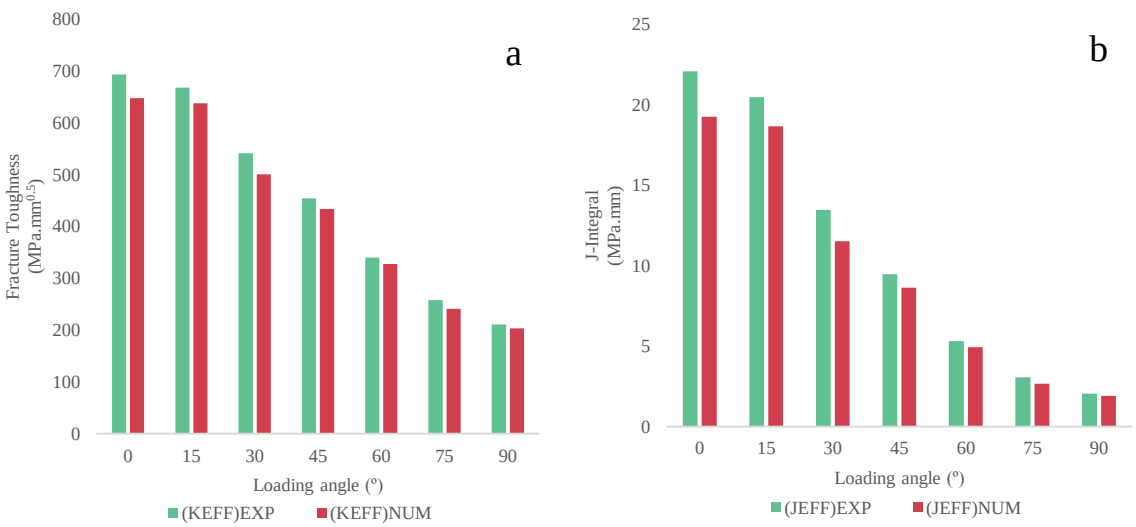

Figure 7.13 The fracture toughness (a) and J-integral (b) variation depending on the loading angles of hybrid glass-carbon knitted composite samples with 12.5mm pattern width (crack initiation from carbon side)

7.2.5. Pure Glass Knitted Composites

The arcan fracture tests were performed for pure glass knitted composite samples subjected to 0°, 30°, 45°, 60°, and 90° loading angles. The four-layered pure glass knitting fabrics were stacked by hand lay-up method and then the pure glass knitted composite plates were cut according to arcan fracture test sample. At the end, the fracture tests and fracture analysis were done and the experimental and numerical fracture images were obtained as illustrated in Figure 7.14.

When the images of experimental damage were analyzed, the crack propagation takes place straight for 0° and 90° loading angles, it was progressed in different directions for 30°, 45°, and 60° loading angles. While examining the numerical damage images, the stresses that concentrated at the crack tip were decreased from 0° to 90° loading angles. As can be seen in Figure 7.15a, the stresses for 15° and 75° loading angles were calculated by a regression approach with 0.58% error. And then this stresses were used in the numerical analysis to obtain the fracture toughness of mentioned angles. The numerical damages, which was obtain from ANSYS finite element analysis, for 15° and 75° loading angles were given in Figure 715b and Figure 7.15c.

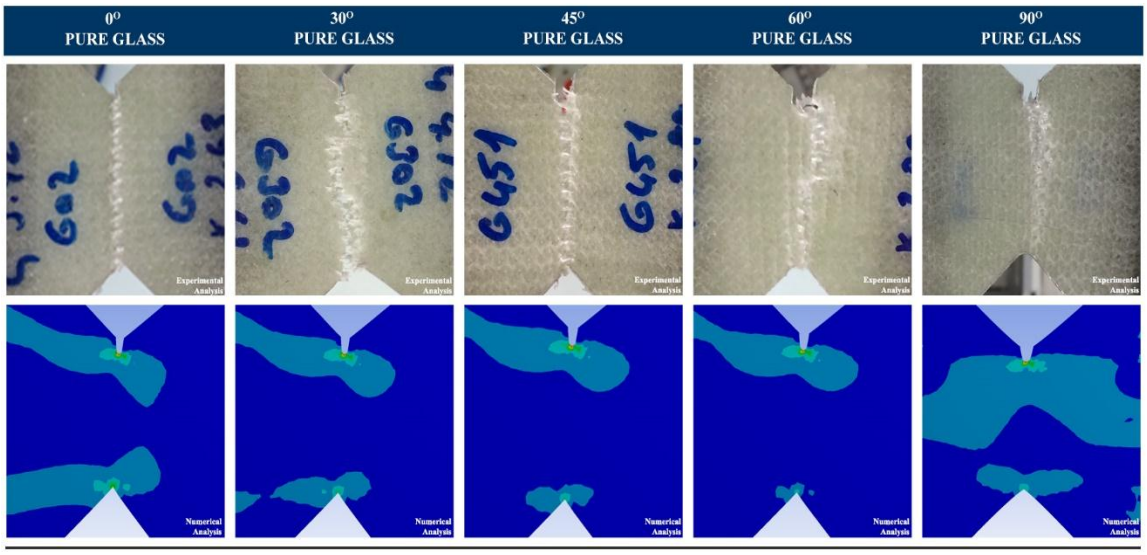

Figure 7.14 The experimental and numerical damage images of pure glass knitted composite samples

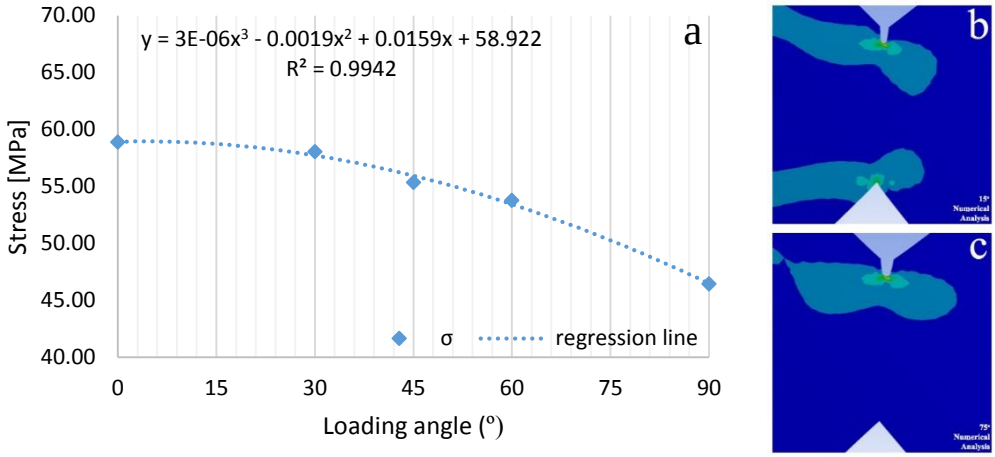

Figure 7.15 The stress-loading angles curve for pure glass knitted composite samples (a) and numerical damage images for 15° (b) and 75° (c) loading angles

The fracture toughness and the J-integral values of pure glass knitted composite samples were given in Table 7.5 and Figure 7.16. When calculating the experimental fracture toughness values, five samples were tested and the average of their results was taken in these table and figure. When the results examined in terms of the fracture toughness values, the highest result was observed in the samples with 0° loading angle and the lowest result was obtained in the samples with 90° loading angles. This trend was also occurred in the J-integral values. While considering the experimental and numerical fracture toughness values, the lowest error was observed as 3.10% for the sample subjected to 30° loading angle and the highest error was obtained as 5.57% in the sample with 45° loading angle. Depending on these values, the highest and lowest error in the J-integral values were also occurred in the samples with 45° as 11.45% and in the samples with 30° as 6.30%.

Table 7.5 The fracture toughness and the J-integral values of pure glass knitted composite samples

Loading angles (°)	$(K_{EFF})_{EXP}$ (Mpa.mm$^{0.5}$)	$(K_{EFF})_{NUM}$ (Mpa.mm$^{0.5}$)	Error (%)	$(J_{EFF})_{EXP}$ (Mpa.mm)	$(J_{EFF})_{NUM}$ (Mpa.mm)	Error (%)
0	508.484	486.329	4.36	10.746	9.830	8.52
15	487.837	468.437	3.98	9.891	9.120	7.80
30	431.082	444.452	3.10	7.723	8.210	6.30
45	353.545	373.244	5.57	5.195	5.790	11.45
60	255.106	243.782	4.44	2.705	2.470	8.68
75	188.493	178.887	5.10	1.477	1.330	9.93
90	110.971	106.341	4.17	0.512	0.470	8.17

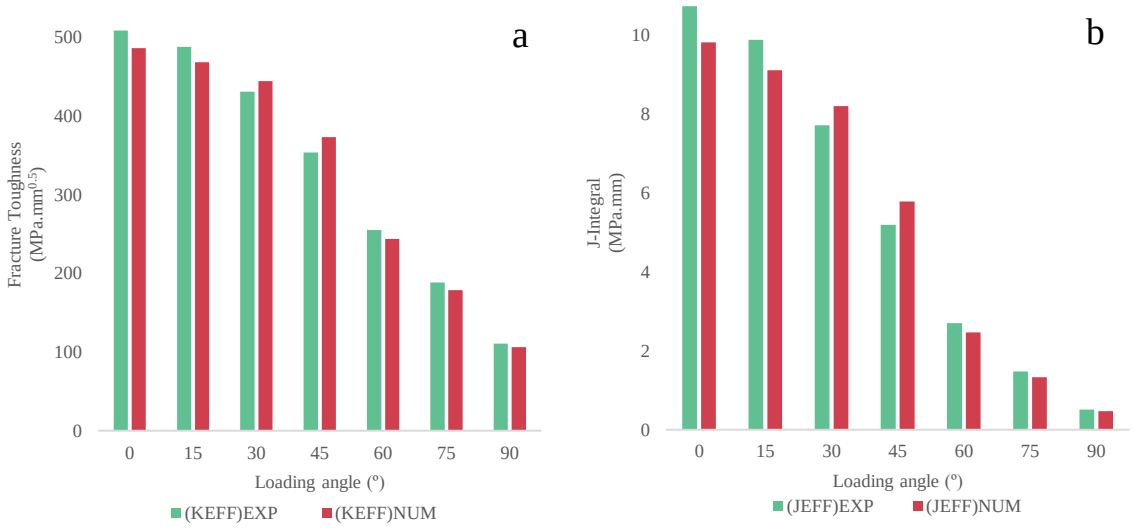

Figure 7.16 The fracture toughness (a) and J-integral (b) variation depending on the loading angles of the pure glass knitted composite samples

7.2.6. Hybrid Knitted Composites with 50mm Pattern Width (Crack Initiation from Glass Side)

The experimental and numerical damage images of hybrid glass-carbon knitted composite samples with 50mm pattern width (crack initiation from glass side) were shown in Figure 7.17. It can be seen from the experimental images that the crack damage in the glass reinforced region was obtained greater than the crack damage in the carbon reinforced regions due to ductility of glass fabrics. The straight crack propagation in the samples subjected to 0° and 90° loading angles were observed, however, the crack propagation was transmitted in different directions for 30°, 45°, and 60° loading angles. When the numerical damage images were examined, it can be said that the stress concentration at the crack tip was decreased from 0° to 90° loading angles (Figure 7.17). The stress-loading angles curve for hybrid glass-carbon knitted composite samples with 50mm pattern width (crack initiation from glass side) was given in Figure 7.18a. As shown in this figure, the stresses were calculated with 2.44% error for 15° and 75° loading angles by using a regression approach. And then these stresses were used in the ANSYS finite element program to obtain the fracture toughness values and the fracture damage images (Figure 7.18b and Figure 7.18c).

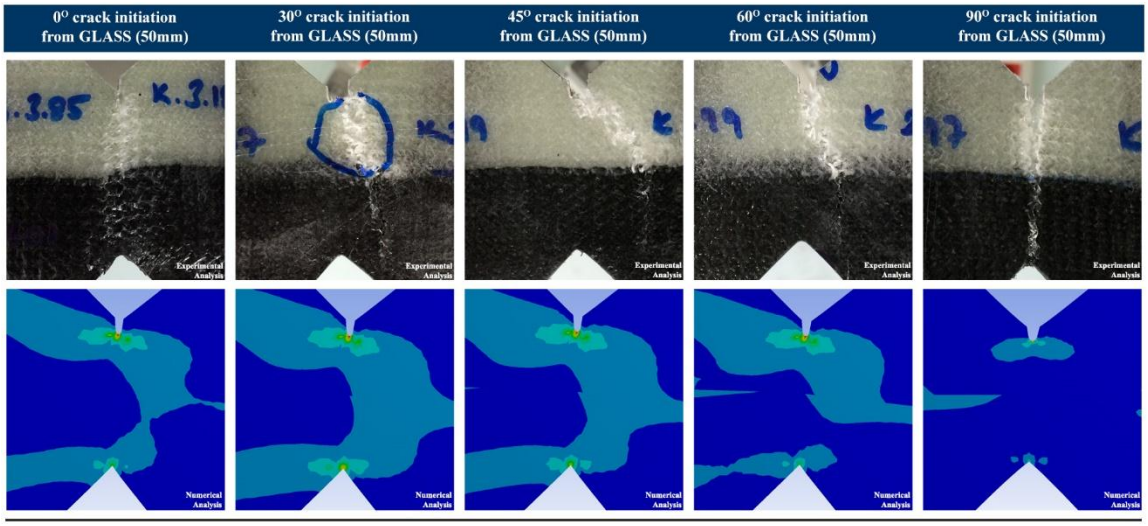

Figure 7.17 The experimental and numerical damage images of hybrid glass-carbon knitted composite samples with 50mm pattern width (crack initiation from glass side)

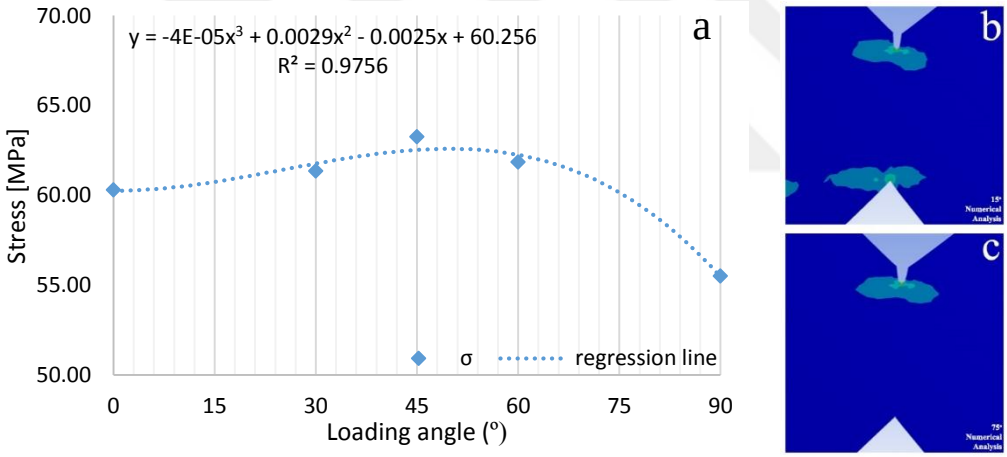

Figure 7.18 The stress-loading angles curve for hybrid glass-carbon knitted composite samples with 50mm pattern width (crack initiation from glass side) (a) and numerical damage images for 15° (b) and 75° (c) loading angles

In Table 7.6 and Figure 7.19, the fracture toughness and the J-integral values obtained from experiments and ANSYS finite element analysis were given. When calculating the experimental fracture toughness values, five specimens were tested and the average of their results was taken. When the Table 7.6 and Figure 7.19 were examined, it can be observed that the J-integral values with experimental and numerical fracture toughness values were decreased towards 0° to 90° loading angles. Again the same trend was obtained in the

numerical calculations. In terms of the fracture toughness values, the highest result was observed in the samples with 0° loading angles and the lowest results was obtained in the samples with 90° loading angles. The maximum and minimum errors were observed as 7.25% for 60° loading angles and as 1.62% for 45° loading angles, respectively.

Table 7.6 The fracture toughness and the J-integral values of hybrid glass-carbon knitted composite samples with 50mm pattern width (crack initiation from glass side)

Loading angles (°)	$(K_{EFF})_{EXP}$ (Mpa.mm$^{0.5}$)	$(K_{EFF})_{NUM}$ (Mpa.mm$^{0.5}$)	Error (%)	$(J_{EFF})_{EXP}$ (Mpa.mm)	$(J_{EFF})_{NUM}$ (Mpa.mm)	Error (%)
0	515.518	532.837	3.36	11.045	11.800	6.83
15	497.913	523.728	5.18	10.304	11.400	10.64
30	458.289	439.553	4.09	8.729	8.030	8.01
45	401.241	407.749	1.62	6.691	6.910	3.27
60	294.930	273.548	7.25	3.615	3.110	13.97
75	191.883	188.067	1.99	1.530	1.470	3.94
90	132.823	126.016	5.13	0.733	0.660	9.99

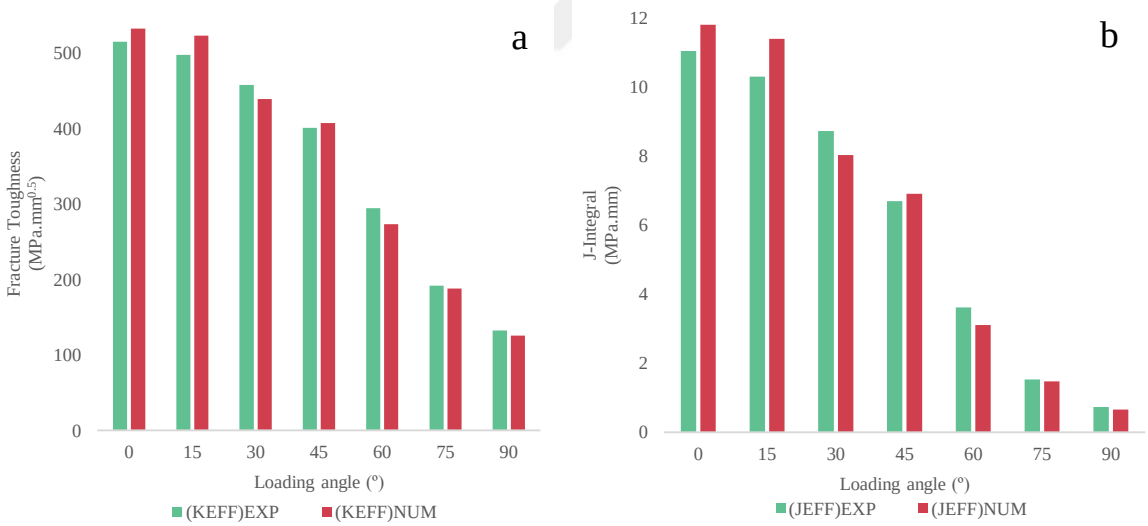

Figure 7.19 The fracture toughness (a) and J-integral (b) variation depending on the loading angles of hybrid glass-carbon knitted composite samples with 50mm pattern width (crack initiation from glass side)

7.2.7. Hybrid Knitted Composites with 25mm Pattern Width (Crack Initiation from Glass Side)

The finite element analysis images and the experimental damage images of hybrid glass-carbon knitted composite samples with 25mm pattern width (crack initiation from glass side) were shown in Figure 7.20. In the fracture tests, the crack was smoothly propagated in the samples subjected to 0° and 90° loading angles. However, the angular crack propagations were occurred in the glass reinforced region due to wale direction of samples subjected to 30°, 45°, and 60° loading angles (Figure 7.20). The regression approach was applied for the 15° and 75° loading angles which cannot calculated as experimentally (Figure 7.21a). As shown in Figure 7.21a, the stresses were obtained with 0.54% error and then finite element analysis was made for 15° and 75° loading angles by using ANSYS package program.

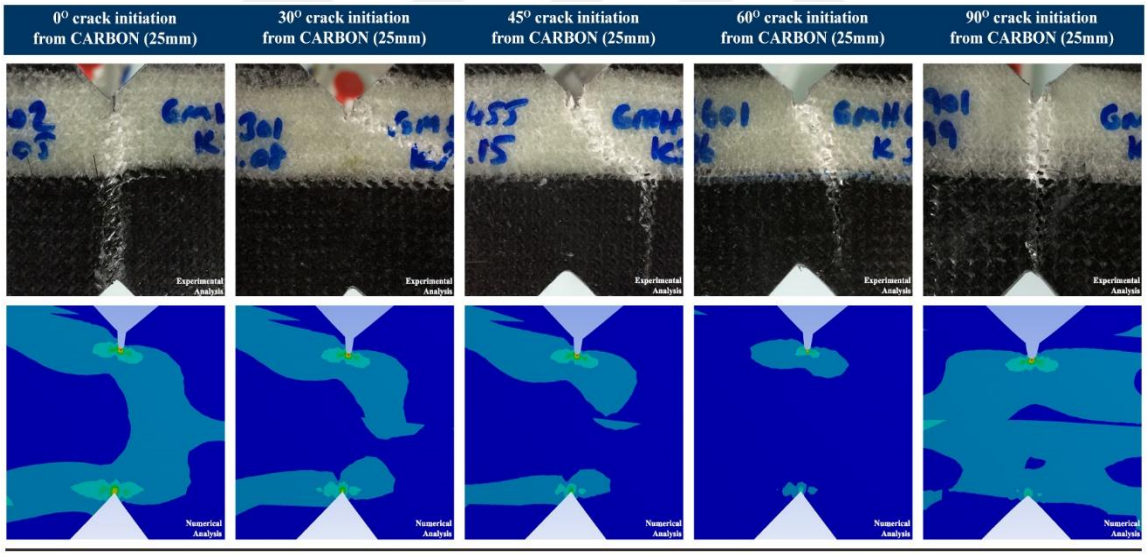

Figure 7.20 The experimental and numerical damage images of hybrid glass-carbon knitted composite samples with 25mm pattern width (crack initiation from glass side)

The five arcan fracture samples were tested during the experiments and the average of their results was taken as fracture toughness values which were given in Table 7.7 and Figure 7.22. When the given table and figure were examined, it can be observed that the J-integral values and the fracture toughness values were decreased from 0° to 90° loading angles. While the highest fracture toughness value was found as 557.984Mpa.mm$^{0.5}$ for 0°

loading angles, the lowest fracture toughness value was found as 145.567 Mpa.mm$^{0.5}$ for 90° loading angles. The numerical fracture toughness values were showed the same trend with the experimental data. When numerical and experimental values were compared to each other, the highest and lowest errors were found as 5.12% for 0° loading angle and as 1.65% for 90° loading angle.

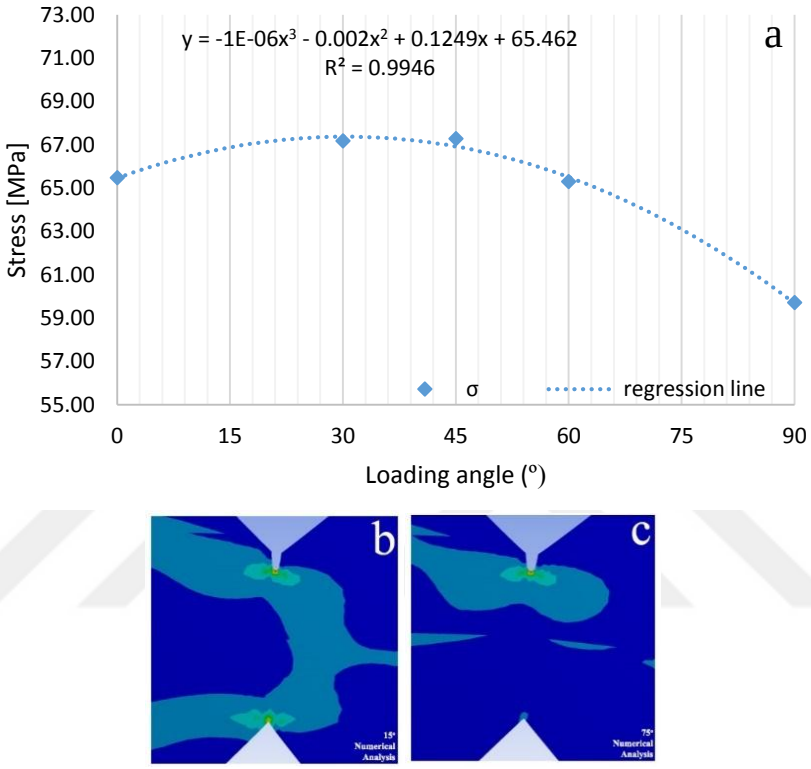

Figure 7.21 The stress-loading angles curve for hybrid glass-carbon knitted composite samples with 25mm pattern width (crack initiation from glass side) (a) and numerical damage images for 15° (b) and 75° (c) loading angles

Table 7.7 The fracture toughness and the J-integral values of hybrid glass-carbon knitted composite samples with 25mm pattern width (crack initiation from glass side)

Loading angles (°)	$(K_{EFF})_{EXP}$ (Mpa.mm$^{0.5}$)	$(K_{EFF})_{NUM}$ (Mpa.mm$^{0.5}$)	Error (%)	$(J_{EFF})_{EXP}$ (Mpa.mm)	$(J_{EFF})_{NUM}$ (Mpa.mm)	Error (%)
0	557.984	586.572	5.12	12.940	14.300	10.51
15	538.837	551.695	2.39	12.067	12.650	4.83
30	499.189	510.467	2.26	10.357	10.830	4.57
45	429.62	450.635	4.89	7.671	8.440	10.02
60	310.871	322.773	3.83	4.017	4.330	7.80
75	209.907	203.431	3.09	1.831	1.720	6.07
90	145.567	147.97	1.65	0.881	0.910	3.33

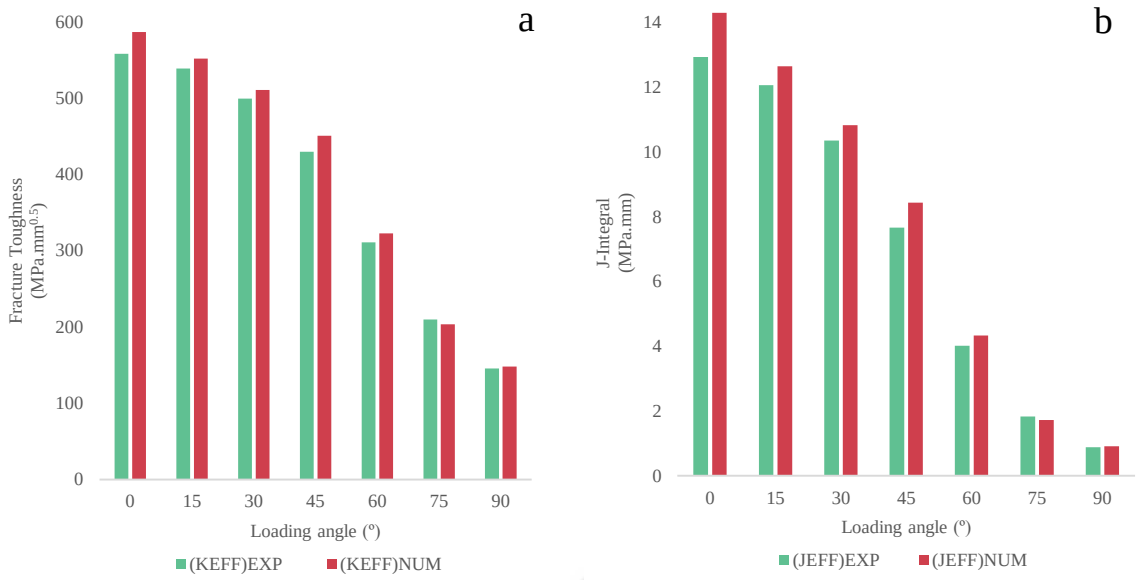

Figure 7.22 The fracture toughness (a) and J-integral (b) variation depending on the loading angles of hybrid glass-carbon knitted composite samples with 25mm pattern width (crack initiation from glass side)

7.2.8. Hybrid Knitted Composites with 12.5mm Pattern Width (Crack Initiation from Glass Side)

The experimental and numerical damage images of hybrid glass-carbon knitted composite samples with 12.5mm pattern width (crack initiation from glass side) were shown in Figure 7.23. In experimental damage images, the crack was straightly propagated in the samples subjected to 0° and 90° loading angles. In the sample loaded with 30°, 45°, and 60° loading angles, though the straight crack propagation was occurred in the carbon fabrics reinforced region, it was propagated depending on the loading direction in glass fabrics reinforced regions (Figure 7.23). In the Figure 7.24a, the regression approach was applied for the 15° and 75° loading angles which cannot calculated as experimentally. As shown in Figure 7.24a, the stresses were calculated with 2.49% error and the numerical damages for these angles were obtained as illustrated in Figure 7.24b and Figure 7.24c.

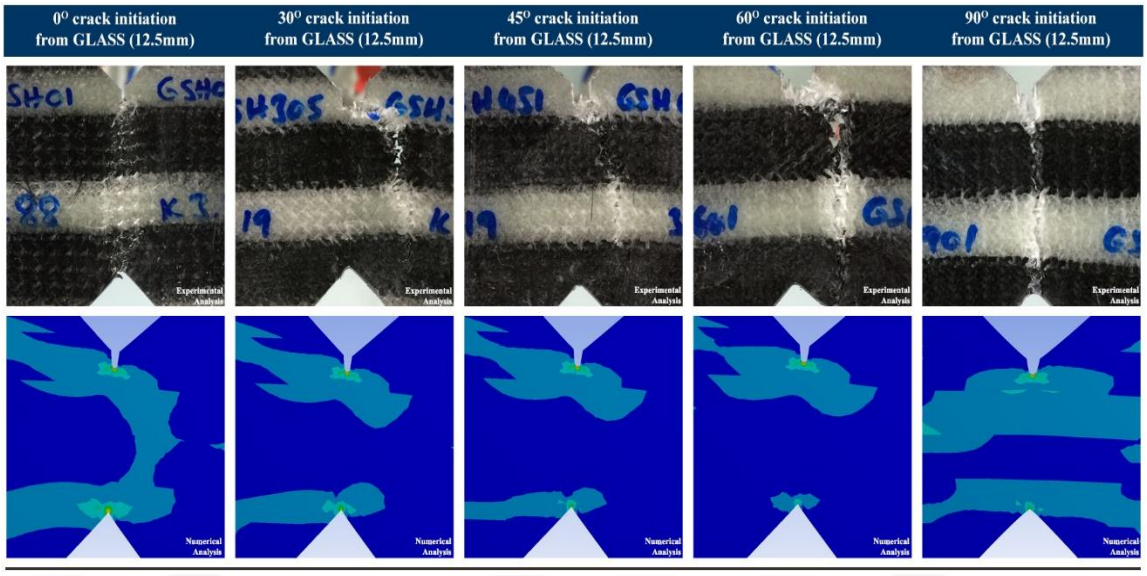

Figure 7.23 The experimental and numerical damage images of hybrid glass-carbon knitted composite samples with 12.5mm pattern width (crack initiation from glass side)

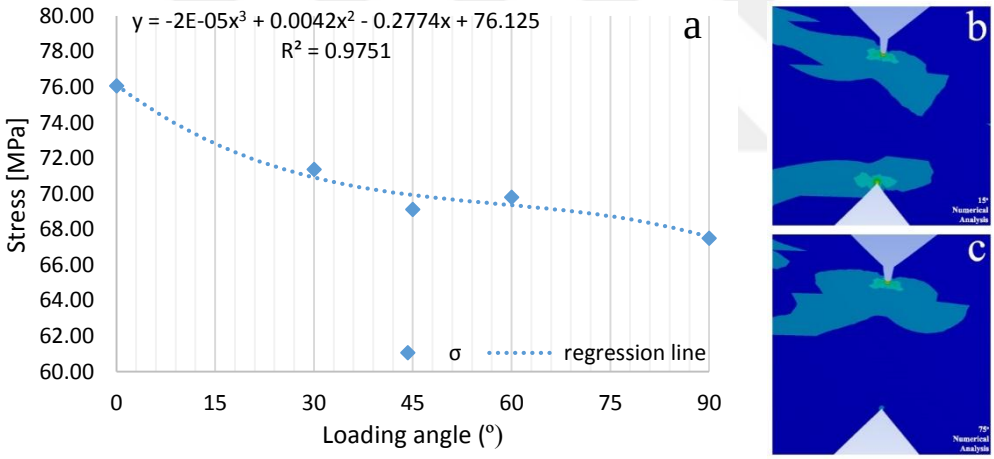

Figure 7.24 The stress-loading angles curve for hybrid glass-carbon knitted composite samples with 12.5mm pattern width (crack initiation from glass side) (a) and numerical damage images for 15° (b) and 75° (c) loading angles

The data's obtained from the average of the results of five arcan test samples were given in Table 7.8 and Figure 7.25. When looking at the given table and figure, the highest fracture toughness and J-integral values were obtained for 0° loading angles. The fracture toughness and J-integral values were decreased from 0° to 90° loading angles, therefore, the lowest fracture toughness and J-integral values were found as 162.961MPa.mm$^{0.5}$ and as

1.104MPa.mm for 90° loading angles, respectively. The same trend was obtained in the numerical fracture toughness and in the numerical J-integral values in the range of 0° to 90° loading angle. In comparison between numerical and experimental fracture toughness values, while the highest error was found as 7.46% for 45° loading angle, the lowest error was found as 3.12% for 30° loading angles. The lowest and highest differences between the experimental and numerical J-integral values were obtained as 6.97% for 75° loading angle and as 15.47% for 45° loading angle.

Table 7.8 The fracture toughness and the J-integral values of hybrid glass-carbon knitted composite samples with 12.5mm pattern width (crack initiation from glass side)

Loading angles (°)	$(K_{EFF})_{EXP}$ (Mpa.mm$^{0.5}$)	$(K_{EFF})_{NUM}$ (Mpa.mm$^{0.5}$)	Error (%)	$(J_{EFF})_{EXP}$ (Mpa.mm)	$(J_{EFF})_{NUM}$ (Mpa.mm)	Error (%)
0	652.178	682.682	4.68	17.678	19.370	9.57
15	631.549	669.694	6.04	16.577	18.640	12.44
30	534.783	551.476	3.12	11.886	12.640	14.34
45	436.881	469.463	7.46	7.933	9.160	15.47
60	329.759	346.153	4.97	4.519	4.980	10.19
75	245.975	254.407	3.43	2.515	2.690	6.97
90	162.961	170.626	4.71	1.104	1.210	10.08

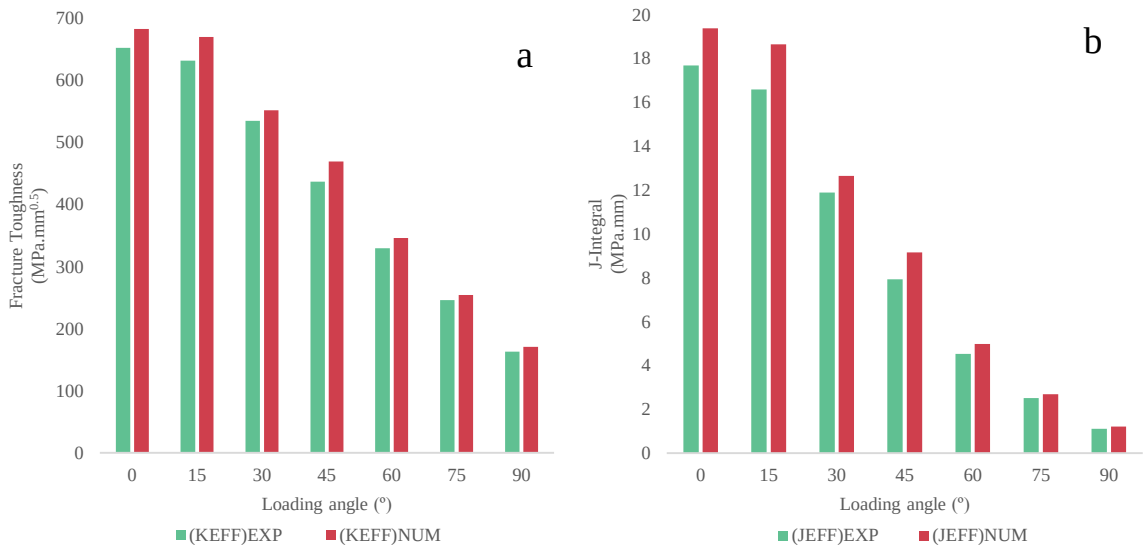

Figure 7.25 The fracture toughness (a) and J-integral (b) variation depending on the loading angles of hybrid glass-carbon knitted composite samples with 12.5mm pattern width (crack initiation from glass side)

7.3. General Evaluation of Results

In this study; the fracture toughness and J-integral values of eight different knitted structures (pure carbon and pure glass knitted non-hybrid structures, crack initiation from carbon side hybrid structures with three different pattern widths as 50mm, 25mm, and 12.5mm, crack initiation from glass side hybrid structures with three different pattern widths as 50mm, 25mm, and 12.5mm) subjected to five different loading directions (0°, 30°, 45°, 60°, and 90°,) were investigated, experimentally and numerically. The critical stresses of samples subjected to 15° and 75° loading angles was not determined, experimentally. These values were calculated by using a regression approach. And then obtained stress values were used in the ANSYS finite element program to obtain the fracture toughness and J-integral values of these structures. The fracture toughness of the glass-carbon hybrid knitted composite samples (with crack initiation from carbon side) and pure carbon non-hybrid knitted composite samples for different loading angles and for different pattern widths were given in Figure 7.26. It can be said from the figure that the highest fracture toughness value was observed in the pure carbon knitted composite samples for all loading angles. When compared to the pure carbon knitted composites, to make hybridization of glass-carbon knitted hybrid composites with different glass pattern width was reduced the fracture toughness of the pure carbon samples. This decrease can be seen for all loading angles. Nevertheless, decreasing the pattern width of the hybrid knitted composites from 50mm to 12.5mm was increased the fracture toughness for all loading angles. However, decreasing the pattern width of the glass knitted composites from 50mm to 12.5mm was slowed down the crack propagation of the carbon knitted structures due to the high ductility of the glass fabrics.

The fracture toughness of the glass-carbon hybrid knitted composite samples (with crack initiation from glass side) and pure glass non-hybrid knitted composite samples for different loading angles and for different pattern widths were given in Figure 7.27. It can be said from this figure that the pure glass knitted reinforced composites was demonstrated the lowest fracture toughness for all loading angles. Making hybrid of the pure glass composite materials with carbon knitted pattern, which has 50mm, 25mm and 12.5mm widths,

respectively, was increased the fracture toughness in all loading angles. It can be seen that decreasing in the pattern width of the samples was increased the brittleness of the material. As a result of crack propagation in the hybrid knitted composites were observed faster than the propagation formed in the pure glass knitted composites.

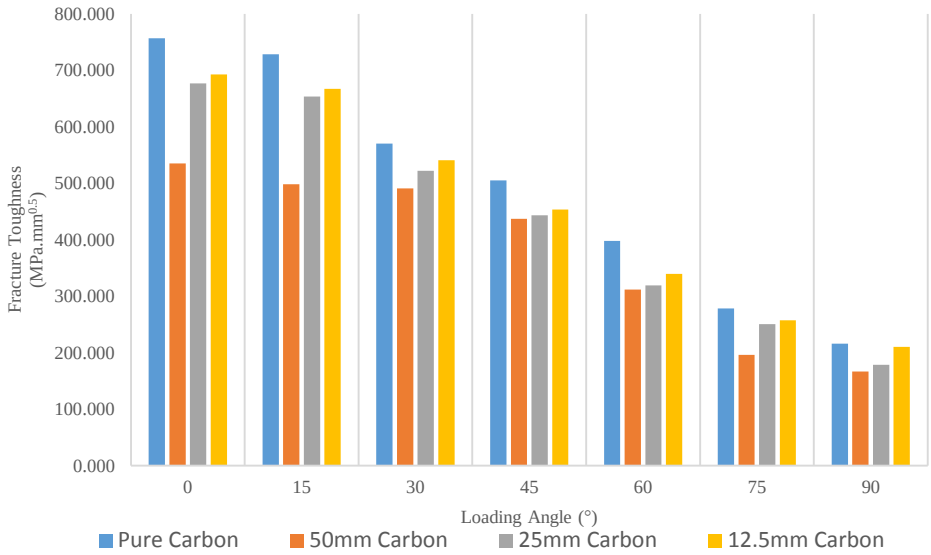

Figure 7.26 The fracture toughness of the glass-carbon hybrid knitted composite samples (with crack initiation from carbon side) and pure carbon non-hybrid knitted composite samples for different loading angles and for different pattern widths

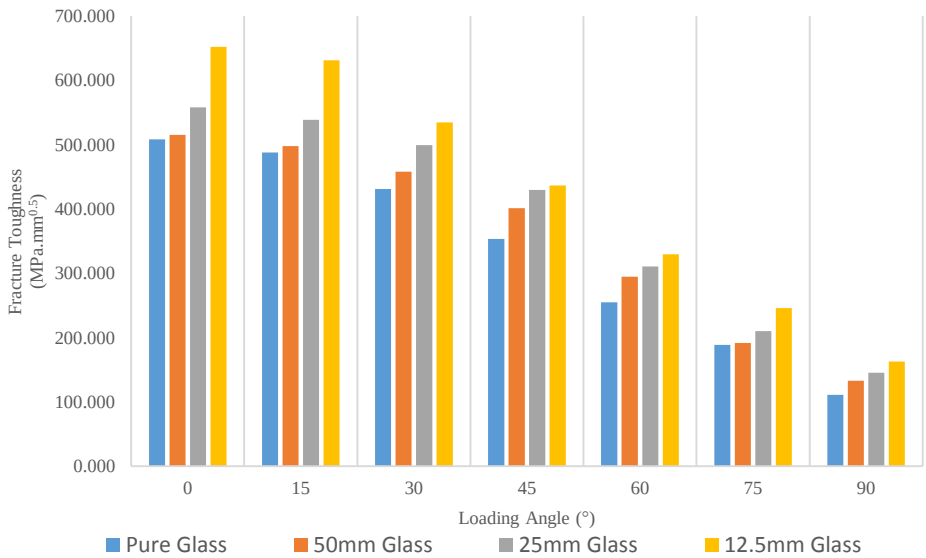

Figure 7.27 The fracture toughness of the glass-carbon hybrid knitted composite samples (with crack initiation from glass side) and pure glass non-hybrid knitted composite samples for different loading angles and for different pattern widths

The fracture toughness values variation depending on the loading angles for all non-hybrid and hybrid structures were shown in Figure 7.28. When the figure was carefully examined, the samples with crack initiation from carbon side were showed higher fracture toughness than the samples with crack initiation from glass side.

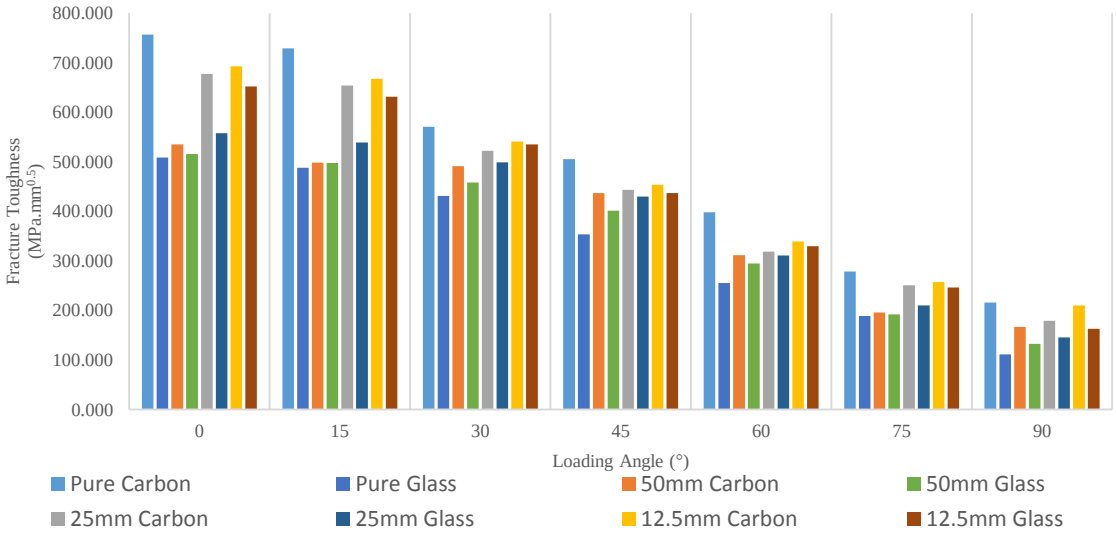

Figure 7.28 The fracture toughness values for all non-hybrid and hybrid structures

7.4. Evaluation of Scanning Electron Microscopy Images

The damages of glass knitted composites, which were obtained from scanning electron microscopy, were given in Figure 7.29. As can be understood from these images, while glass composites were faced with damage, fiber fractures were occurred mostly in the region which the crack propagates. The homogeneous matrix density of almost each region of the glass knitted composites show that the production process of the producing samples by hand lay-up method was successful.

Scanning electron microscopy images of carbon knitted composites and the matrix damages in the pure glass knitted composites during crack propagation were shown in Figure 7.30 and Figure 7.31, respectively. When examined the images in the Figure 7.30, it is obviously seen that the fiber fractures of the carbon knitted composites differ from the glass knitted composites. In the glass knitted composites, the glass knitted fibers were undergone

fracture by getting free from the matrix. However, the carbon knitted fibers were broken to pieces. Establishing stronger bonds with epoxy matrix material of the carbon knitted fibers was increased the fracture toughness of carbon knitted composites.

Figure 7.29 The fracture damage images of the glass knitted fibers in the pure glass knitted composites

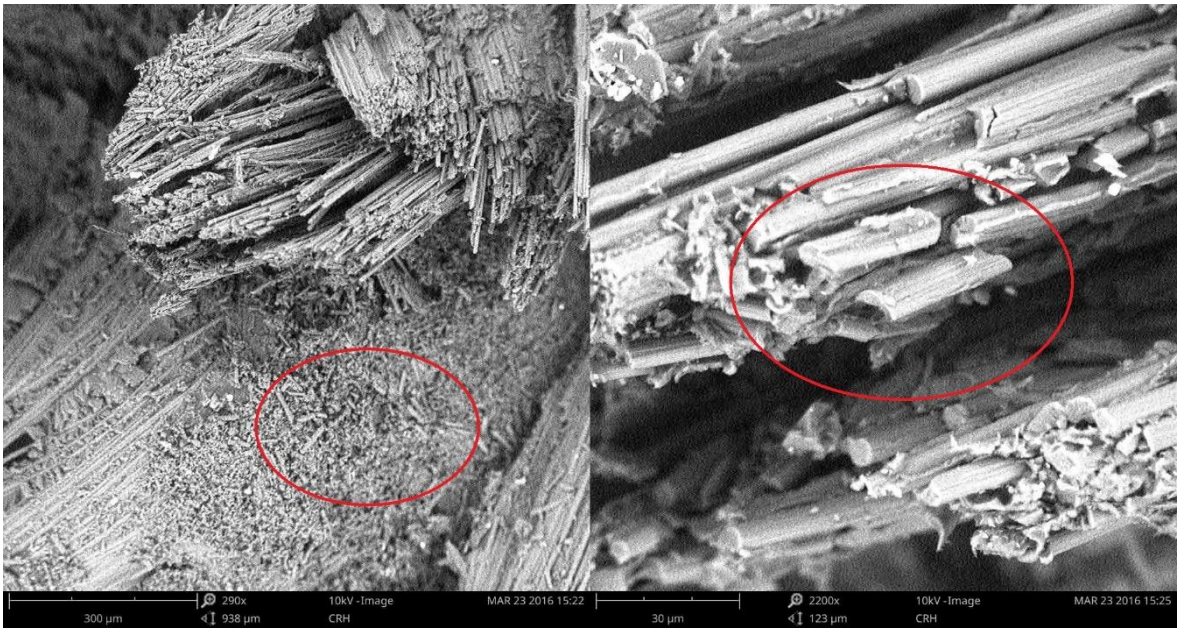

Figure 7.30 The fracture images of the carbon knitted fibers in the pure carbon knitted composites

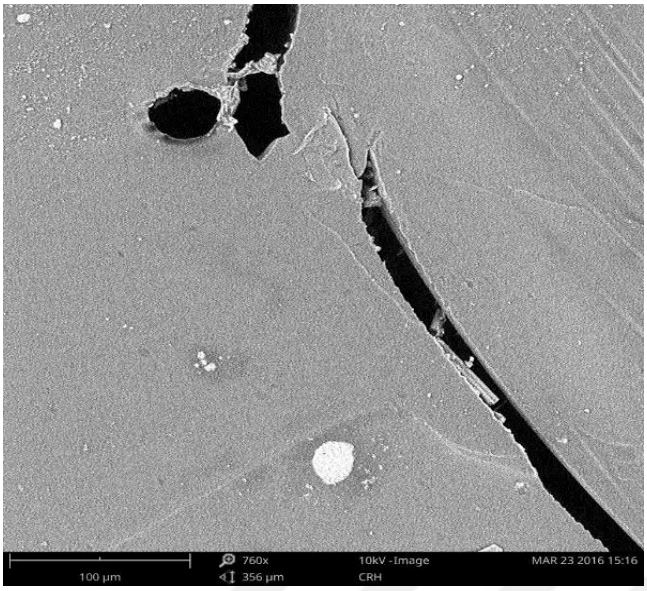

Figure 7.31 The matrix damages in the pure glass knitted composites during crack propagation

7.5. Discussion

In this thesis, the experimental and numerical fracture toughness of the non-hybrid (pure carbon and pure glass knitted composite samples) and hybrid (50% glass and 50% carbon fabrics with different pattern widths as 50mm, 25mm, and 12.5mm) knitted composites in the mode I (0°), mode I-II (30°, 45°, and 60°) and mode II (90°) loading conditions were determined. In addition, all required mechanical properties of each structure for numerical study (E_W, E_C, W_t, C_t, W_c, C_c, G_{WC}, S_{WC} and S_{CW}) were determined, experimentally. At the end of the experimental studies, the information regarding damages of knitted composite samples was reached by using scanning electron microscopy. The experimental results were compared with results obtained from numerical studies. The inferences, which were obtained from all these studies, were specified below;

- The fracture toughness was decreased from 0° to 90° loading angles.
- The highest fracture toughness was obtained from pure carbon knitted composites for 0° loading angle.
- The lowest fracture toughness was obtained from pure glass knitted composites for 90° loading angle.

- The samples with crack initiation from carbon side have higher fracture toughness values than the samples with crack initiation from glass side due to ductility of glass and fragility of carbon fabrics.
- In plane hybridization of pure carbon knitted composites with the glass knitted composites was reduced the fracture toughness of pure carbon knitted composites.
- In plane hybridization of pure glass knitted composites with the carbon knitted composites was increased the fracture toughness of pure glass knitted composites.
- The fracture toughness of carbon knitted structures were increased by decreasing the pattern width of the glass knitted fabrics in the carbon knitted structures. This situation was increased the speed of the fracture due to fragility of carbon knitted fabrics.
- When examined the scanning electron microscopy images, it was observed that the carbon fibers were broken to pieces in the carbon knitted composites, however, in the glass knitted composites, glass fibers have undergone fracture by getting free from the matrix.

REFERENCES

1. Vieille, B., Casado, V.M., Bouvet, C., 2013, "About the impact behavior of woven ply carbon fiber-reinforced thermoplastic- and thermosetting-composites: A comparative study", *Composite Structures*, vol. 101: 9–21.

2. Dai G., Mishnaevsky L., 2014, "Fatigue of hybrid glass/carbon composites: 3D computational studies", *Composites Science and Technology*, vol. 94: 71–79.

3. Dong C., Davies I. J., 2014, "Flexural and tensile strengths of unidirectional hybrid epoxy composites reinforced by S-2 glass and T700S carbon fibres", *Materials & Design*, vol. 54: 955–966.

4. Maples H. A., Wakefield S., Robinson P., Bismarck A., 2014, "High performance carbon fibre reinforced epoxy composites with controllable stiffness", *Composites Science and Technology*, vol. 105: 134–143.

5. Boroujeni A. Y., Tehrani M., Nelson A. J., Al-Haik M., 2014, "Hybrid carbon nanotube–carbon fiber composites with improved in-plane mechanical properties", *Composites Part B: Engineering*, vol. 66: 475–483.

6. Pérez M. A., Martínez X., Oller S., Gil L., Rastellini F., Flores F., 2013, "Impact damage prediction in carbon fiber-reinforced laminated composite using the matrix-reinforced mixing theory", *Composite Structures*, vol. 104: 239–248.

7. Elanchezhian C., Ramnath B. V., Hemalatha J., 2014, "Mechanical Behaviour of Glass and Carbon Fibre Reinforced Composites at Varying Strain Rates and Temperatures", *Procedia Materials Science*, vol. 6: 1405–1418.

8. Ochola R. O., Marcus K., Nurick G. N., Franz T., 2004, "Mechanical behaviour of glass and carbon fibre reinforced composites at varying strain rates", *Composite Structures*, vol. 63, no. 3–4: 455–467.

9. Tehrani M., Boroujeni A. Y., Hartman T. B., Haugh T. P., Case S. W., Al-Haik M. S., 2013, "Mechanical characterization and impact damage assessment of a woven carbon fiber reinforced carbon nanotube–epoxy composite", *Composites Science and Technology*, vol. 75: 42–48.

10. Qi Y., Li J., Liu L., 2014, “Tensile properties of multilayer-connected biaxial weft knitted fabric reinforced composites for carbon fibers”, *Materials & Design*, vol. 54: 678–685.

11. Leong K. H., Falzon P. J., Bannister M. K., Herszberg I., 1998, “An investigation of the mechanical performance of weft-knit Milano-rib glass/epoxy composites”, *Composites Science and Technology*, vol. 58(2): 239–251.

12. Sugie T., Nakai A., Hamada H., 2009, “Effect of CF/GF fibre hybrid on impact properties of multi-axial warp knitted fabric composite materials”, *Composites Part A: Applied Science and Manufacturing*, vol. 40(12): 1982–1990.

13. Solaimurugan S., Velmurugan R., 2008, “Influence of in-plane fibre orientation on mode I interlaminar fracture toughness of stitched glass/polyester composites”, *Composites Science and Technology*, vol. 68(7–8): 1742–1752.

14. Aktaş A., Tercan M., Aktaş M., Turan F., 2013, “Investigation of knitting architecture on the impact behavior of glass/epoxy composites”, *Composites Part B: Engineering*, vol. 46: 81–90.

15. Pandita S. D., Verpoest I., 2004, “Tension–tension fatigue behaviour of knitted fabric composites”, *Composite Structures*, vol. 64(2): 199–209.

16. Ma P., Zhang F., Gao Z., Jiang G., Zhu Y., 2014, “Transverse impact behaviors of glass warp-knitted fabric/foam sandwich composites through carbon nanotubes incorporation”, *Composites Part B: Engineering*, vol. 56: 847–856.

17. Yang B., Kozey V., Adanur S., Kumar S., 2000, “Bending, compression, and shear behavior of woven glass fiber–epoxy composites”, *Composites Part B: Engineering*, vol. 31(8): 715–721.

18. Kim K.-Y., Curiskis J. I., Ye L., Fu S.-Y., 2005, “Mode I interlaminar fracture behaviour of weft-knitted fabric reinforced composites”, *Composites Part A: Applied Science and Manufacturing*, vol. 36(7): 954–964.

19. Ramesh M., Palanikumar K., Reddy K. H., 2013, “Mechanical property evaluation of sisal–jute–glass fiber reinforced polyester composites”, *Composites Part B: Engineering*, vol. 48: 1–9.

20. Arthanarieswaran V. P., Kumaravel A., Kathirselvam M., 2014, “Evaluation of mechanical properties of banana and sisal fiber reinforced epoxy composites: Influence of glass fiber hybridization”, *Materials & Design*, vol. 64: 194–202.

21. Zhang Y., Li Y., Ma H., Yu T., 2013, “Tensile and interfacial properties of unidirectional flax/glass fiber reinforced hybrid composites”, *Composites Science and Technology*, vol. 88: 172–177.

22. Stamenkovic D., 2006, “Determination of Fracture Mechanics Parameters using FEM and J-Integral Approach”, *Proceedings of the 2nd WSEAS International Conference on Applied and Theoretical Mechanics*, 25–29.

23. Rashedi A., Sridhar I., Tseng K. J., 2016, “Fracture characterization of glass fiber composite laminate under experimental biaxial loading”, *Composite Structures*, vol. 138: 17–29.

24. Gliesche K., Hübner T., Orawetz H., 2005, “Investigations of in-plane shear properties of ±45°-carbon/epoxy composites using tensile testing and optical deformation analysis”, *Composites Science and Technology*, vol. 65(2): 163–171.

25. Elarabi S. M., 2005, “The Effect of Transversely Aligned Fibers on the Axial Tensile Strength of Carbon Epoxy Composites”, *Journal of Industrial Textiles*, vol. 35(1): 39–45.

26. Zhang M., Mason S. E., 1999, “The Effects of Contamination on the Mechanical Properties of Carbon Fibre Reinforced Epoxy Composite Materials”, *Journal of Composite Materials*, vol. 33(14): 1363–1374.

27. Reis P. N. B., Ferreira J. A. M., Antunes F. V., Richardson M. O. W., 2009, “Effect of Interlayer Delamination on Mechanical Behavior of Carbon/Epoxy Laminates”, *Journal of Composite Materials*, vol. 43(22): 2609–2621.

28. Suresha B., Chandramohan G., 2007, “Effect of Normal Load and Sliding Velocity on Friction and Wear Behavior of Carbon Fiber Reinforced Epoxy Composites”, *Journal of Reinforced Plastics and Composites*, vol. 26(16): 1695–1703.

29. Yang L., Ran L., Yi M., 2011, “Carbon fiber knitted fabric reinforced copper composite for sliding contact material”, *Materials & Design*, vol. 32(4): 2365–2369.

30. Wonderly C., Grenestedt J., Fernlund G., Cĕpus E., 2005, “Comparison of mechanical properties of glass fiber/vinyl ester and carbon fiber/vinyl ester composites”, *Composites Part B: Engineering*, vol. 36(5): 417–426.

31. Deng S., Ye L., 1999, “Influence of Fiber-Matrix Adhesion on Mechanical Properties of Graphite/Epoxy Composites: II. Interlaminar Fracture and Inplane Shear Behavior”, *Journal of Reinforced Plastics and Composites*, vol. 18(11): 1041–1057.

32. Shan Y., Lai K.-F., Wan K.-T., Liao K., 2002, “Static and Dynamic Fatigue of Glass-Carbon Hybrid Composites in Fluid Environment”, *Journal of Composite Materials*, vol. 36(2): 159–172.

33. Luo Y., Verpoest I., 2002, “Biaxial tension and ultimate deformation of knitted fabric reinforcements”, *Composites Part A: Applied Science and Manufacturing*, vol. 33(2): 197–203.

34. Khondker O. A., Leong K. H., Herszberg I., Hamada H., 2005, “Impact and compression-after-impact performance of weft-knitted glass textile composites”, *Composites Part A: Applied Science and Manufacturing*, vol. 36(5): 638–648.

35. Rogers C.A., Hancock G.J., 2001, “Fracture toughness of G550 sheet steels subjected to tension”, *Journal of Constructional Steel Research*, vol. 57(1): 71–89.

36. Zappalorto M., Salviato M., Quaresimin M., 2013, “Mixed mode (I+II) fracture toughness of polymer nanoclay nanocomposites”, *Engineering Fracture Mechanics*, vol. 111: 50–64.

37. Chandrasekaran S., Sato N., Tölle F., Mülhaupt R., Fiedler B., Schulte K., 2014, “Fracture toughness and failure mechanism of graphene based epoxy composites”, *Composites Science and Technology*, vol. 97: 90–99.

38. Ashby M. F., 2005, “Materials Selection in Mechanical Design”, 3rd ed., Pergamon Press, *Jordan Hill*, Oxford, UK.

39. Chung D. D. L., 2010, “Composite Materials - Science and Applications”, 2nd ed., Springer Science & Business Media, *Dordrecht Heidelberg*, New York, USA.

40. Ravi K.B.M., Harish S.N., Preetham B.M., 2013, " Study On Mechanical Properties Of TiB2 Reinforced Al7075 Metal Matrix Composite Material", *International Journal of Advanced Scientific and Technical Research*, Vol.4: 439-434.

41. Shi M. F., Brindza J. A., Michel P. F., Bucklin P., Belanger P. J., Prencipe J. M., 1997, “Static and Dynamic Dent Resistance Performance of Automotive Steel Body Panels”, *SAE Technical Paper 970158*, Michigan, 1-9.

42. Armstrong K., 1997, “Care and repair of advanced composites”, Society of Automotive Engineers Publisher, *Warrendale*, Pennsylvania, USA.

43. Morita H., Adachi T., Tateishi Y., Matsumot H., 1997, "Characterization of Impact Damage Resistance of CF/PEEK and CF/Toughened Epoxy Laminates under Low and High Velocity Impact Tests", *Journal of Reinforced Plastics and Composites*, vol. 16(2): 131–143.

44. Peters S.T., 2013, "Handbook of Composites", 2nd ed., Springer Science & Business Media, *Dordrecht Heidelberg*, New York, USA.

45. Dahotre N. B., Samant A., 2011, "Laser Machining of Advanced Materials". CRC Press, *Boca Raton*, Florida, USA.

46. Giurgiutiu V., 2015, "Structural Health Monitoring of Aerospace Composites", Elsevier Academic Press, *San Diego*, California, USA.

47. Edward M.L., 2012, "Fibrous Composites in Structural Design", Springer Science & Business Media, *Dordrecht Heidelberg*, New York, USA.

48. Mouritz A. P., Bannister M. K., Falzon P. J., Leong K. H., 1999, "Review of applications for advanced three-dimensional fibre textile composites", *Composites Part A: Applied Science and Manufacturing*, vol. 30(12):1445–1461.

49. Hollaway L.C., Teng J.G., 2008, "Strengthening and Rehabilitation of Civil Infrastructures Using Fibre-Reinforced Polymer (FRP) Composites", CRC Press, *Padstow*, Cornwall, UK.

50. Poornakumar S.L.S., Karthick A.V.T.S.S., 2015, "Fabrication and Experimental Strength Analysis of Natural Fiber Composite Material", *International Journal for Scientific Research & Development*, vol. 3(2): 2240–2242.

51. Richardson, T., 1987, "Composites: A Design Guide", Industrial Press Inc., *Madison*, New York, USA.

52. Bensadoun F., Vallons K.A.M., Lessard L. B., Verpoest I., Vuure A.W.V., 2015, "Fatigue behaviour assessment of flax-epoxy composites", *Composites Part A: Applied Science and Manufacturing*, vol. 82: 253–266.

53. Boyer R.R., Cotton J.D., Mohaghegh M., Schafrik R. E., 2015, "Materials considerations for aerospace applications", *MRS Bulletin*, vol. 40(12): 1055–1066.

54. Evaristo R., Ricardo D.-C., Margarita P., Rosa M., Catalina S., 1999, "Polymer Viscoelasticity: Stress and Strain in Practice", Marcel Dekker Inc., *Madison*, New York, USA.

55. James K.W., 2004, "The Handbook of Advanced Materials: Enabling New Designs", John Wiley & Sons Publishers, *Hoboken*, New Jersey, USA.

56. Mangalgiri P.D., 1999, "Composite materials for aerospace applications," *Bulletin of Materials Science*, vol. 22(3): 657–664.

57. Campbell F.C., 2003, "Manufacturing Processes for Advanced Composites", Elsevier Ltd., *Kidlington*, Oxford, UK.

58. Harle J.V.S., 2000, "High-Performance Fibres", Woodhead Publishing Limited, *Abington*, Cambridge, UK.

59. Campbell F. C., 2010. "Structural Composite Materials", ASM International, *St Louis*, Missouri, USA.

60. George W., 2015, "Handbook of Fillers", 2nd ed., ChemTec Publishing, *Toronto*, Ontario, CA.

61. Paiva M.C., Bernardo C.A., Nardin M., 2000, "Mechanical, surface and interfacial characterisation of pitch and PAN-based carbon fibres", *Carbon*, vol. 38(9):1323–1337.

62. Paris O., Loidl D., Peterlik H., 2002, "Texture of PAN- and pitch-based carbon fibers," *Carbon*, vol. 40(4): 551–555.

63. Anthonio M., 1999, "3-D textile reinforcements in composite materials", Woodhead Publishing Limited, *Cornwall*, England, UK.

64. Morán-López J.L., Sánchez J.M., 2012, "Advanced Topics in Materials Science and Engineering", Springer Science & Business Media, *New York*, USA.

65. Buckley J.D., Edie D.D., 2012, "Carbon-Carbon Materials and Composites", Noyes Publications, *Park Ridge*, New Jersey, USA.

66. Campbell F.C., 2012, "Fatigue and Fracture: Understanding the Basics", ASM International, *St Louis*, Missouri, USA.

67. Campbell F.C., 2011, “Manufacturing Technology for Aerospace Structural Materials”, Elsevier Ltd., *Kidlington*, Oxford, UK.

68. Thomas S., Sinturel C., Thomas R., 2014, “Micro- and Nanostructured Epoxy/Rubber Blends”, Wiley-VCH Publisher, *Weinheim*, DE.

69. Ellis B., 1993, “Chemistry and Technology of Epoxy Resins”, Springer Science & Business Media, *Glasgow*, UK.

70. Mark H. F., 2007, “Encyclopedia of Polymer Science and Technology, Concise”, 3rd ed., John Wiley & Sons Publishers, *Hoboken*, New Jersey, USA.

71. Mallick P.K., 2007, “Fiber-Reinforced Composites: Materials, Manufacturing, and Design”, 3rd ed., CRC Press, *Boca Raton*, Florida, USA.

72. Verrey J., Wakeman M.D., Michaud V., Månson J.-A.E., 2006, “Manufacturing cost comparison of thermoplastic and thermoset RTM for an automotive floor pan”, *Composites Part A: Applied Science and Manufacturing*, vol. 37(1): 9–22.

73. Chawla S.L., 1993, “Materials Selection for Corrosion Control”, ASM International, *St Louis*, Missouri, USA.

74. Vodicka R., 1996, “Thermoplastics for Airframe Applications: A Review of the Properties and Repair Methods for Thermoplastic Composites”, DSTO-TR-0424, *DSTO Aeronautical and Maritime Research Laboratory*, Melbourne, AU.

75. McAuley M., 2015, “Contemporary Methods for Repairing Composite Materials”, *DSIAC Journal: A Quarterly Publication of the Defense Systems Information Analysis Center*, vol. 2(1): 27-34.

76. Roesler J., Harders H., Baeker M., 2006, “Mechanical Behavior of Enginerring Materials”, Springer Science & Business Media, *Verlag*, Berlin Heidelberg, DE.

77. Donald R.A., Fulay P.P., 2015, “Essentials of Materials Science and Engineering”, 2nd ed., Cengage Learning, *Birchmount Road*, Toronto, CA.

78. Askeland D., Wright W., 2014, “Science and Engineering of Materials”, 7th ed., Cengage Learning, *Boston*, Massachusetts, USA.

79. Unger D.J., 1995, “Analytical Fracture Mechanics”, Academic Press Inc., *San Diego*, California, USA.

80. Internet: Wikipedia the Free Encyclopedia, 2013, “Plane Stress”, https://en.wikipedia.org/wiki/Plane_stress#cite_note-Meyers-1, 7 August 2013.

81. Wang C.H., 1996, “Introduction to Fracture Mechanics”, DSTO-GD-0103, *DSTO Aeronautical and Maritime Research Laboratory*, Melbourne, AU.

82. Yayla P., 2007, “Fracture Mechanics”, Caglayan Press, *Beyoglu*, Istanbul, TR.

83. Liu A.F., 2005, “Mechanics and Mechanisms of Fracture: An Introduction”. ASM International, *St Louis*, Missouri, USA.

84. Benson H.D., Gregory H.H., 1992, “Performance of Resin Transfer Molded Multiaxial Warp Knit Composites”, *Third NASA Advanced Composites Technology Conference*, 231-261.

85. Internet: 3K A-38 Technical Data Sheet, 2016, “Fiber Properties”, http://www.dowaksa.com/wp-content/uploads/2016/03/3K-A-38.pdf, February 2016.

86. Miloš B.V., 1990, “Technical approach to glass”, Elsevier Science Publisher Co, *New York*, USA.

87. Campilho R.D.S.G., 2016, “Natural Fiber Composites”, CRC Press, *Boca Raton*, Florida, USA.

88. Bank L.C., 2006, “Composites for Construction: Structural Design with FRP Materials”, John Wiley & Sons Publishers, *Hoboken*, New Jersey, USA.

89. Balasubramanian M., 2014, “Composite Materials and Processing”, CRC Press, *Boca Raton*, Florida, USA.

90. Aktaş, M., 2007, “Temperature effect on impact behavior of laminated composite plates”, PhD Thesis, Dokuz Eylül University, İzmir, TR.

91. Choupani N., 2008, “Experimental and numerical investigation of the mixed-mode delamination in Arcan laminated specimens”, *Materials Science and Engineering A*, vol. 478: 229–242.

92. Balcıoğlu H.E., Aktaş M., “An investigation on lateral buckling of laminated composites with delaminations”, *Indian Journal of Engineering and Materials Sciences*, vol. 20: 367-375.

93. Karakuzu R., Taylak N., İçten B.M., Aktaş M., 2008, “Effects of geometric parameters on failure behavior in laminated composite plates with two parallel pin-loaded holes”, *Composite Structures*, vol. 85:1-9.

94. Karakuzu R., Çalışkan C.R., Aktaş M., İçten B.M., 2008, “Failure behavior of laminated composite plates with two serial pin-loaded holes”, *Composite Structures*, vol. 82: 225-234.

95. Aktaş M., 2009, “Buckling behavior of carbon/epoxy laminated composite plates under biaxial loading”, *Advanced Composite Letters*, vol. 18(3): 85-93.

96. Tercan M., Aktaş M., 2009, “Buckling behavior of 1x1 rib knitting laminated plates with cutouts”, *Composite Structures*, vol. 89: 245-252.

97. Garcia-Manrique J., Camas D., Lopez-Crespo P., Gonzalez-Herrera A., 2013, “Stress intensity factor analysis of through thickness effects”, *International Journal of Fatigue*, vol. 46: 58–66.

98. Kaman M.O., 2011, “Effect of fiber orientation on fracture toughness of laminated composite plates”, *Engineering Fracture Mechanics*, vol. 78(13): 2521-2534.

99. Hoha H.J., Panga J.H.L., Tsanga K.S., 2016 “Stress intensity factors for fatigue analysis of weld toe cracks in a girth-welded pipe”. *International Journal of Fatigue*, vol. 87: 279–287.

100. Nikbakht M., Choupani N., 2008, “Fracture Toughness Characterization of Carbon-Epoxy Composite using Arcan Specimen”, *International Journal of Mechanical, Aerospace, Industrial, Mechatronic and Manufacturing Engineering* Vol: 2(5): 690-696